A Study on the Effects of Deposition Strategies and Shapes on Thermo-mechanical Characteristics in the Vicinity of the Deposited Region by a DED Process

조 선 대 학 교 대 학 원

기 계 공 학 과

ALIYEV ALISSULTAN

A Study on the Effects of Deposition Strategies and Shapes on Thermo-mechanical Characteristics in the Vicinity of the Deposited Region by a DED Process

적층 경로 및 적층 형상이 DED 공정으로 적층된 적층부 인근의 열-기계 특성에 미치는 영향에 관한 연구

2022 년 8 월 26 일

조 선 대 학 교 대 학 원

기 계 공 학 과

ALIYEV ALISSULTAN

A Study on the Effects of Deposition Strategies and Shapes on Thermo-mechanical Characteristics in the Vicinity of the Deposited Region by a DED Process

지도교수 안 동 규

이 논문을 공학 사학위신청 논문으로 제출함

2022 년 4 월

조선대학교 대학원

기 계 공 학 과 대학원

ALIYEV ALISSULTAN

ALIYEV ALISSULTAN 의 석사학위논문을 인준함

위원장 조선대학교 교 수 김 창 래 (인)

위　원 조선대학교 교 수 이 정 원 (인)

위　원 조선대학교 교 수 안 동 규 (인)

2022 년 5 월

조선대학교 대학원

TABLE OF CONTENTS

LIST OF FIGURES

LIST OF TABLES

NOMENCLATURE

ρ	Density
ε	Emissivity
α	Thermal diffusivity
β	Volumetric thermal expansion coefficient of fluid
σ_s	Stefan-Boltzmann constant
η	Efficiency of laser
Q_0	Maximum heat flux at the center of beam
r	Radial distance from the center of beam
r_0	Effective radius of beam
r_b	Radius of beam
r_e	Effective radius of beam at z_e
r_i	Effective radius of beam at z_i
z_e	Top coordinates of source
z_i	Bottom coordinates of source
$\hat{h}_{conv}$	Coefficient of natural convection
$\hat{h}_{rad}$	Coefficient of radiation
Nu_L	Nusselt number
L_c	Characteristics length
k	Thermal conductivity
c	Shape factor
P	Laser power
δ	Penetration of heat source

R	Effective distance from stagnation point
Ra_L	Rayleigh number
Re_L	Reynolds number
Gr_L	Grashof number
g	Gravitational acceleration
ν_k	Kinematic viscosity
T	Temperature
T_∞	Ambient temperature
T_f	Gas temperature
T_s	Surface temperature
A_r	Nozzle area
H	Distance from the nozzle to impingement surface
D	Nozzle diameter
R	Distance from the stagnation point
t	time
C_p	Specific heat
$q_{conv}^{"}$	Convective loss
$q_{rad}^{"}$	Radiative losses
ε	Emissivity
σ_s	Stefan-Boltzmann constant
$q_{loss}^{"}$	Combined convective and radiative losses

ABSTRACT

A Study on the Effects of Deposition Strategies and Shapes on Thermo-mechanical Characteristics in the Vicinity of the Deposited Region by a DED Process

Aliyev Alissultan

Advisor: Prof. Ahn Dong-Gyu, Ph.D.

Department of Mechanical Engineering

Graduate School of Chosun University

Additive manufacturing is one of the important parts of industrial revolution 4.0 because its capability to create free form objects with minimum wastage and reduced energy usage. The ability to create customizable, personalized parts and components can be used to improve other areas of manufacturing as well as efficiency of tools and machines. Metals are one of the most important engineering materials due to their properties such as strength, durability, fatigue strength and recyclability. Directed energy deposition (DED) is one of the metal AM processes. Depending on the feeding method DED can be divided into powder and wire feeding type. DED can be used in order to create complex geometry objects, functional materials and can be used for repair and remanufacturing purposes. However, during the deposition process high temperature gradients due to rapid heating and cooling of the metal undesired effects occur such as residual stress, distortion and deflection. In order to manufacture high quality parts by DED information of proper deposition strategies is required. In order to investigate various deposition

strategies to find best process parameters numerical analysis method is proposed in this work. Finite element analysis (FEA) can help reduce cost and time required for performing numerous experiments. Hence, investigation of different process parameters is required in order to acquire information about proper deposition strategies.

The goal of this thesis to analyze DED process and evaluate the effects of various deposition strategies in order to find methods for improved quality of deposited parts. Control over temperature histories one of the most important methodology to improve the quality and mechanical properties of parts manufactured by DED. One of the methods to control temperature during DED process is applying different scanning patterns. Change in scanning pattern leads to changes in temperature histories and as a result residual stresses and distortion is modified. Deposition pattern can affect mechanical properties, surface quality and density of the part. Hence, evaluation of various deposition pattern is proposed in this work.

The shape of deposited material can have effect on residual stress and, more importantly, distortion and deflection in case of cantilever beam shape substrate. The effect deposited width and length can have different effects. Investigation of this effects can provide and insight on substrate requirement depending on deposited shape as well as this information can serve as a guideline for the cases when additional pre-processing measures must be taken in order to avoid failure or unusable condition of deposited part. FEA of different width and length as well as height of deposited region were analyzed on cantilevered shape substrate in order to evaluate post process thermos-mechanical properties of metal parts. In the next step selected proper deposition pattern was applied to build thin wall structure and results were compared to the deposition of simple wall structure deposited by zig-zag deposition strategy. The results of the analysis showed that selected deposition pattern resulted in improved residual stress and displacement when Inconel 718 powder is deposited over AISI 1045 substrate. However, in case of G6 powder deposited in SCM 440 substrate proper deposition pattern helped to reduce

effective and 1st principal stress but failed to improve displacement of the substrate.

초록

적층 경로 및 적층 형상이 DED 공정으로 적층된 적층부 인근의 열-기계 특성에 미치는 영향에 관한 연구

Aliyev Alissultan

Advisor: Prof. Ahn Dong-Gyu, Ph.D.

Department of Mechanical Engineering

Graduate School of Chosun University

적층제조는 산업혁명 4.0의 중요한 부분 중 하나로서 낭비를 최소화하고 에너지 사용을 줄이면서 자유로운 형태의 물체를 만들 수 있다. 사용자 정의 및 개인화된 부품과 구성 요소를 생성하는 기능은 다른 제조 영역뿐만 아니라 도구 및 기계의 효율성을 향상시키는 데 사용할 수 있다. 금속은 강도, 내구성, 피로강도 및 재활용성과 같은 특성으로 인해 제일 중요한 엔지니어링 재료 중 하나이다. 직접용착방식(DED)은 금속 적층 제조(AM) 공정 중 하나이다. 공급방식에 따라 DED는 분말 및 와이어 공급 유형으로 나눌 수 있다. DED는 복잡한 가하학 객체 및 기능성재료를 생성하는 데 사용할 수 있으며 수리 및 재제조 목적으로 또한 사용할 수 있다. 다만, 증착공정 과정에서 금속의 급속 가열 및 냉각으로 인한 고온 구배는 잔류응력, 디스토션 및 편향과 같은 바람직하지 않은 효과가 발생한다. DED로 고품질 부품을 제조하려면 적절한 증착공정 전략에 대한 지식이 요구된다. 본고에서는 최적의 증착공정 매개변수를 찾기 위한 다양한 증착공정 전략을 조사하도록 수치 분석 방법이 제안된다. 유한 요소 해석(FEA)은 수많은 실험을 수

행하는 데 필요한 비용과 시간을 줄이는 데 도움이 될 수 있다. 따라서 적절한 증착 전략에 대한 정보를 얻으려면 다양한 증착공정 매개 변수에 대한 조사가 요구된다.

본 논문의 목적은 증착된 부품의 품질을 향상시키는 방법을 모색하기 위해 DED 공정을 분석하여 다양한 증착 전략의 효과를 평가하는 것이다. 온도 이력 제어는 DED에 의해 제조된 부푸의 품질 및 기계적 성질을 향상시키는 것은 제일 중요한 방법론 중 하나이다. DED의 공종 중에서 온도를 제어하는 방법 중 하나는 서로 다른 스캐닝 패턴을 적용하는 것이다. 스캐닝 패턴의 변경은 온도 이력의 변화로 이어지면서 그 결과 잔류 응력과 디스토션이 영향을 받게 된다. 증착 패턴은 부품의 기계적 성질, 표면 품질 및 밀도에 영향을 미칠 수 있다. 따라서 본고에서 다양한 증착 패턴에 대한 평가가 제안된다.

증착된 재료의 모양은 잔류 응력에 영향을 미칠 수 있으며, 더욱 중요한 것은 외팔 보 모양 기판의 경우 디스토션 및 편향에 영향을 줄 수 있다. 이러한 효과의 조사는 증착된 모양에 따른 기판의 요구 사항과 관련하여 통찰력을 제공할 수 있다. 또한, 이 정보는 증착된 부품의 고장 혹은 사용불능 상태를 방지하기 위해 추가적인 전처리 조치를 취해야 하는 경우에 대한 지침의 역할을 할 수 있다. 금속 부품의 후처리 열-기계적 특성을 평가하기 위해 캔틸레버 모양 기판에서 다양한 폭과 길이의 FEA와 증착된 영역의 높이를 분석하였다. 다음 단계에서 미리 선택된 적절한 증착 패턴은 얇은 벽 구조를 구축하기 위해 적용되었다. 결과는 지그재그 증착 전략에 의해 증착된 간단한 벽 구조의 증착과 비교되었다. 분석 결과는 Inconel 718 분말이 AISI 1045 기판 위에 증착될 때 선택된 증착 패턴이 장류 응력과 변위를 향상시킬 수 있음을 보여주었다. 단, SCM 440 기판에 증착된 G6분말의 경우 적절한 증착 패턴은 유효 및 1차 주응력을 줄이는 데 도움이 되었지만 기판의 변위 개선에는 실패하였다.

I. INTRODUCTION

A. Research Backgrounds

1. Additive Manufacturing Technology

Additive manufacturing (AM) is a process of building 3D objects by adding material based on computer aided design (CAD) model[1]. This is in contrast with traditional manufacturing processes where material is subtracted to produce a part, AM techniques rely on the process of continuously adding material layer by layer in order to fabricate tools and components[2]. Major applications of AM are prototyping (rapid prototyping), end user products, and tools like dies and molds which are used for mass production of parts (rapid tooling) [2].

Prototyping. At first AM was used in order to create prototypes for visual aids and as a presentation models[3]. Prototyping is very compelling application, as 3D representations help people understand design of the object better compared to 2D models[3]. With improvement of material properties, parts build by AM started to be used in functional models and for assembly, eventually this brought AM to be a part of long phase of prototyping[3]. AM build prototypes became irreplaceable part of product development cycle after new AM systems were developed, which were office friendly and cost efficient. Even today, many engineering companies use rapid prototyping technology as standard of product development[3].

Tooling. Another type of application which has wide range of uses is manufacturing of patterns, dies and other equipment for tooling. For long time, production of investment castings was aided by AM[3]. Production of urethane castings using silicone rubber is another area where AM patterns were widely applied. These castings produced by AM patterns were mainly utilized as prototypes, however sometimes they were also used as a final component. Additionally, AM patterns were applied for sand castings. Dies with conformal cooling is the area where AM

showed superiority over conventional manufacturing processes.

End user products. The most rapidly growing area where AM is used is direct manufacturing of end use products[3]. This is in contrast to other applications such as prototyping and tooling where AM is used as one of the steps towards manufacturing ready to use products. This application showed outstanding growth with the increase from 3% to 20% between 2003 and 2010 years[3]. Improved material properties, increased understanding of potential of AM and decreasing cost have all contributed to surge in direct manufacturing of parts.

Repair and remanufacturing. Application of AM is growing quickly in the area of repair and remanufacturing especially in the cases where longer lead time or high cost is associated with replacement of broken part by new product[4]. The capability of AM to repair part to near net shape is extremely advantageous compared to manufacturing of new parts primarily in case of large components which are damaged in small areas[5]. In addition, AM is superior to traditional repair techniques and can be applied in cases where traditional repair approaches not suitable. Moreover, utilization of AM for repair application creates metallurgical bond between base and repair material and reduces heat affected zone (HAZ) considerably[3]. Hence, AM creates very strong bond with reduced residual stress and distortion which is why AM is a perfect solution for repair of metal parts highly sensitive towards distortion caused by high heat input[6].

According to American Society for Testing Materials (ASTM) there are total of seven categories of AM which include: directed energy deposition (DED), powder bed fusion (PBF), sheet lamination, material jetting, binder jetting, material extrusion and vat polymerization[1].

DED is a metal AM process which uses high heat sours to melt material as it is being supplied. Material is supplied in the form of powder or wire. DED is a promising metal AM process which can be used to create large parts with complex geometry and for repair and remanufacturing.

Powder bed fusion is metal AM process which selectively melts metal powder in powder bed layer by layer. Electron beam and laser can be used as a heat source. After each layer the powder bead is moving downward by a specified distance and powder roller is spreading metal powder

over previously melted layer. When electron beam power source is applied the manufacturing process is performed in vacuum environment.

Sheet lamination AM process can be divided into two types according to bonding process: ultrasonic additive manufacturing (UAM) and laminated object manufacturing (LOM). Metal sheets are bonded by ultrasonic welding in UAM. Various metals can be used in this process to create complex three-dimensional parts. While in LOM process paper sheets and glue are utilized to create 3D objects, primarily fashionable and visually appealing.

Material jetting process performed in similar conventional two-dimensional ink jet printer. The jetting or deposition is performed by continuous or drop on demand method. Material ejection onto the building platform is performed by moving nozzle. Photo curable polymers and waxes typically used in material jetting process. After deposition of the layer it is hardened by UV light and next layer is applied. Polymers and waxes are ideal for the process due to their physical properties such as thick nature and capability to form droplets.

Binder jetting process consist of alternating deposition of two materials onto the build platform. The main material which is base material of manufactured part is used in the form of powder while the binding material is in the form of liquid. Binding material is applied between powder layers in order to bind powder material.

In material extrusion technology the material is drown from the nozzle and heat is applied with the following deposition process. During the process nozzle can move in two dimensions over the build table while the building table moves up and down. Similarly, to other AM processes the part build layer by layer. The strength of deposited layers can be improved by temperature control.

Vat photopolymerization involves fabrication of the three-dimensional model layer by layer from a vat of liquid photo curable polymers. Typically, UV light is utilized in order to selectively irradiate photopolymers inducing complex chemical reactions which results in polymers hardening. Support structure is required due to the nature of the process which involves moving

the hardened part downwards after curing of each successive layer.

AM has shown incredible growth on the past three decades[7]. Commercial development and investigation of AM begun since 1980s[7]. Such incredibly rapid growth of AM became possible due to development of AM technologies and materials for use by AM driven by market factor which had necessities for its use such as growing demand for personalized goods, decreased cycles of product development, reduction of lead times and cost of manufacturing[8]. New techniques and methods in AM were developed and implemented during past decade and applied in areas such as aerospace, automotive and biomedical[7]. Developed techniques in AM include fused deposition modeling (FDM), stereolithography (SLA), laser metal deposition (LMD), selective laser sintering (SLS), laminated object manufacturing (LOM) and three-dimensional printing (3DP)[7]. Table 1 shows additive manufacturing technologies names and names of companies that invented them, including purpose of technology and materials used. Due to development in precision of AM machines, variety of available materials and mechanical properties close to other manufacturing processes, AM reached sophisticated level, hence AM

Table 1 Additive manufacturing technology summary[3]

Technology	Manufacturing Companies	Materials	Usage
Material extrusion	3D Systems, Solidscape	Polymers	Prototyping
Binder Jetting	ExOne, Voxeljet, 3D Systems	Metals, Polymers and Foundry stand	Casting Molds, Prototyping and Direct manufacturing
Sheet lamination	Mcor, Fabrisonic	Metals and Paper	Direct manufacturing and Prototyping
Vat Photopolymerization	Envisiontec, 3D Systems	Photopolymers	Prototyping
Directed Energy Deposition	POM, Optomec	Metals	Direct manufacturing and Repair
Powder Bed Fusion	3D Systems, Arcam	Metals and Poymmers	Prototyping and Direct manufacturing
Material Jetting	3D Systems, Object	Polymers and Waxes	Casting patterns and Prototyping

has a potential to position itself as a new manufacturing standard. The main goal of AM is to manufacture final functional tool or component by combining advantages of prototyping and engineering design[9].

2. Design for Additive Manufacturing

Capabilities of AM include manufacturing of complex of geometry, functionality, personalization of products and mass customization[10]. In light of these unique characteristics of AM the difficulty for engineers and designers is assuring AM technologies production capabilities and cost of manufacturing in order to build high quality products.

Advantages of AM in freedom of design and material creates huge number of possibilities. However, due to manufacturability limitations of AM at its current state not all designs can be produced in cost efficient manner which includes hanging features, small poles, overhang structures, thin walls, small holes and slots[11]. The fact worth mentioning is that limitations of AM depend on AM process. Investigation of limitations and capabilities of AM can help engineers and designers to develop parts suitable for production by AM technologies[12]. The three main objectives of design for additive manufacturing (DfAM): 1) provide set of guidelines and procedures and ensure them to be within the limitations and constraints of manufacturing processes, 2) improve quality of the product through evaluation of design techniques on manufacturing process, 3) establish relationships between design and manufacturing process[12]. As far as design and usability of the part is concerned DfAM can be classified into five groups: 1) geometry of the part, 2) part consolidation, 3) materials, 4) support structure, 5) sustainability[13].

Geometry. AM can be used to create high aesthetic, economic and functional parts due to its capabilities to fabricate freeform geometry. One of the most useful features of AM in industrial applications is ability to produce complex internal features of fabricated parts, such as pathways to improve acoustic dumping, micro-vanes for ocular medical devices, integrated air ducts and

mentioned earlier, conformal cooling channels which are the most extensively used feature produced by AM[4,7,13].
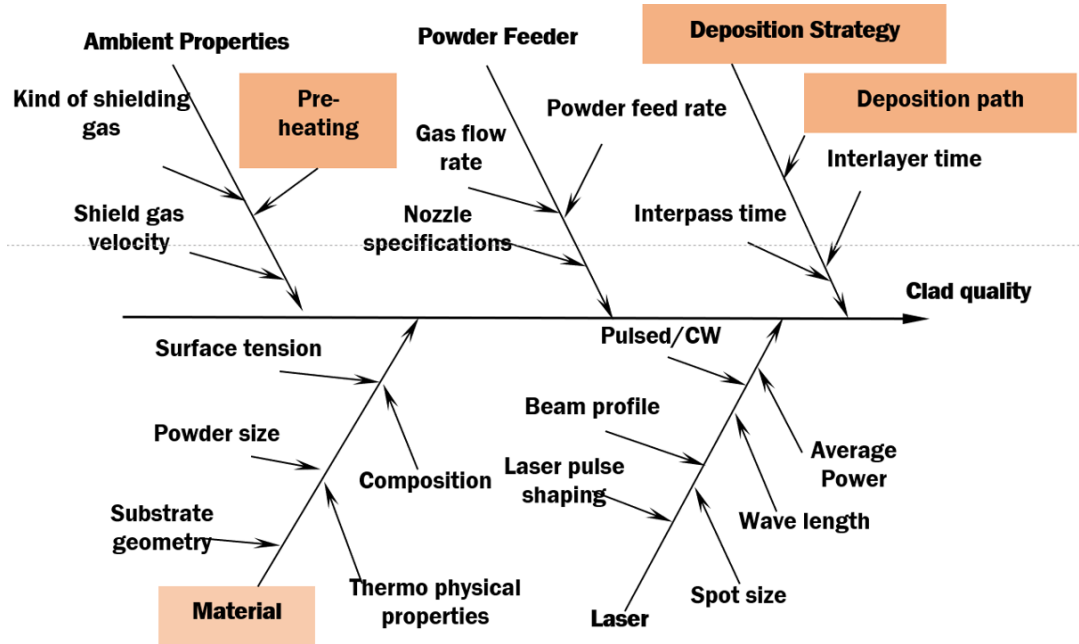
Fig. 1 Process parameters of DED[7)]

Part consolidation. Part consolidation is a prominent strategy of reducing the number of parts in the design through design simplification. The main goal of this approach is to enhance performance and at the same time reduce weight and manufacturing cost. This has become possible due to capability of AM of free form fabrication and freedom to distribute material as required which made possible reduction of number of parts of design[7)]. Researches and industries showed great motivation in investigation and applying this feature of AM for design innovation[14)]. Well known example of part which is also the first reported case of part consolidation using AM is redesign of aircraft duct[4)]. When conventional manufacturing processes were used a total of 16 part were required to complete fabrication of aircraft duct but only one part was required when part consolidation by AM was used[4)]. Another example, General Electric consolidated helicopter

engine from 900 parts, including fasteners, down to just 14. Moreover, the weight of new design is reduced by around 40% and cost by 60%[7].

Materials. Large number of materials is already used in order to manufacture parts by AM and research of developing these materials as well as development of new materials is in progress[7]. Currently, different types of materials are applied, including metals, ceramics, polymers and etc. Metal AM offers high growth potential. AM technology can be used to create a variety of metals and alloys, including stainless steel, titanium, nick el and aluminum alloys[7]. Versatility and simplicity of use in 3D applications made polymers and their composites the most widely used materials in AM industry[7]. In addition, AM developed into fundamental technology for the production of sophisticated materials such as ceramics.

Support structure. During manufacturing process by AM, the part undergoes multiple states in which it can be affected by a number of different forces, including residual forces and in case of overhang structures gravitational forces and etc. and supporting structures become increasingly important. To mitigate the negative effect of these forces on quality, accuracy, strength of the part, various methods are employed such as positioning the part in such a way that it does not require any support during deposition process, designing self-supporting parts e.g. parts that do not require support and incorporation of support structure[7].

Sustainability. Optimization of design in such way that it has positive economic and social effect while negative impact on environment is minimized[7]. AM has capabilities to create goods that are both economically and environmentally sustainable. Fabrication of lasting products, employing recyclable and recycled materials, applying highly efficient production technologies, minimization or elimination of usage of hazardous materials and establishing good relationships between consumers and goods are all part of sustainable applications of AM[7].

Apart from the design prospective, aspects of DfAM directly related to design and functionality of the part, another area of researches based on improvement of quality of goods produced by AM. Examples include surface finish, durability, strength, accuracy and etc. These

attributes of parts fabricated by AM require different approaches of investigation and are referred to as deposition strategies. Numerous process parameters can affect the quality of deposition, as shown on the Fig. 1[7]. Each process parameter can affect quality of deposition. One example is deposition path. Every type of AM technology except sheet lamination requires deposition path for fabrication of 3D objects[15]. Deposition path has direct relation to dimensional accuracy, surface roughness and mechanical properties of the fabricated part, hence path planning is crucial in AM[15]. Moreover, different deposition path means different movement of the moving table or the print head which affects completion time of deposition[15]. As a result, effective path planning can result in better quality of manufactured part or shorter production time[15].

3. Directed Energy Deposition

Number of metal AM processes were developed after patent of SLS 1986 by Professor Joseph Beaman and Carl Deakard including DED, PBF, SL and other processes[16]. Laser and electron

(a) Co-axial material supply system   (b) Off-axial material supply system
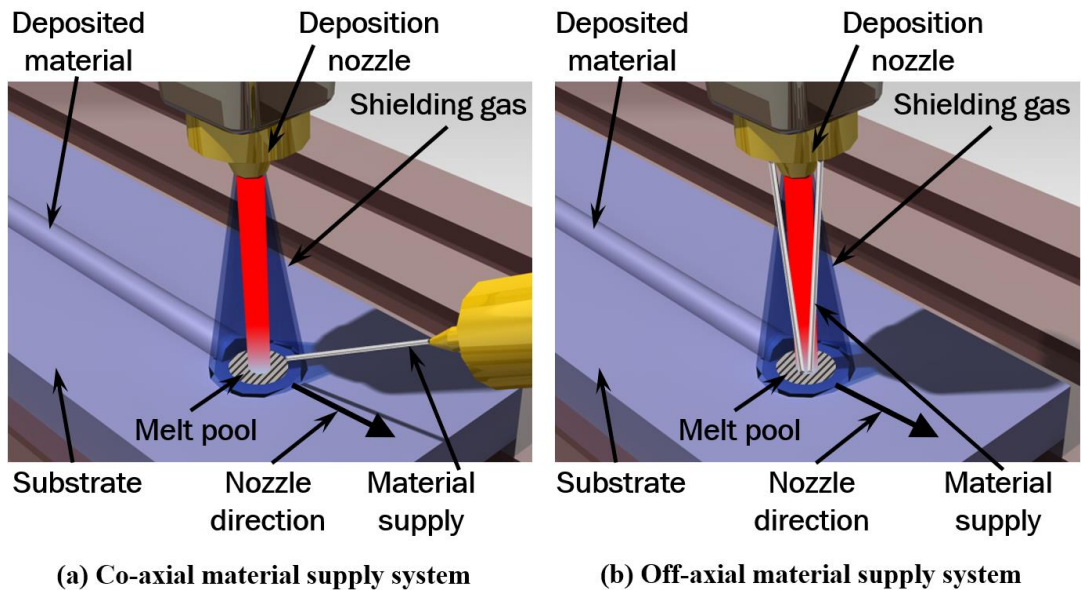
Fig. 2 DED process scheme

beam heat source can be used for melting metal powder during PBF and three processes can be distinguished which are selective laser melting (SLM), direct metal laser sintering (DMLS) and electron beam melting (EBM)[4]. Metal AM processes including DED and PBF were academically researched, used in industrial applications as well as commercially[16]. When DED compared to PBF, DED shows higher build rate and volume density while finer surface finish and lower thickness of the layers is attributed to PBF process[16]. In DED metal powder or wire is supplied to the surface of the substrate or previously deposited layer and simultaneously melted by high intensity heat source creating a pool of molten material upon solidification of which deposition bead is created. Fig. 2 shows schematics of DED process. PBF uses laser or electron beam to selectively melt powder in powder bed. DED process can be used to deposit material over even and uneven surface along the arbitrary trajectory which makes it excellent solution for deposition of complex shapes as well as being used in repair and remanufacturing, unlike PBF[17]. Some DED systems were developed with multiple powder or wire feeding supply systems which made possible to produce parts with heterogeneous properties by depositing different materials in sequence as well as combining them[16, 17]. This resulted in substantial rise in research and development of DED technology over the past years.

According to the material supply system DED feedstock can be classified as powder and wire feeding types[16]. Heat source in powder feeding type DED is a laser, while wire feeding type

Table 2 DED process nozzle types[4]

Feeding Type	Feeder axis type	Energy source	Deposition Method	Process
Powders	Co-axial and off-axis (lateral) feeding	Laser (CO_2, Nd:YAG,etc.)	Cladding	LAM-DED
Wire	Co-axial and off-axis (lateral) feeding	Electric arc	Welding	WAAM
		Plasma arc	Welding	
		Laser	Cladding and Welding	WLAM
		Electron beam	Welding	WEAM

Table 3 DED process summary[4]

Technology	Laser Engineering Net Shaping	WLAM	WAAM
Feeding type	Powder	Wire	Wire
Layer thickness (μm)	100-380	>1000	1000-2000
Material deposition rate (g/min)	6.5	1.5-48.0	16.7-66.7

DED can utilize electron beam, laser, plasma arc or electric arc[16]. Feedstock delivery system with regards to feeding process can be classified into two types which are co-axial and lateral supply technologies[16]. Powder feeding type DED which uses laser as a heat source is called a laser additive manufacturing (LAM) – DED[17]. In case of wire DED, it can be classified into three types depending on energy source used which are electron beam (WEAM), arc (WAAM) and laser (WLAM) [16]. Energy density primarily depends on heat source type and is 10^4, 10^6, 10^8 W/mm^2 for arc, laser and electron beam, respectively[18]. WEAM. WAAM and LAM-DED utilizes inert gas shielding during deposition process to protect molten pool from oxidation, while WEAM is performed in the vacuum chamber[18]. Among four of these process WAAM system is the cheapest compared to other processes[18]. The surface roughness of parts manufactured by LAM-DED is higher compared to WLAM process[4]. When build rate is compared wire feeding type has considerably higher build rates and layer thickness as well as greater residual stresses compared to powder feeding type DED[4].

B. Research Motivation

Parts produced by AM showed mechanical properties equivalent to wrought materials. In order to obtain required quality of deposition proper process parameters must be carefully chosen. Applying experimental techniques in order to characterize empirical data from experiment as a function of parameters is a common practice among researchers. However, experimental methodology is costly and requires a lot of time due to necessary adjustments including equipment set up and calibration of equipment, post processing and in some cases pre-processing of specimen, testing and measurements of experimental results. Numerical simulation of the deposition process in order to predict thermo-mechanical characteristics of manufactured part is cost and time efficient alternative[19, 20].

Number of studies have employed finite element analysis (FEA) for modeling deposition process by DED[21, 22]. In order to investigate post process parameters of DED three dimensional FEA models with boundary constraints and moving heat flux were utilized to simulate real DED process[23]. Continuous research and development of methods and techniques for FEA of DED process brought quiet good results in terms of accuracy and reliability[24]. Researches on heat source calibration as well as investigation of convective losses, both natural and forced were investigated and reported for several materials. The methodologies for proper estimation, assumption and simplifications were established by previous studies. Thus, the goal of this study by using these methods and techniques to further develop strategies and techniques for improved quality of deposition using FEA.

C. Previous Research Works

1. Finite Element Analysis of DED

Thermo-mechanical analysis is performed in two steps, first heat transfer analysis with the following mechanical analysis. The essential part of FEA is heat transfer analysis which simulates DED process by applying temperature field throughout deposition process by using moving heat source technique. Boundary conditions and deposition strategies are part of thermos-mechanical analysis. Heat transfer analysis is performed in order to obtain transient temperature field. These results are applied in mechanical analysis. Some similarities can be observed in terms of process characteristics between DED and welding technologies.

In 1999, Nickel at al. investigated the effects of powder feeding type shape deposition manufacturing process on distortion and residual stresses[25]. The project was developed in cooperation with Carnegie Mellon and Stanford Universities. However, in order to simplify the process, during analysis heat source was applied on the surface of the substrate without including material deposition.

In 2006, Mughal et al. used 3 dimensional FEA method to analyze GMAW based AM process, Temperature dependent properties of material and process of material addition were considered in the study[26]. Single layer deposition by different deposition strategies based on raster scanning pattern were analyzed to investigate residual stress distribution and distortion of the substrate. Deposition of seven rows of beads were considered in the analysis. For passive cooling during deposition process inter-pass time of one minute between rows was applied.

In 2006, Deus and Mazumder proposed FEA model for the deposition of a single track by laser cladding process which was performed in ABAQUS software. In their work, dilution model was applied in order to investigate the composition of materials during surface cladding of different materials of substrate and deposit[27]. They compared the effects of curved and planar

front melt on residual stress. It was estimated that stress is formed in the vicinity of the deposited region close to end of straight bead. According to their results added material to the front of melt pool induces small constraint in melt pool area, hence regardless of outline of melt front similar stress magnitude was observed.

In 2010, Chiumenti et al. performed FEA for fully coupled thermo-mechanical analysis on in-house finite element software[28]. In their analysis phase change phenomenon was considered and represented as a shrinkage effect and released latent heat during process. Shape metal deposition (SMD) AM process was used to deposit ten layer of Inconel 718 alloy with straight beads. The applied heat source model was calibrated depending on volume of feeding wire. Mechanical properties for solid, liquid and mushy state of the metal were considered in the analysis. Compared to experimental results the estimated results errors were in the range of 10% on average.

In 2011, Ding et al. applied a steady state Eulerian heat transfer analysis of WAAM process for deposition of large multi-layer clad[29]. Model was simplified such that elements are activated for the whole layer which results in smaller distortion magnitude when compared to sequential element activation method. When compared to conventional Lagrangian heat transfer analysis their technique is 80% faster.

In 2011, Zhang et al. used ANSYS FEA for thermo-mechanical analysis of pulsed laser powder deposition AM process for multi-bead deposition[30]. They defined cross-section of the bead through dimensions of bead width, length and area as well as wetting angle. In order to simulate pulsing laser effect, the elements in the layer with melting temperature as initial temperature were added during irradiation of each pulse on deposit.

In, Farahmand and Kovacevic used ANSYS software to design transient thermal elastic model to analyze multi-bead laser cladding through evaluation of temperature field and residual stress[31]. Laser heat source power distribution with top hat model was adopted for the study. The laser dimensions are 12 mm and 3 mm for width and length, respectively. In the proposed FEA

model latent heat and convection were incorporated and in case of temperature higher that melt pool temperature modified thermal conductivity and specific heat were applied. The results of the study showed increased residual stress for slower deposition speed after cooling process as a result of higher heat input.

In 2010, Crespo and Vilar performed thermo-mechanical analysis to investigate the effects of deposition speed and inter-layer cooling time during laser powder deposition process[32]. In their study they considered phase transformation of metals. According to their results, the inter-layer cooling time plays an important role for control over uniformity of grain distribution because proper inter-layer cooling can prevent excessive heat accumulation in the vicinity of deposited bead.

In 2016, Denlinger et al. investigated the effects of inter-layer cooling time for deposition of wall structure on thermo-mechanical characteristics of Inconel 625 and Ti-6Al-4V deposited by powder DED[33]. For the moving heat source Goldak double ellipsoidal laser distribution model was adopted. In the model conductive losses through the clamping fixtures was considered. In order to obtain agreement between analysis results and experimental results they applied zero stress to the model when temperature rise above relaxation temperature of the metals.

In 2018, Chua et al. investigated the effects of single layer deposition by wire DED process on thermo-mechanical characteristics depending on scan speed and power of laser using FEA software SYSWELD[20]. They estimated the hatch distance between beads in order to minimize residual stresses due to negative effects of heat affected zone (HAZ).

In 2018, Lee et al. used FEA in order to investigate effects of dwell time between layers on thermo-mechanical characteristics of Ti-6L-4Al deposited by wire feeding type laser metal deposition[34]. The point-concentrated heat source model was proposed to analyze deposition of the wall of ten layers using ABAQUS software. The dwell time was analyzed between 91s and 200 s and predicted results showed error in distortion near 37%.

2. Application of Inconel 718 & AISI 1045

AISI 1045 carbon steel was selected for substrate and Inconel 718 as a deposition powder. Inconel 718 is Ni-Cr-Fe based super alloy which became fundamental material of gas turbine applications since its invention in 1963[35]. Despite being considerably harder to process compared to stainless or carbon steel, it is has great level of forgeability among other super alloys and been used to fabricate rings, shells and structural components[35]. In addition, Inconel 718 properties such as ability to maintain its superior properties at elevated temperatures which made parts such as aircraft engines, nuclear parts, rockets manufactured of Inconel 718[4]. AISI is a medium carbon steel with good properties in terms of strength and toughness and can be easily heat treated to obtain required properties. The properties of AISI 1045 make it easy to work with to produce various parts but it is also easily affected when high heat is applied such as in welding or during metal AM deposition process. AISI 1045 is used to produce wide range of metal parts such as bolts, shafts, gears, axles, crankshafts and etc[4]. For the improved accuracy of the analysis temperature dependent properties of AISI 1045 were assigned to substrate material and for powder temperature dependent properties of Inconel 718. All six phases were considered in the analysis for AISI 1045 with the initial conditions of 75% ferrite and 25% pearlite phase, while only single phase was used in the analysis for Inconel 718.

3. Objective & Methodology

Finite element methods (FEM) for the investigation of thermos-mechanical characteristics of deposition process is still under development worldwide. After many years of research and development of thermo-mechanical analysis acceptable methodologies and techniques are estimated for acceptable results. Necessary simplifications such as rectangular cross-section of the bead for powder feeding type DED process are made. This gives results with error of acceptable range because the dimensions of bead cross-section for powder feeding type is very small compared to wire feeding type DED process. For more accurate results volumetric heat source is required which is essential for proper bead melting process simulation. Gaussian volumetric heat flux distribution and Goldak double ellipsoidal heat flux distribution are numerical representation of heat source which is usually applied. Due to high number of unknown variables which required adjustment researches around the world before they can start calibration of the heat source model must assume efficiency and distribution of heat flux. After years of research method to quantify acceptable range of error was proposed[24]. In addition, the effect of different process parameters such as nozzle speed influence on the heat flux was investigated too[24]. Several researches proposed methods to estimate heat losses due to free and forced convection in order to improve the accuracy of the results. Based on previous investigations and research methods to estimate effects of various process parameters on thermal and mechanical characteristics of DED process using FEA farther investigation and development of DED process is required. In other words, systematic investigation of shape of deposition as well as effect of deposition strategies is required for the continuous development of FEA models for DED technology.

The main goal of this thesis is to propose method for development of FEA model for powder DED process. The flowchart of research work is shown in Fig. 3. It includes, firstly estimate various parameters for improved accuracy of the analysis based on previous researches
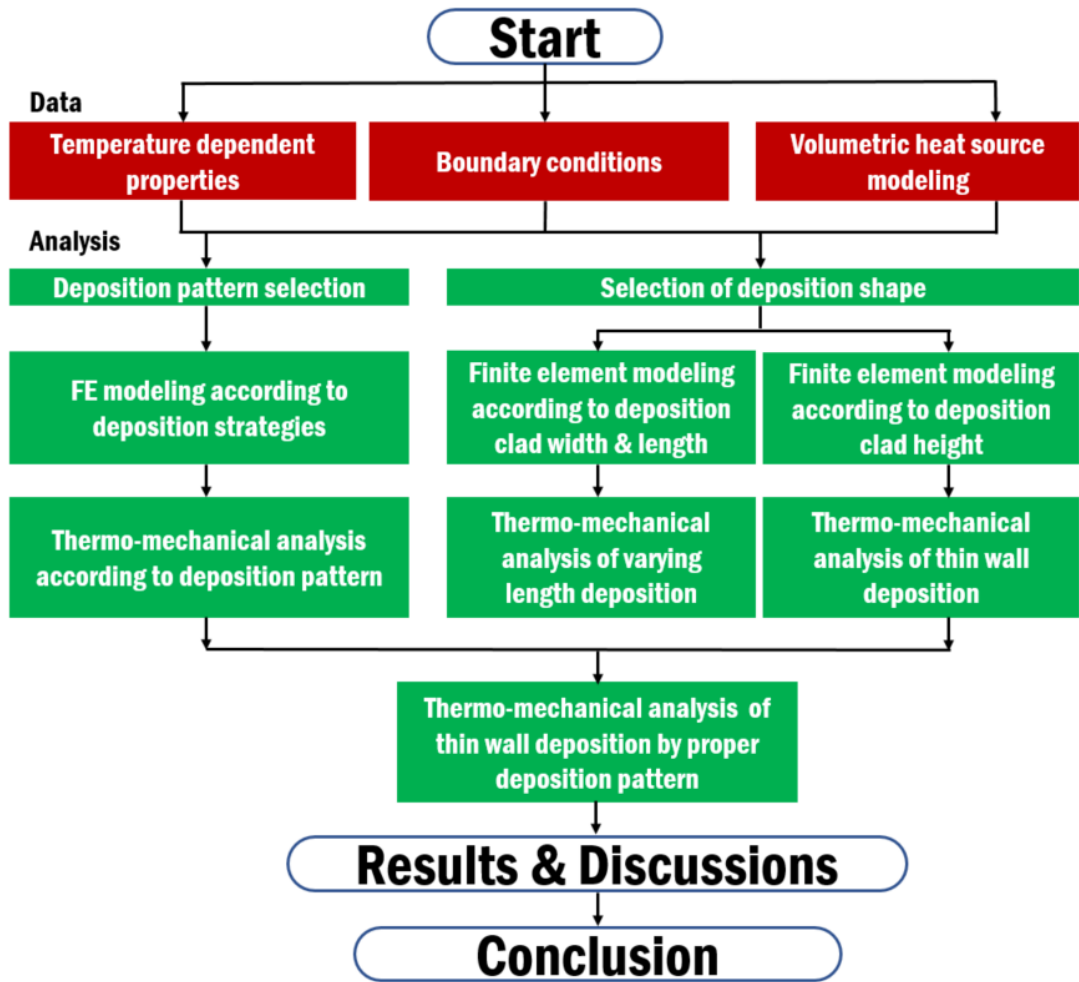
Fig. 3 Flow chart of research work

methodologies and data. In particular, methods of estimation volumetric heat flux parameters, heat losses due to natural convection and due to forced convection, bead height and width and layer thickness. Using necessary assumptions and estimated data the effects of shape of deposited bead, deposition path and pre-heating effects on thermos-mechanical characteristics of Inconel 718 powder deposited on AISI 1045 substrate are investigated in this study.

In Chapter 2, the methodology to investigate the effects of deposition shape on thermos-mechanical characteristics in the vicinity of the deposited bead are estimated. In particular, the

effects of various width and length of deposition. The power of laser, travel speed of heat source and efficiency of the heat source are same for all cases. In Chapter 3 the effects of deposition path are analyzed in terms of HAZ, residual stress distribution and magnitude and distortion evaluation. The best deposition path with uniform stress distribution, comparatively low maximum stresses, lower distortion and lower twisting effect are selected. In Chapter 4, different pre-heating temperatures are applied on the selected deposition paths in order to reduce temperature gradient during deposition and reduce undesired effects of deposition process such as stress and distortion.

II.　THERMO-MECHANICAL CHARACTERISTICS IN THE VICINITY OF DEPOSITED REGION ACCORDING TO DEPOSITION STRATEGIES

A.　Deposition Strategies and Related Works

AM can be described as a key manufacturing process of industrial revolution 4.0 because it has necessary functions and capabilities which satisfy IE standards such as ability to manufacture completely customizable and personalized goods with complex shape, functionality and reduced energy consumption and waste[42, 43]. However, AM still has a long way to go until it can become major manufacturing process and replace conventional manufacturing processes. This is because the quality of parts manufactured by AM still need a lot of improvements such as surface finish, mechanical properties and accuracy. If proper process parameters and settings are used powder DED can be used to fabricate parts with high quality and ready to use with minimal post processing. However, a lot of research and development is required in order to obtain information about right deposition properties to satisfy the needs of majority of industrial applications. The major problems of parts produced by DED are stress and distortion. The high heat flux applied during deposition process causes negative effects such as residual stress due to high temperature gradients across the part[44].

In order to reduce time required for multiple experiments FEA methods can be used to evaluate and estimate the results of the effects of various process parameters. One of the methods to improve the quality of the deposited part is to modify temperature histories which can be accomplished by changing deposition path. Thus, study on deposition path can help to improve the properties of deposited parts. However, currently majority of researches related to investigation of process parameters of DED are about single bead deposition and only some of

the researchers analyzed deposition of complex geometry with various scanning patterns[36].

In 2002, Dai and Shaw numerically investigated the effects of deposition strategies on residual stress and distortion using ANSYS software for the case of zig-zag and offset out deposition strategies[45]. They used simplified model which did not include expansion and shrinkage of the material due to temperature changes and in simplified model convection in the molten pool was not considered.

In 2014, Parisa et al. studied the effects of high-power direct diode laser cladding process on fabricated part in terms of residual stress and distortion, molten pool size, temperature and stress-strain fields[56]. In order to analyze single and multi-bead deposition three-dimensional FEA model was developed for uncoupled transient heat transfer and plastic-elastic model and experimentally validated with predicted error around 3.5%.

In 2018, Lei et al. proposed three-dimensional FEA model with simplified clamping fixture of substrate[47]. The model was experimentally calibrated and applied for the analysis of thin wall deposition using direct laser deposition process. Various volumetric heat flux models based on Gaussian distribution were applied in order to find strategy for reducing residual stress.

In 2019, Ren et al. performed thermo-mechanical analysis of deposition process by laser aided AM process to investigate the effect of deposition patterns on temperature evolution and its effects on residual stress and distortion for single layer deposition process[36]. The element activation technique and Gaussian heat flux moving heat source were applied using MATLAB and COMSOL software.

In 2021, Kim et al. investigated various deposition patterns for LENS process for small volume deposition and selected best deposition strategies for FEA of large volume deposition[48]. In addition, they investigated the effects of pre-heating. Their results have shown that proper deposition pattern combined with pre-heating can greatly reduce residual stress.

The goal of this study is to apply the knowledge from previous studies in order further contribute for farther development of FEA methods for analyses of residual stresses and

distortion when powder DED is applied. The evaluated deposition patterns are based on raster and zig-zag deposition strategies. These strategies were selected due to their robustness and simplicity to use on any geometry.

B. Thermo-Mechanical Analysis

1. Heat Source

Because thermo-mechanical analysis depend on temperature history heat source model is highly important for the accuracy of the thermo-mechanical FEA simulation. For this study conical Gaussian heat source was adopted, as shown in Fig. 3[39].

The real laser beam heat flux distribution is very close to Gaussian distribution as shown in Fig. 4. The highest power density is at the center of the beam and it exponentially decreases away from the center. At any plane perpendicular to z-axis within the effective penetration depth or "keyhole" heat flux can be described by Equation (1) [39]:

$$Q(x, y, z) = Q_0 * \exp\left(\frac{-cr^2}{r_z}\right) \tag{1}$$

$$r = \sqrt{x^2 + y^2} \tag{2}$$

$$r_z = r_{e+}\frac{r_i - r_e}{z_i - z_e}(z - z_e) \tag{3}$$

Where, $Q(x, y, z)$ is volumetric heat flux at any point within heat source volume. Q_0 is the maximum heat flux density at the center of the beam, r is distance from the center of the beam, r_i is conical source radius at any depth which reduces linearly. r_e, r_i are "keyhole" top and bottom radius, respectively and z_e and z_i are top and bottom coordinates of heat source,

respectively. c is a shape factor and x, y, z are coordinates.

Q_0 can be expressed by energy conservation Equation (4)[39]:

$$Q_0 = \frac{3P}{\pi\delta(r_i^2 + r_i*r_e + r_e^2)} \tag{4}$$

Where P, δ are laser power and penetration depth of heat source, respectively. Volumetric heat flux is estimated by Equation (5) [39]:

$$Q(x, y, z) = \eta * \frac{3P}{\pi\delta(r_i^2 + r_i*r_e + r_e^2)} * exp\left(-\frac{(x-vt)^2 + y^2}{c*(r_e + \frac{r_i - r_e}{z_i - z_e}(z - z_e))}\right) \tag{5}$$

Where, η is the efficiency of laser deposition process which attributes to losses related to material evaporation, reflection of laser rays and other physical phenomenon.
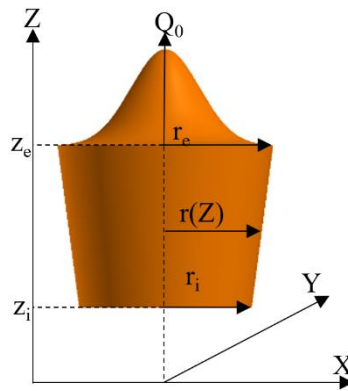
Fig. 4 Heat source model

2. Heat Loss

During DED process surface temperature varies across surfaces of the specimen. The buoyancy of air causes variation of natural convection depending on surface temperature[24]. In addition, inert gas, which is Argon is this case study, is applied during deposition process to protect melt pool from oxidation. For more accurate results of the simulation which includes long cooling process until the part is in steady state conditions it is necessary to define proper cooling conditions. The average coefficient of natural convection (h_{conv}) based on temperature dependent properties of Argon and Air was implemented into the model as shown in Fig. 5. It was estimated by Equation (6) [24]:

$$h_{conv} = \frac{Nu_L \cdot k}{L_c} \tag{6}$$

Where, Nu_L , k and L_c are average Nusselt number, thermal conductivity of gas and the characteristics length of the specimen, respectively.

Depending on surface orientation average Nusselt number is determined by Equations. (7-9) [24]:

$$Nu_L = 0.54 Ra_L^{1/4} \quad (10^4 \leq Ra_L \leq 10^7, \mathrm{Pr} \geq 0.7) \text{ for top surface} \tag{7}$$

$$Nu_L = 0.52 Ra_L^{1/5} \quad (10^4 \leq Ra_L \leq 10^9, \mathrm{Pr} \geq 0.7) \text{ for bottom surface} \tag{8}$$

$$Nu_L = 0.68 + \left(\frac{0.6704 Ra_L^{1/4}}{(1+(0.492/Pr)^{9/16})^{4/9}} \right) \quad (Ra_L \leq 10^9) \text{for vertical surfaces} \tag{9}$$

Where, Pr, is Prandtl number and Ra_L is Rayleigh number.

The air temperature (T_f) and Rayleigh number can be obtained from Equations (10-11) [24]:
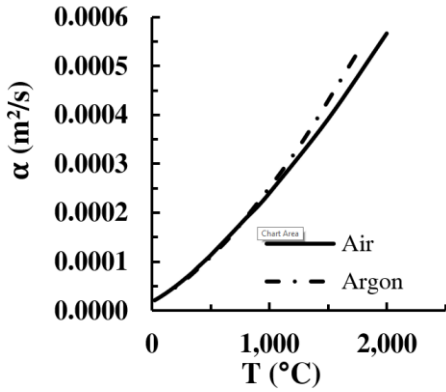
(a) Thermal diffusivity
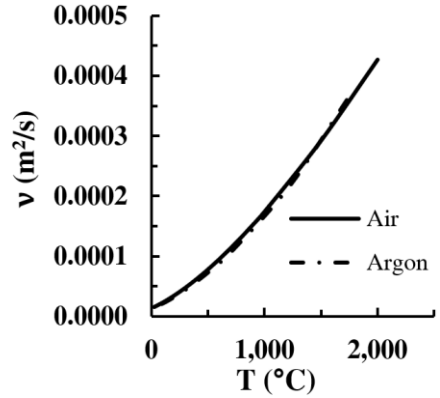
(b) Kinematic viscosity
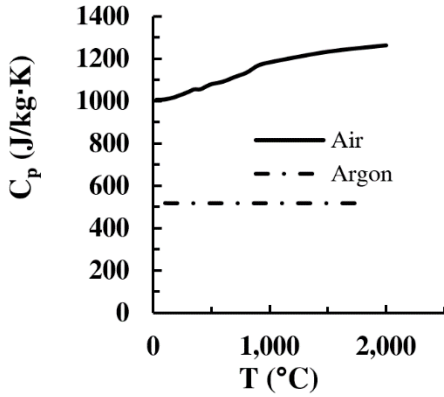
(c) Specific heat
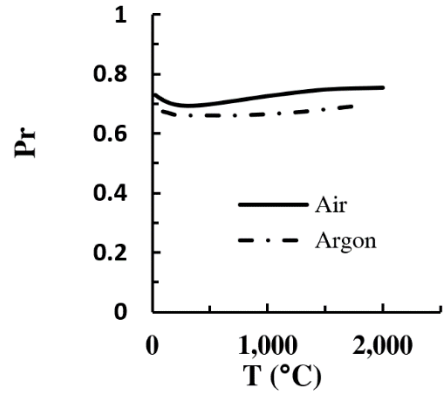
(d) Prandtl number
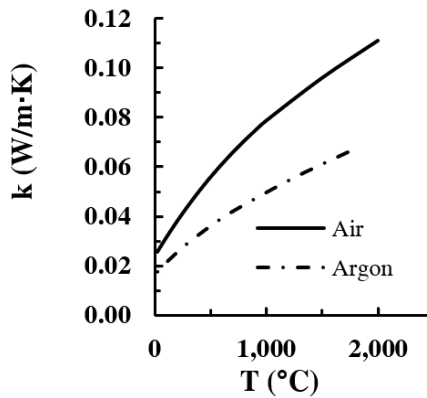
(e) Thermal conductivity

Fig. 5 Thermo-physical Properties of Air and Argon[24]
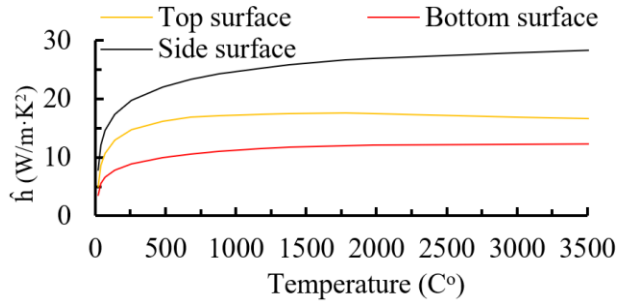
Fig. 6 Equivalent Heat Loss from Different Surfaces of the Model

$$Ra_L = \frac{g(T_s - T_\infty)L_c^3}{\nu_k \cdot \alpha \cdot T_f} \tag{10}$$

$$T_f = \frac{(T_s + T_\infty)}{2} \tag{11}$$

Where $g, T_s, T_\infty, \nu_k, \alpha$ are gravitational acceleration, temperature of the surface, ambient temperature, kinematic viscosity and thermal diffusivity of air, respectively. The calculated average coefficient of natural convection for top, bottom and vertical surfaces is plotted in Fig. 6.

For Argon shielding applied during DED process first should be determined if forced convection should be considered in FEA model which can be accomplished by relation between buoyancy to inertial forces which must be less than one (eq. 12) [24]:

$$\frac{Gr_L}{Re_L} < 1 \tag{12}$$

Where Gr_L is Grashof number and Re_L is Reynolds number. This relation is estimated based on melting temperature of AISI 1045 to determine applicability of forced convection effect at the melt pool. Grashof and Reynolds numbers can be determined by Equations (13-14) [24]:

$$Gr_L = \frac{g\beta(T_s - T_\infty)L_c^3}{\nu_k^2} \tag{13}$$

$$Re_L = \frac{V_f D}{\nu_k} \tag{14}$$

Where, β is thermal expansion coefficient of gas and V_f is velocity of gas.

Based on results from Equation (12) Argon shielding causes forced convection. Average Nusselt number for impinging jet can be determined from Equation (15-16) which is estimated from empirical correlation for the blow from single round nozzle, as shown in Fig. 7[24].

$$Nu_L = Pr^{0.42} \left(\frac{2A_r^{0.5}(1 - 2.2A_r^{0.5})}{1 + 0.2\left(\frac{H}{D} - 6\right)A_r^{0.5}} \right) (2Re^{0.5}(1 + 0.005Re^{0.55})^{0.5}) \tag{15}$$

$$A_r = \frac{D^2}{4R^2} \tag{16}$$

Where A_r, H, D, R are nozzle area, distance from nozzle to impingement surface, nozzle diameter, and distance from stagnation point, respectively.

By substituting temperature dependent material properties into Fourier's heat transfer equation thermal history or temperatures (T) at (x, y, z, t) were obtained in FEA of transient heat conduction (eq. 17) [24]:

$$\frac{\partial}{\partial x}\left(k(T)\frac{\partial T}{\partial x}\right) + \frac{\partial}{\partial y}\left(k(T)\frac{\partial T}{\partial y}\right) + \frac{\partial}{\partial z}\left(k(T)\frac{\partial T}{\partial z}\right) + Q(x, y, z, t) = \rho(T)C_p(T)\frac{\partial T}{\partial t} \tag{17}$$

Where, $Q(x, y, z, t)$ is heat input, t is time and $\rho(T), C_p(T), k(T)$ are temperature dependent density, specific heat and thermal conductivity of the material, respectively.

Ambient temperature was set to be 20°C and initial temperature of the model is the same as

ambient. Heat dissipation from the model to the environment was considered from all the open surfaces and beads. Convective losses were estimated by Newton's Law of cooling Equation (18) [24]:

$$q_{conv}^{"} = h_{conv}(T_s - T_\infty) \tag{18}$$

Where, $q_{conv}^{"}$ is convective loss, T_s and T_∞ are surface temperature and ambient temperature, respectively.

Radiative losses ($q_{rad}^{"}$) were calculated by Stefan-Boltzmann law (eq. 19) [24]:

$$q_{rad}^{"} = \varepsilon\sigma_s(T_s^4 - T_\infty^4) \tag{19}$$

Where, ε is emissivity of the material and σ_s is Stefan-Boltzmann constant which has a value of $5.670*10^{-8}$ W/m/K^4. Equation (19) can be rewritten and represented by the Newton's law of cooling Equation (20) [24]:

$$q_{rad}^{"} = h_{rad}(T_s - T_\infty) \tag{20}$$

The radiation coefficient h_{rad} can be calculated by Equation (21) [24]:

$$h_{rad} = \varepsilon\sigma_s(T_s^2 + T_\infty^2)(T_s + T_\infty) \tag{21}$$

For better efficiency of FEA analysis combined losses ($q_{loss}^{"}$) from convection and radiation can be interpreted into single Equation (22) [24]:

$$q_{loss}^{"} = (h_{conv} + h_{rad})(T_s - T_\infty) \tag{22}$$
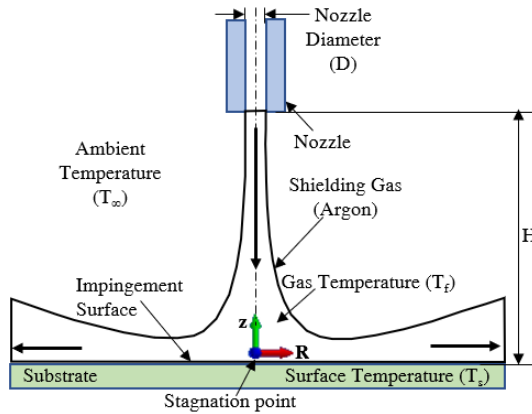
Fig. 7 Schematic representation of forced convection from a single nozzle[24]

C. Effect of Deposition Strategies on Inconel 718 Powder Deposited on AISI 1045 Substrate

3. Material Properties

In order improve accuracy of the analysis temperature dependent properties of Inconel 718 were assigned to the bead material and properties of AISI 1045 to the substrate. The data was obtained from commercial software SysWeld and JmatPro[40, 41]. The graphs on the Fig. 8 and 9 are showing temperature dependent conductivity, specific heat, yield strength, modulus of elasticity and Poison's ratio. In case of Inconel 718 single phase was assumed while all six phases were considered for AISI 1045. Initial conditions of AISI 1045 are 25% Pearlite and 75% Ferrite phases. Chemical composition of AISI 1045 and Inconel 718 are shown in the Table 4.

Table 4 Chemical composition of AISI 1045 and Inconel 718

Material	Fe	C	Si	Ni	Cr	Mn	Cu	Mo	Other
AISI 1045	Balance	0.444	0.247	0.005	0.015	0.757	0.01	0	≤ 0.1
Inc. 718	Balance	0.08	0.35	50	19	1.15	0	3.05	0
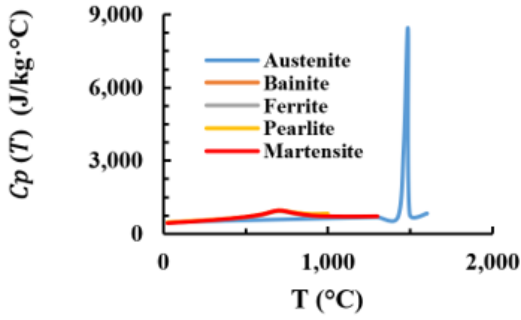
(a) Specific heat
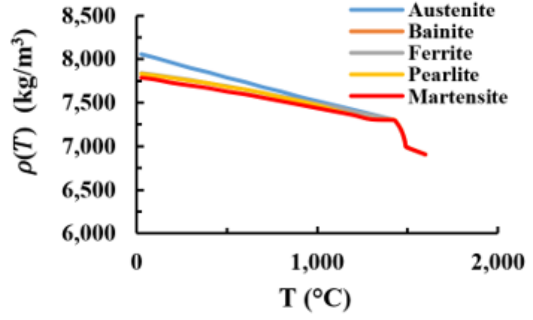
(b) Density
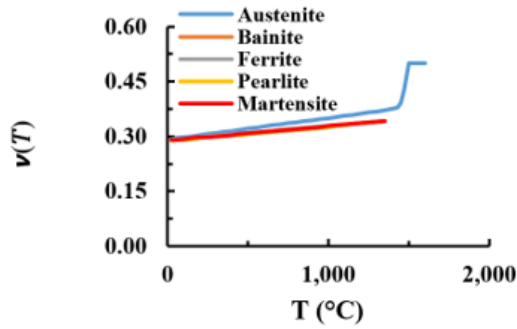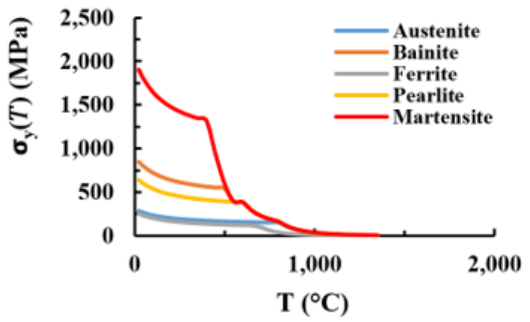
(c) Poisson's ratio
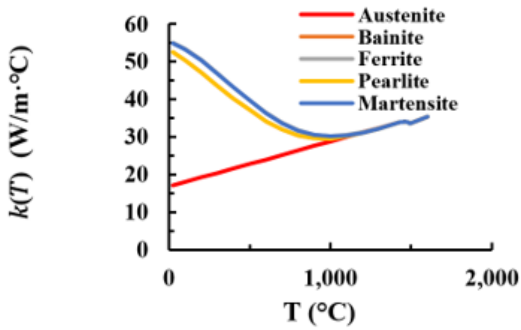
(d) Yield strength

(e) Thermal conductivity
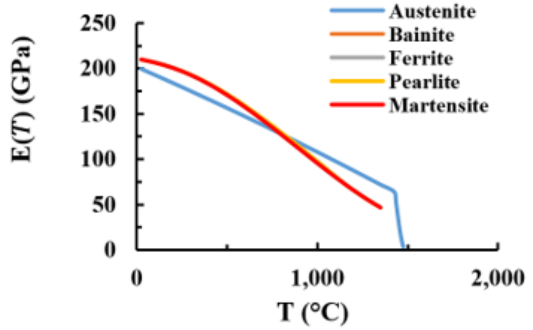
(f) Modulus of elasticity

Fig. 8 Temperature dependent properties of AISI 1045[40, 41]
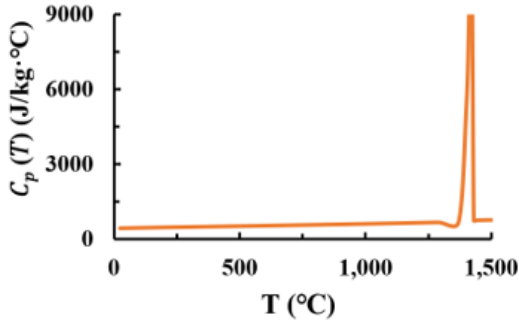
(a) Specific heat
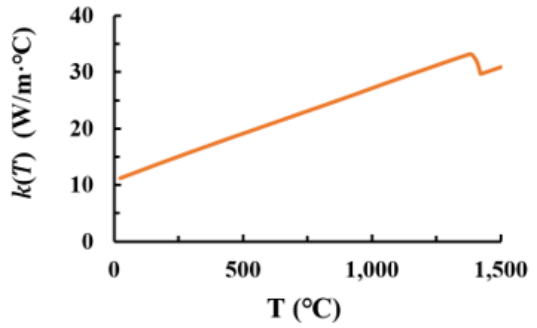
(b) Modulus of elasticity
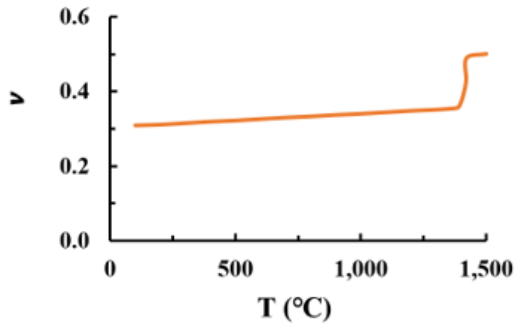
(c) Poisson's ratio
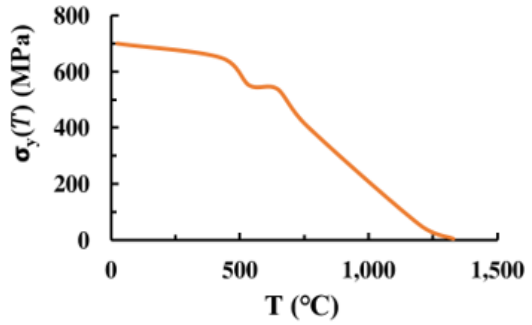
(d) Yield strength
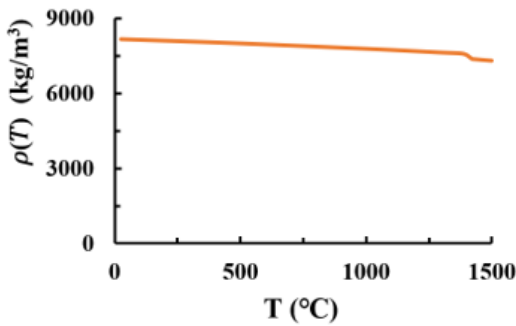
(d) Density
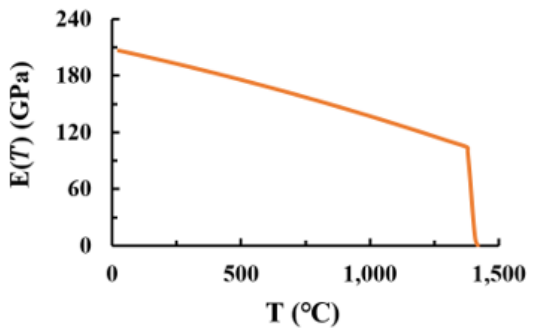
(d) Modulus of elasticity

Fig. 9 Temperature dependent properties of Inconel 718[24)]

4. Finite Element Models

A total of 16 FEA models were developed to investigate the effects of scanning patterns. Dimensions and boundary conditions of FEA models are shown on the Fig 10. Temperature dependent material properties of AISI 1045 were incorporated into substrate and Inconel 718 to powder model. Similarly, to the previous model cases mesh was structured in such a way that fine mesh applied only in the HAZ region and surrounding area. The purpose of this strategy is to minimize computational time while retaining high accuracy because high temperature flux, change and gradients are in vicinity of deposited clad and require accurate estimations of temperature field. This as a result makes improves results of mechanical analysis because it primarily depends on temperature histories. Eight deposition strategies based on zig-zag and eight based on raster deposition strategies are studied in this research. The four strategies in each type are combination of different direction of deposition in each layer marked as Z-1, Z-2, Z-3, Z-4 in case of zig-zag strategies and R-1, R-2, R-3, R-4 for raster scanning patterns, as shown in Fig. 11 (a) and 12 (a), respectively. The other four are the strategies with contour bead scan
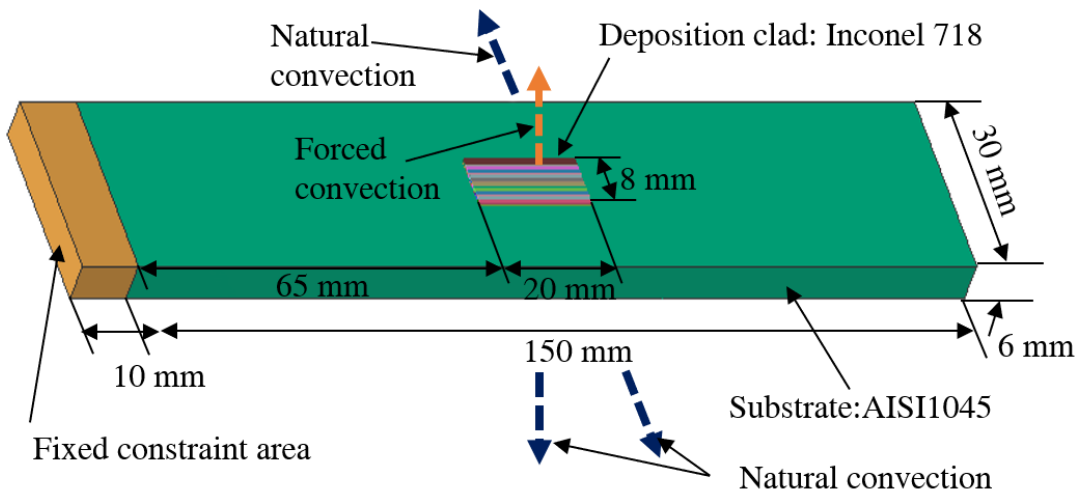
Fig. 10 Boundary conditions of FE model for investigation of the effects of deposition strategies (Deposition material: Inconel 718, substrate: AISI 1045)
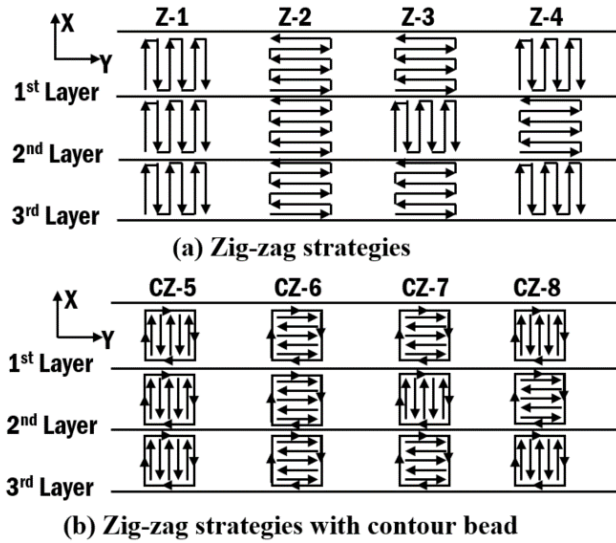
Fig. 11 Zig-zag deposition strategies (Deposition material: Inconel 718, substrate: AISI 1045)

applied first over the perimeter of the deposition area and then the inside layer is filled. These strategies are referred as CZ-5, CZ-6, CZ-7 and CZ-8 in case of zig-zag scanning patterns and
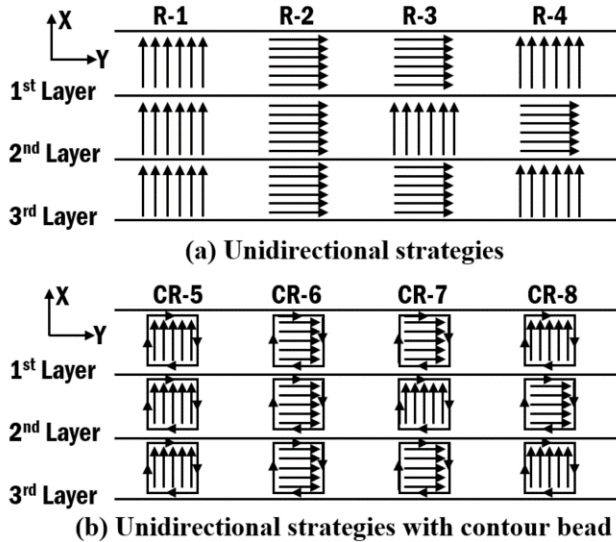
Fig. 12 Raster deposition strategies (Deposition material: Inconel 718, substrate: AISI 1045)

CR-5, CR-6, CR-7, CR-8 for the case of raster deposition strategies, as illustrated on Fig. 11 (b) and 12 (b) respectively.

The majority of studies related to deposition patterns are evaluating the deposition of square shape bead. These results might be less accurate when the deposition clad has different width and length. Thus, this study is investigating the effect of scanning pattern on rectangular shape of deposition clad with length to width around 3 which can be applied in the cases with higher ratio. The evaluation of the results is based on HAZ, residual stress and distortion.

5.   Results & Discussions

HAZ is the area around the deposition region which was affected by high temperatures and had its microstructure modified without melting. Due to the change in microstructure thermo-mechanical properties are also changed.

The knowledge of the link between thermal history and mechanical behavior is crucial to achieve required properties of parts by AM. Fig. 13 shows ISO view of temperature distribution at the end of deposition process. It can be observed that temperature distribution is different for different deposition strategies. In other words, higher temperatures can be observed in the larger area in the vicinity of deposited region. Note that the average temperature in substrate and deposited clad away from heat source is not higher than 300℃. This is due to conduction process which takes away most of the heat from the melt pool.

Temperatures in the vicinity of deposited region are lower for raster deposition strategies due to the effect of inter-pass time cooling. In other words, when raster strategy is used the deposition nozzle moves to the starting point of the subsequent bead after completion of previous bead allowing substrate to cool. The inter-pass time control can also be used to alter mechanical properties of deposited clad however the process time is increased as well.

All the deposition patterns investigated in this study are based on 4 deposition strategies type
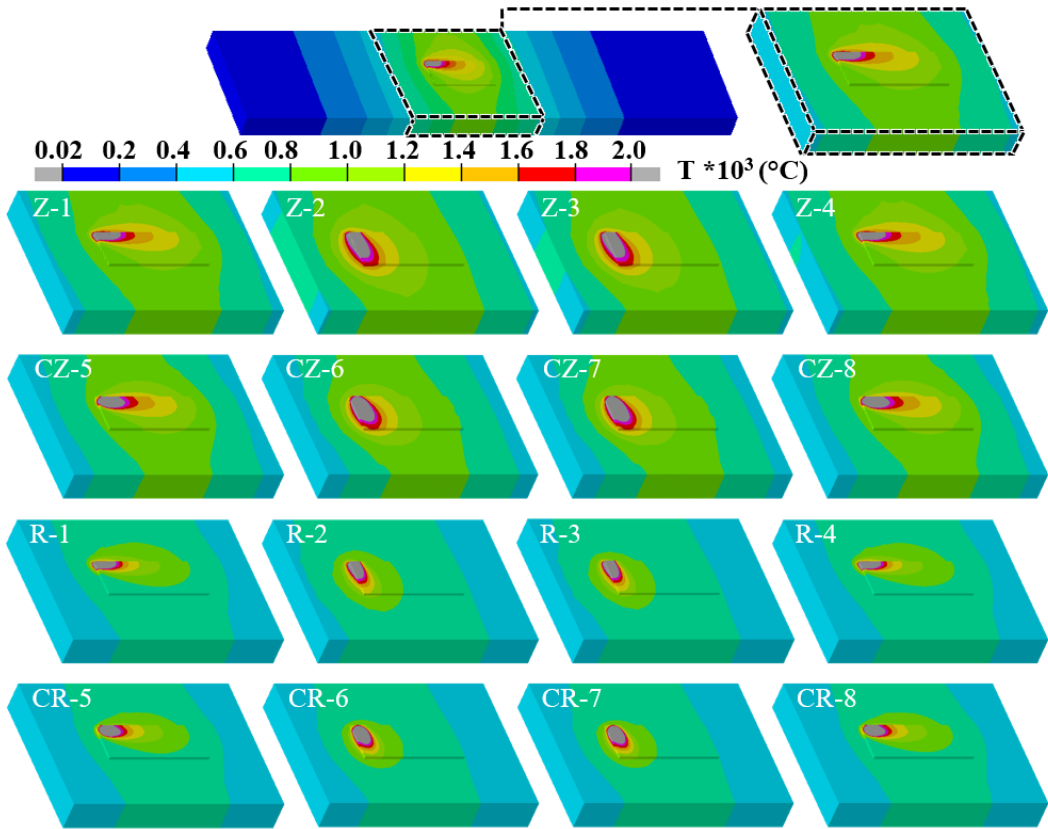
Fig. 13 Influence of deposition strategies on the temperature distribution at the end of cooling process (Deposition material: Inconel 718, substrate: AISI 1045)

Z-1, Z-2 and R-1, R-2, hence these patterns were selected to analyze predicted thermal histories at points A, B and C, as illustrated at Fig 14 (a). Fig. 14 (b) shows thermal histories for Z-1 and Z-2 deposition patterns and Fig. 14 (c) shows results for Type R-1, R-2. The results show that at selected points A, B, C for Z-1 pattern, temperature rise more quickly and continuously until it reaches local peak temperature. This is contrary to Z-1 where temperature rise occurred via short heating and cooling cycles until it gradually reached its peak temperature. For each selected points the peak temperatures for Z-1 were higher than Z-1. From this result it can be noted that during deposition process Z-1 allows better cooling at selected surface points. The differences in temperature are drastically reduced during the cooling process.
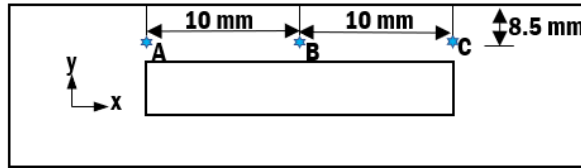
(a) Selected locations for measurement
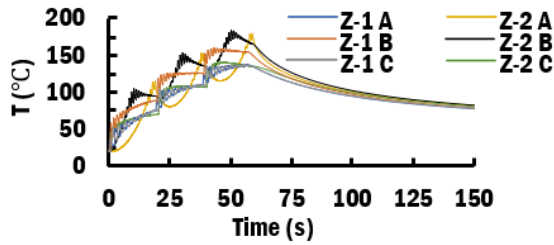
(b) Temperature histories for zig-zag strategies
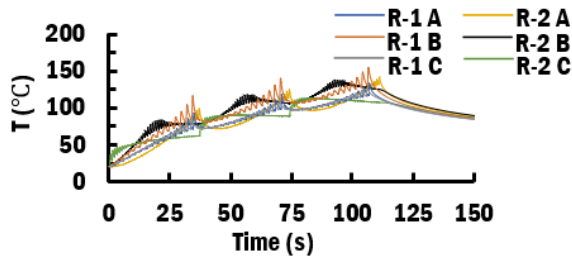
(c) Temperature histories for raster strategies

Fig. 14 Temperature histories according to deposition strategies (Deposition material: Inconel 718, substrate: AISI 1045)
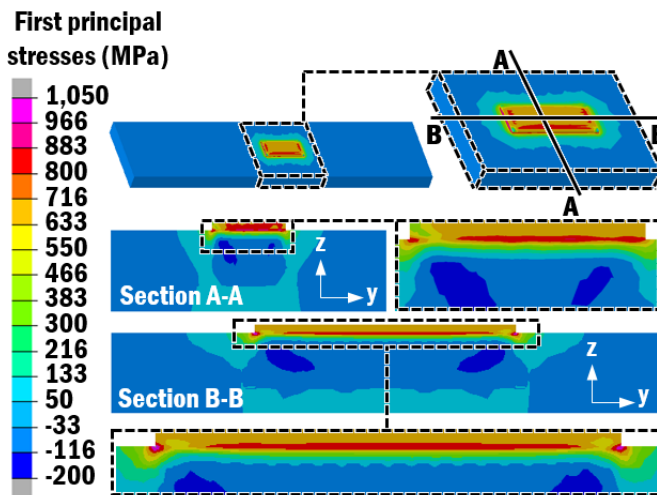
(a) Selected cross-sections
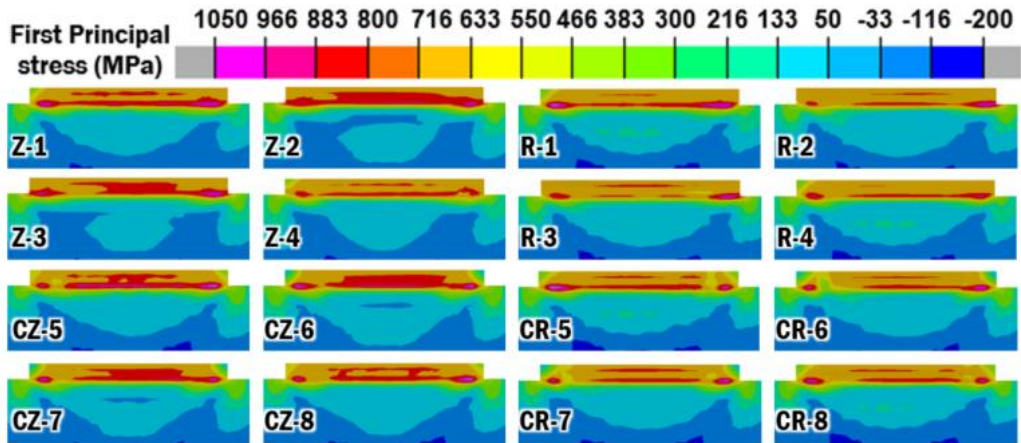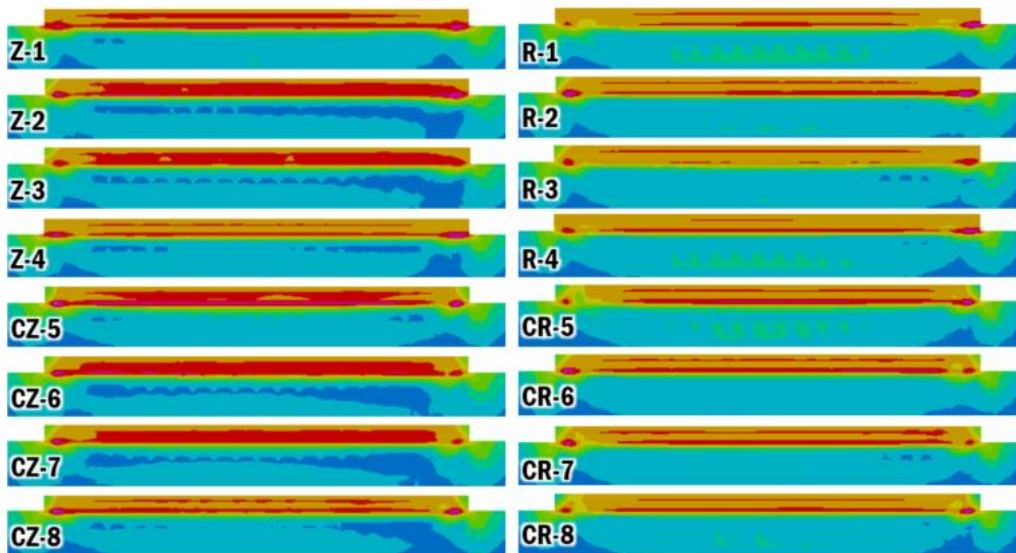
Fig. 15 Influence of deposition strategies on 1st principal stress distribution in the vicinity of deposited bead (Deposition material: Inconel 718, substrate: AISI 1045)

In case of raster deposition strategy R-1 shows higher peak temperatures at point B lower peaks at points A and C. This is due to nozzle movement after each deposited bead. Since R-2 scanning patterns has shorter beads it cooled more often during deposition process and shows gradual increase in temperature. This in contrast to R-1 strategy where temperature rises higher

after each deposited bead. For all deposition strategies points A and C show the lower peak temperatures when compared to point B. This is due to relatively cooler substrate edges compared to the center region hence higher conduction rate occurs at the points closer to the edges of substrate.

Cut through the center cross-sections are selected for stress evaluation, as shown in Fig. 15 (a). Predicted results for 1st principal stress and effective stress according to scanning pattern are shown in Fig. 15 (b) and Fig. 15 (c). The total cooling time of all the specimens is 40 minutes after which uniform temperature of 28-30°C distributed for all models.

The distribution of residual stress in the area surrounding deposition region is highly varied according to deposition pattern. The stress concentration region is under the deposition region close to upper surface of the substrate. All non-contour bead scanning strategies show excessive stress region in the corners between substrate and clad. The stress in this case is partially distributed on the surface of deposited clad and substrate. This is much undesired because tension stresses on the surface are more prone to crack initiations rather than inside stresses. In cases where contour bead is applied the effect of surface stress is lowered to some degree.

(a) Selected cross-sections
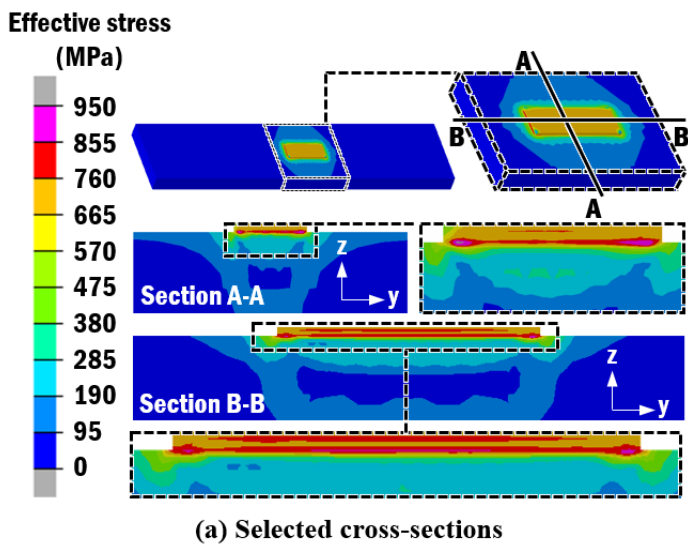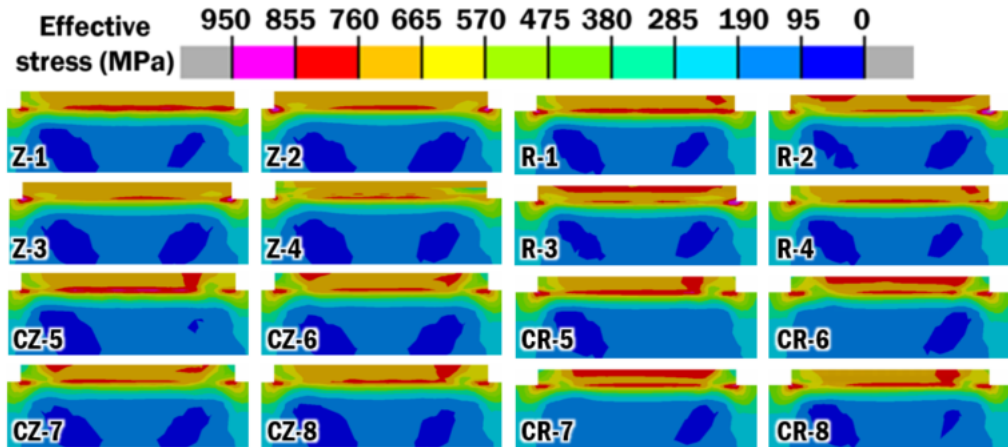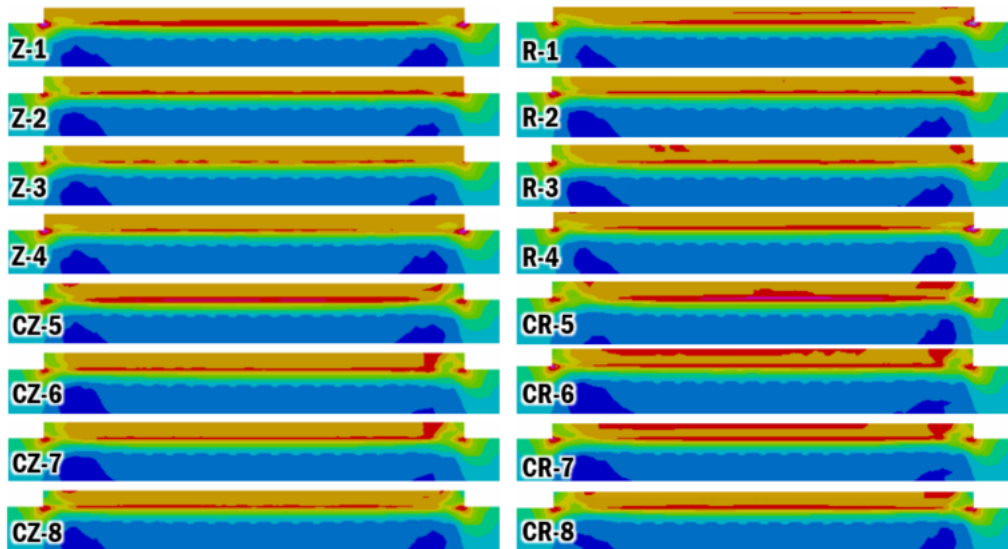
Fig. 16 Influence of deposition strategies on effective stress distribution in the vicinity of deposited bead (Deposition material: Inconel 718, substrate: AISI 1045)

In case of the zig-zag deposition strategies concentration of the 1st principal stress is observed inside the deposited clad and gradually decreased from contact region, as shown in Fig. 15 (c) and Fig 15 (b). Investigation of effective stress distribution in the midline cross sections shows highest stress concentration in the contact region between deposited clad and substrate regardless,

(a) Selected locations

(b) 1st principal stress distribution
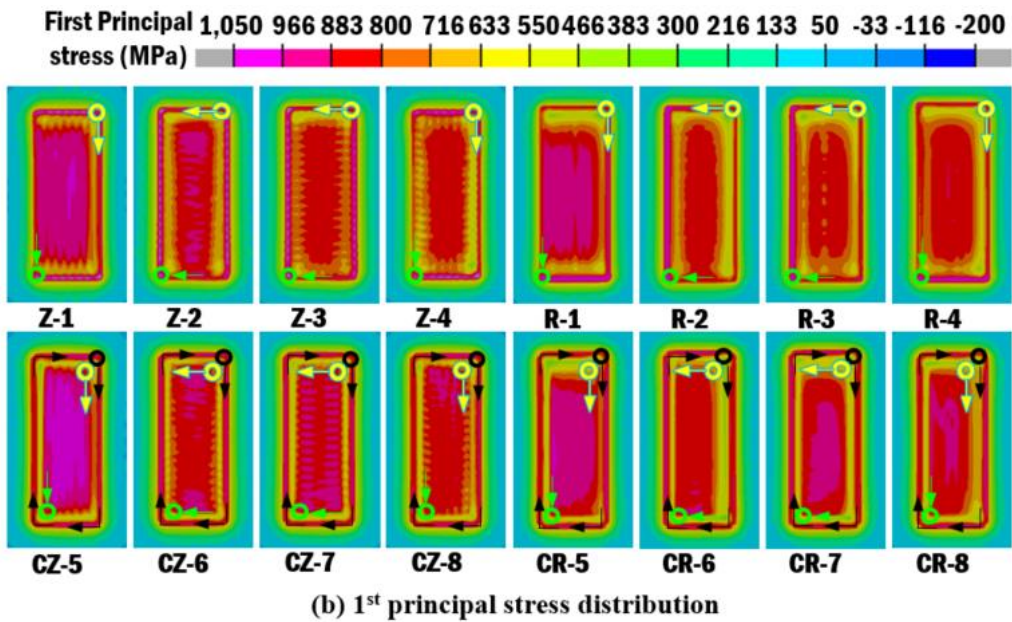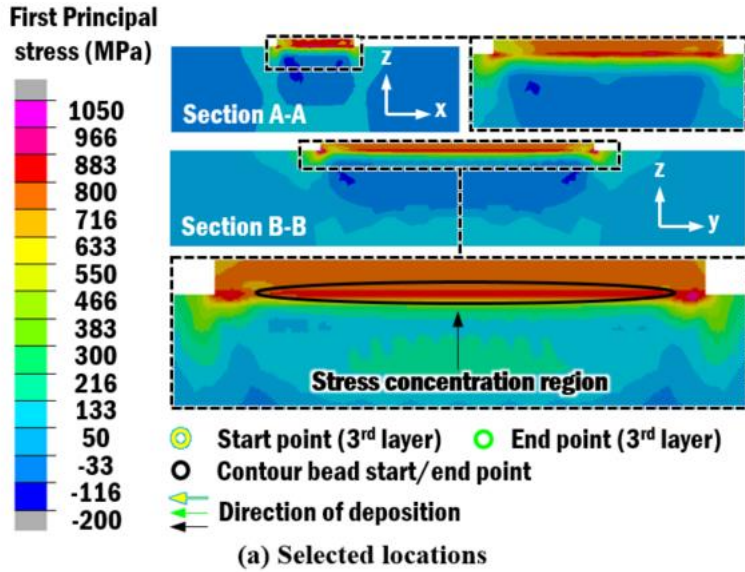
Fig. 17 Effect of deposition strategies on planar 1st principal stress distribution (Deposition material: Inconel 718, substrate: AISI 1045)

(a) Selected locations

(a) Effective stress distribution
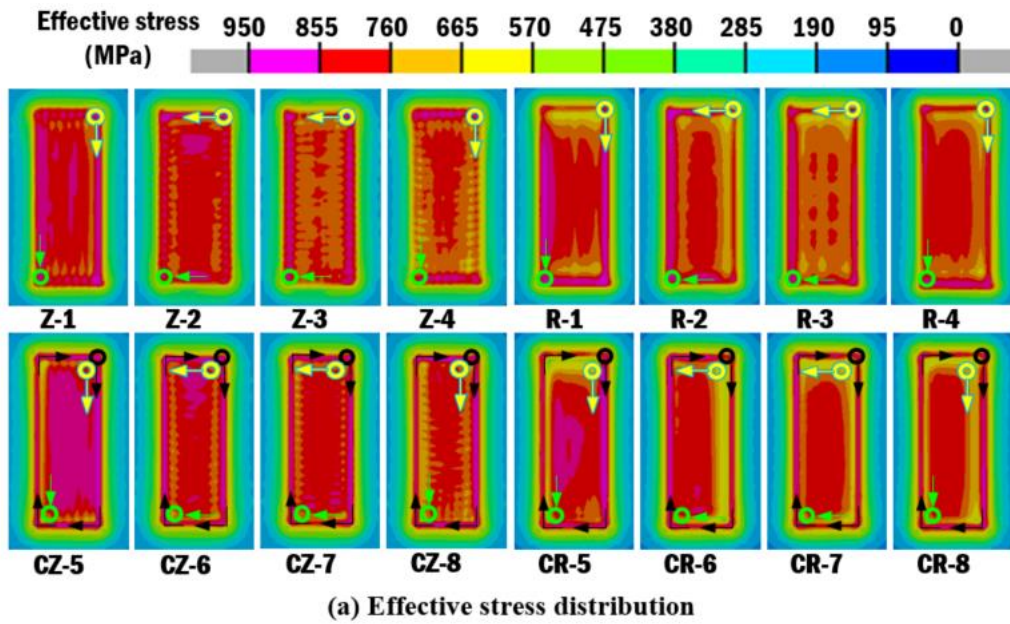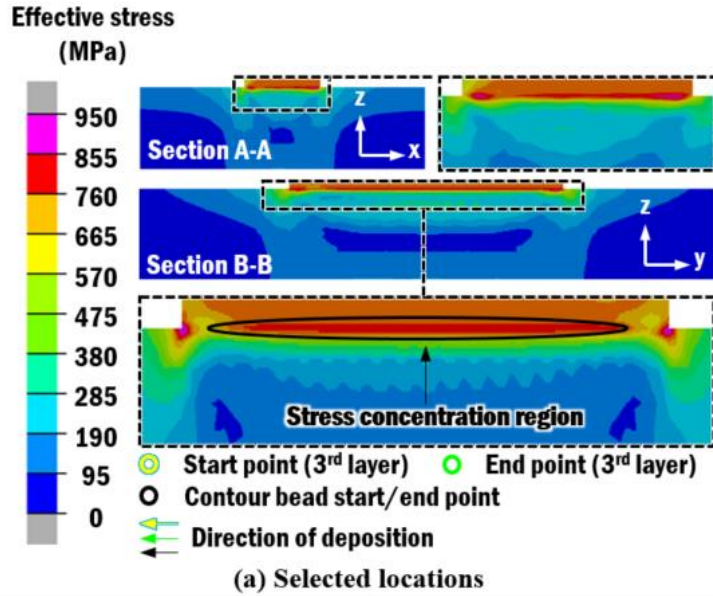
Fig. 18 Effect of deposition strategies on planar effective stress distribution (Deposition material: Inconel 718, substrate: AISI 1045)

of the deposition strategy as illustrated in Fig. 16 (b) and Fig. 16 (c). In addition, all deposition strategy cases show stress concentration along the corners between substrate and deposited clad. However, lower stresses along the corner are observed in contour bead cases.

High stress concentration is primarily observed under the deposition close to top surface of substrate. The depth of excessive stress concentration is nearly 150 µm. Deposition patterns Z-1, CZ-5, R-1 and CR-2 consist of longer beads in each layer which are oriented in the direction perpendicular to width of substrate. These strategies show deeper distribution of highly concentrated stress region. The distribution of stress in cross-section view considerably different between raster and zig-zag deposition strategies. Distribution of 1st principal stress for the case of zig-zag strategy show better symmetry when compared to raster deposition strategy.

The predicted results of planar stress distribution is assessed on top surface of the substrate below deposited clad as can be seen on Fig 17 (a) and 18 (a). Zig-zag scanning pattern shows symmetrical stress distribution, except Z-1 and CZ-5 which shows asymmetric stress distribution, as shown in Fig 17 (b). Both of these strategies have similar scanning patterns, except that CZ-5 has contour bead. Thus, it can be concluded that deposition of longer beads perpendicular to shorter side of substrate produces non-uniform stress distribution. Scanning patterns Z-3 and Z-4 are grid-like deposition strategies and CZ-7 and CZ-8 are respectively, similar patterns but they have contour bead deposited first. Scanning patterns Z-3 and RZ-7 show comparatively better uniformity of stress distribution, both effective and 1st principal. Thus, it can be concluded that stress distribution primarily affected by 1st layer deposition direction and proper following stress distribution can improve uniformity of stress distribution.

Planar residual stress distribution predicted for raster deposition strategies shows non-uniform distribution as can be seen on Fig 18 (b). Zig-zag deposition pattern exhibits comparatively symmetrical stress distribution when compared to raster scanning patterns. Strategies R-1 and CR-5 show similar tendency as in the case of zig-zag strategies. Comparing to other raster scanning patterns R-1 and C-R5 predicted to have significantly more irregular stress distribution.
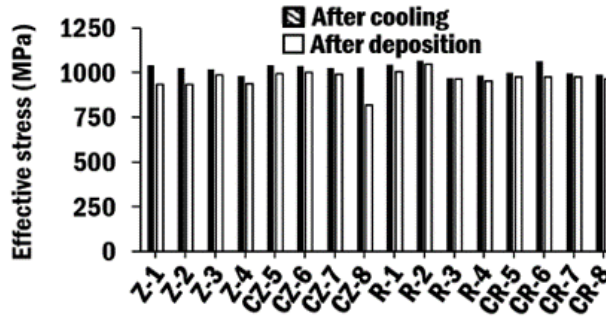
Fig. 19 Maximum effective stress accroding to deposition strategy (Deposition material: Inconel 718, substrate: AISI 1045)
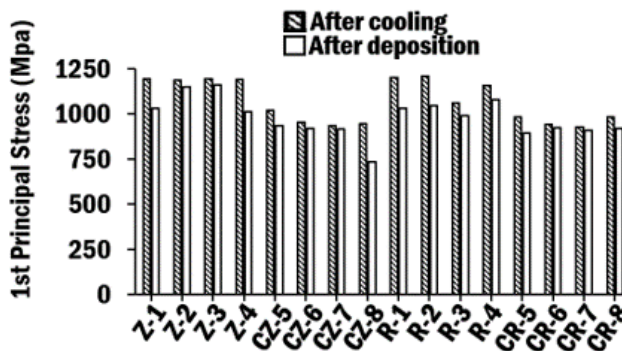
Fig. 20 Maximum 1st principal stress according to deposition strategy (Deposition material: Inconel 718, substrate: AISI 1045)

R-3, R-4, CR-7 and CR-8 are the patterns with grid and show better uniformity compared to other raster deposition patterns, as shown on Fig 18 (b). The influence of scanning pattern on stress distribution is predicted to be more significant in case of raster strategy compared to zig-zag pattern.

Irrespective of scanning pattern predicted results show that maximum residual stress is located in the surrounding area of stress concentration region, as shown in Fig 17 (b) and Fig. 18 (b). According to this result it can be concluded that weakest point of deposited clad and region where fracture initiation can occur. Maximum stress location is different for each scanning pattern. From this result, it is noted that maximum stress location is highly influenced by the deposition pattern.

(a) Typical displacement distribution
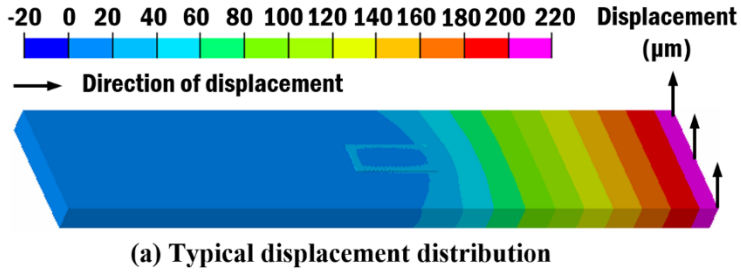
Fig. 21 Typical displacement distribution (Deposition material: Inconel 718, substrate: AISI 1045)

Predicted results of maximum stresses are shown on Fig 19 and 20. These graphs show results for maximum 1st principal and effective stress at the end of cooling process and immediately at the end of deposition process. During cooling process stresses are increased for the case of effective stress the increase in stress is between 0.4-20.4 % while 1st principal stress rose between 1.7- 22.5 %. From this result it can be noted that during natural cooling stresses increase in magnitude and that deposition pattern can affect the increasing value. In addition, predicted results show that side constraints effect on stresses in not significant. In case of effective stress, deposition pattern influence on maximum stress is insignificant as shown in Fig. 19. However, maximum 1st principal stress is significantly affected by scanning pattern. Contour bead show considerably lower maximum stresses. This can be result of preheating effect when contour bead is deposited and temperature of substrate is increased. Deposition strategies CZ-7 and CR-7
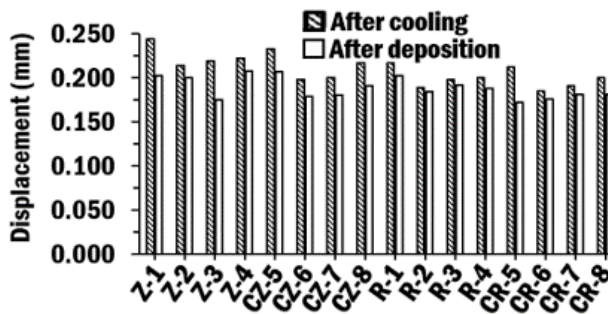
Fig. 22 Maximum displacement according to deposition strategies (Deposition material: Inconel 718, substrate: AISI 1045)

(a) Selected locations

Time (s)
(b) Distortion histories
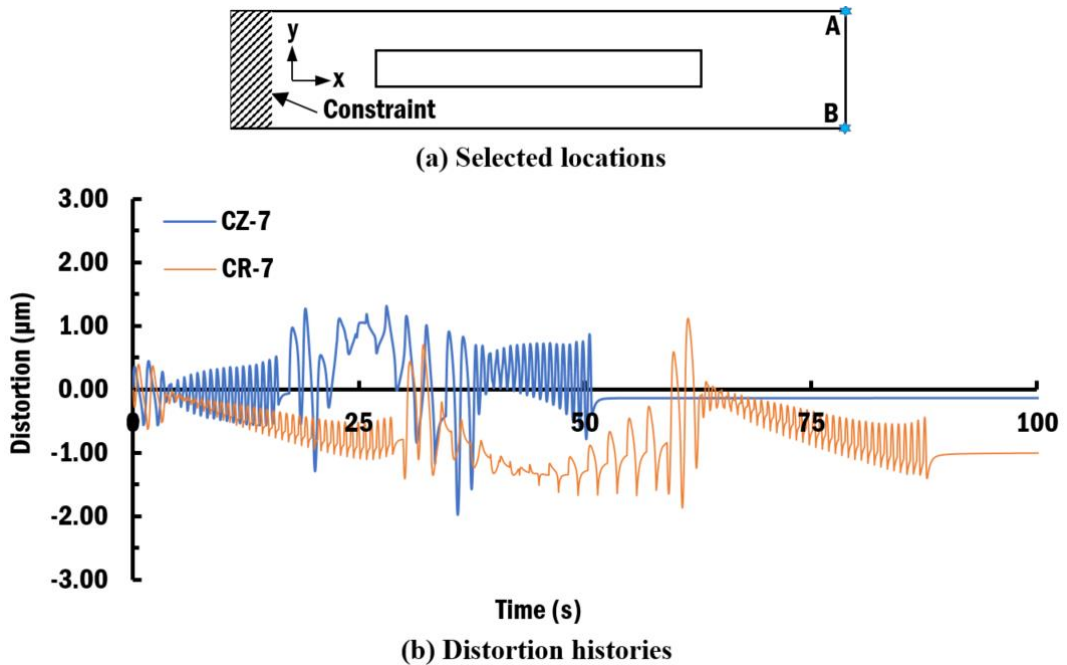
Fig. 23 Distortion histories for selected deposition strategies (Deposition material: Inconel 718, substrate: AISI 1045)

showed lowest maximum 1st principal stress.

For both zig-zag and raster deposition strategies for the case of contour bead the residual stress estimated to have higher maximum effective stress than max 1st principal stresses. This is due to hydrostatic effect which appears as a result of deposited clad being surrounded by pre-deposited contour bead creating compressive stresses.

As has been estimated in previous sections the 1st principal stresses are considerably lower when contour bead is applied. Fig. 22 depicts comparison between 1st principal stress and thermal histories. Starting point of the deposition on the substrate was selected for the evaluation due to its location being same for all models. The lower stresses in deposition strategies with contour bead can be explained by higher initial peak temperature with the following relaxation effect as deposition progresses. Similar behavior is observed for both zig-zag and raster strategies.

Predicted results of the analysis show similar pattern of distortion after end of cooling and

before cooling irrespective of deposition strategy. Analysis results show upward displacement at the tip of free end of all models irrespective of deposition pattern, as shown in Fig. 21. The starting location of displacement is at the edge of deposition bead and it reaches maximum at the free end of the models.

This result is expected because bending effect appears at the location of deposition region. Maximum displacement before and after cooling process are shown of Fig. 22. As a result of higher temperatures at the end of deposition process zig-zag patterns shows higher increase in maximum displacement due to cooling process. Maximum displacement is significantly affected by deposition pattern varying from 198µm to 244µm for zig-zag strategies and between 185µm to 217µm for raster strategies. Overall zig-zag deposition strategies show higher displacement at the end of cooling and at the end of deposition process due to overall higher temperature during processing.

Fig. 23 shows graph of distortion over time for CZ-7 and CR-7. The graph is based on difference in displacement at points A and B. The deposition process time of raster strategies is almost double of zig-zag patterns. According to predicted results on the graph, the accumulation of distortion is significantly affected by processing time. In addition, the inter-pass time in case of CU-7 strategy has negative effect on the accumulation distortion and final distortion at the end of deposition of each layer as well as at the end of processing. The graph shows that CZ-7 strategy has lower distortion during the processing at after the end of deposition. Although displacement of CZ-7 is strategy is higher than CR-7, 200µm versus 185 µm, analysis result shows significant increase in distortion when CR-7 strategy is applied. From this result it can be noted that CZ-7 deposition strategy is suitable for reduced distortion. Additionally, CZ-7 strategy showed low maximum residual stresses and more uniform stress distribution, hence CZ-7 is preferred deposition strategy.

D. Effect of Deposition Strategies on G6 Powder Deposited on SCM 440substrate

1. Boundary Conditions and Analysis Parameters.

Among investigated strategies five strategies which has shown comparatively uniform residual stress distribution and lower maximum stresses were selected. These strategies were

Table 6 Characteristics dimensions of DED process (Deposition material: G6, substrate: SCM 440)

Bead width (μm)	Hatch distance (μm)	1st Layer height (μm)	2nd Layer height (μm)
2,000	1,200	500	625

Table 5 Analysis parameters (Deposition material: G6, substrate: SCM 440)

Power of laser (W)	Scan speed (mm/min)	Feed rate (g/min)	Efficiency
1,400	1,200	8	0.44

applied for deposition of G6 powder over SCM 440 substrate. Selected strategies are shown in Fig. 24.

Boundary conditions of FE models are shown in Fig. 25. Substrate dimensions, clamping
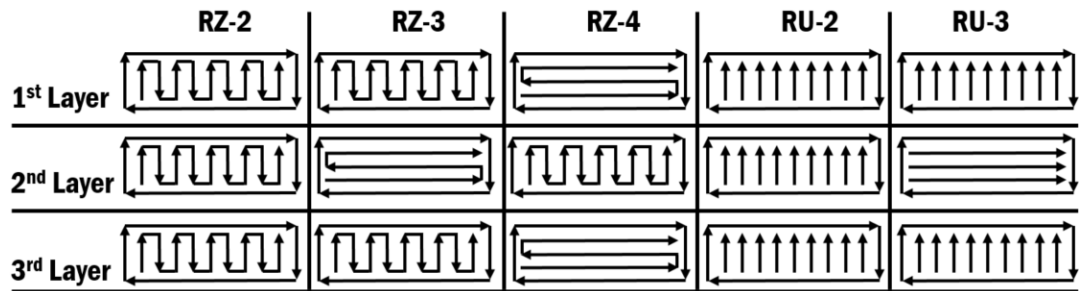
Fig. 24 Selected deposition strategies (Deposition material: G6, substrate: SCM 440)
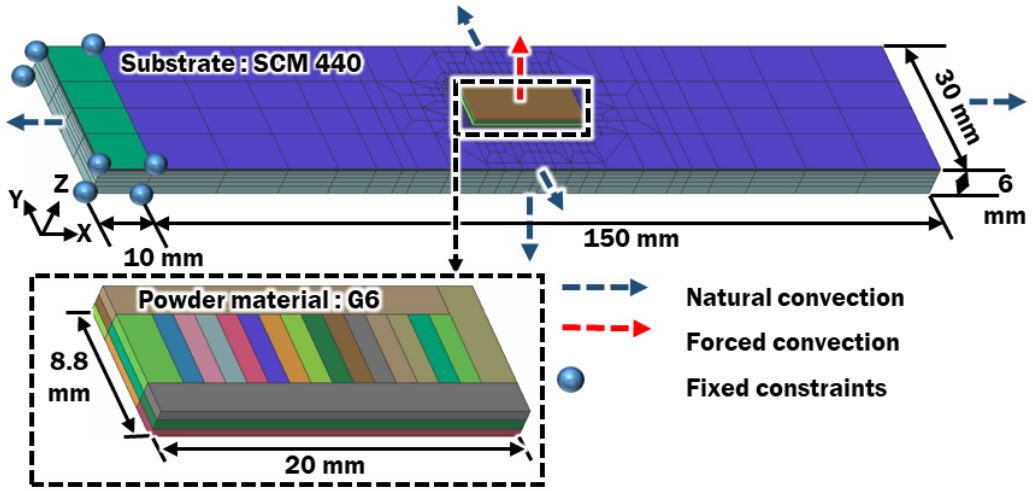
Fig. 25 Boundary conditions of FE models for investigation of the effects of deposition strategies (Deposition material: G6, substrate: SCM 440)

conditions and deposition bead dimensions are similar to the case of Inconel 718 deposition. The heat loss was considered from all surfaces, including heat loss from forced convection, and were applied to the model for improved accuracy. The analysis parameters and characteristics dimensions are shown on Table 5 and Table 6.

In order to obtain accurate results temperature dependent material properties of G6 steel were assigned to powder material and temperature dependent material properties of SCM 440 were assigned to substrate material. Properties of G6 and SCM 440 are show on Fig. 26 and Fig 27, respectively.

2. Results & Discussion

In order to evaluate inside residual stresses cross-sections through mid-section were selected as shown in Fig 28 (a). Fig. 28 (b) shows 1st principal stress distribution in cross-section A-A'. According to the results of the analysis the depth of concentrated stresses is deeper in case of zig-zag deposition strategies. In case of unidirectional deposition strategies, the stresses are

(a) Specific heat

(b) Density

(c) Poisson's ratio

(d) Yield strength

(e) Thermal conductivity

(f) Modulus of elasticity
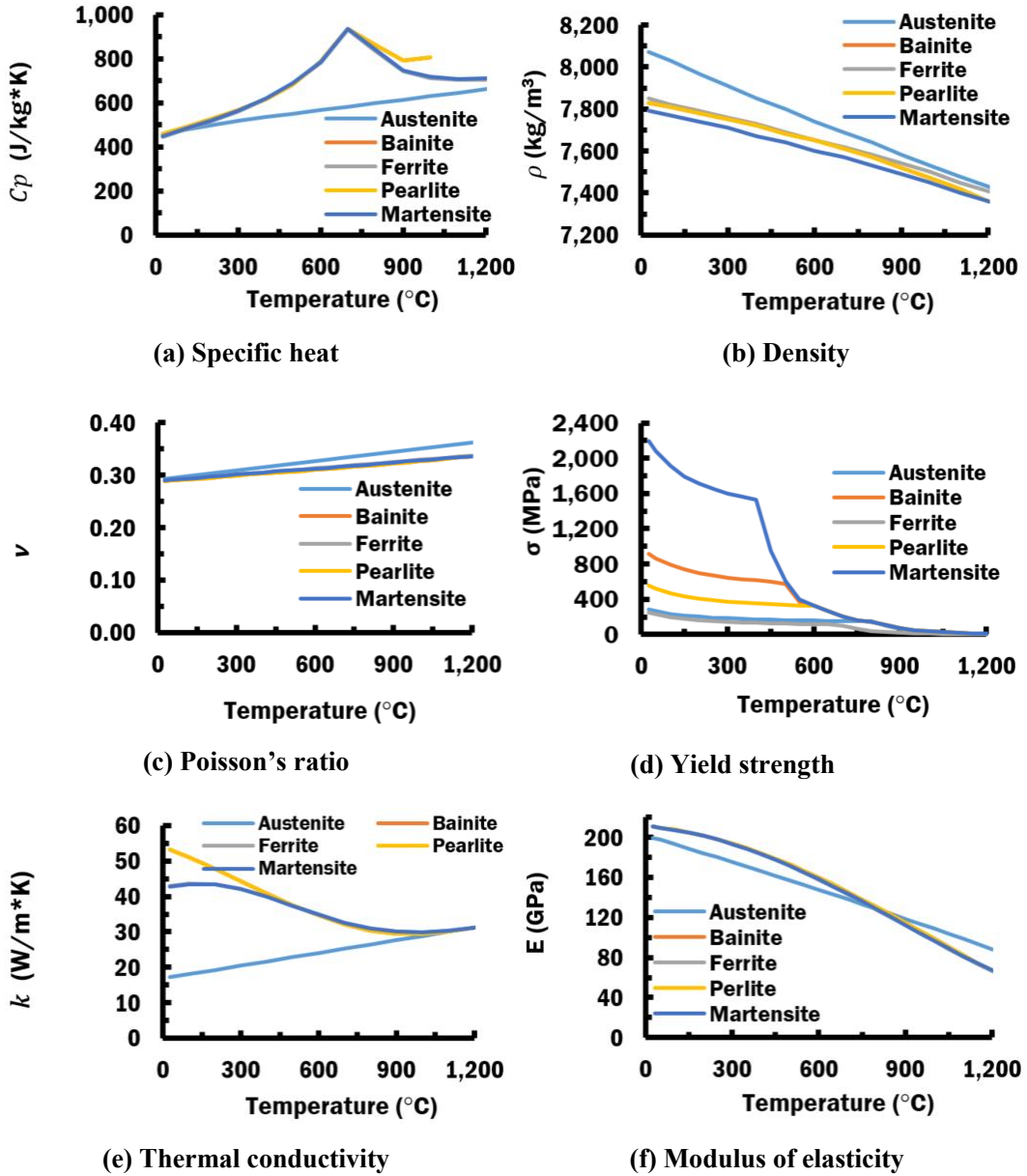
Fig. 26 Temperature dependent properties of G6[40, 41)
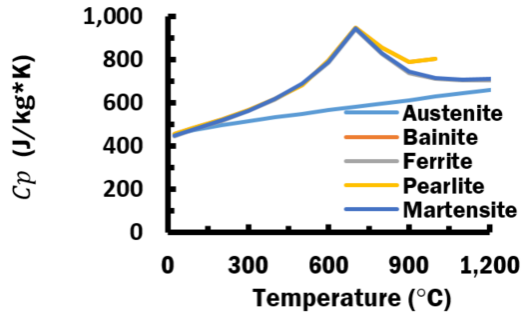
(a) Specific heat
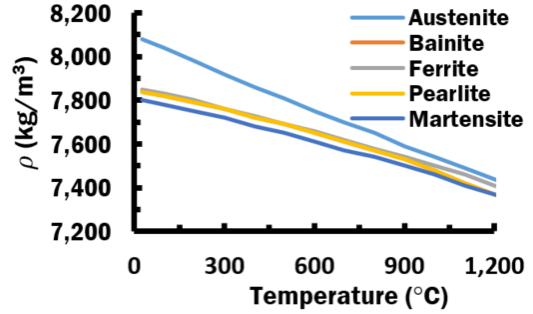
(b) Density
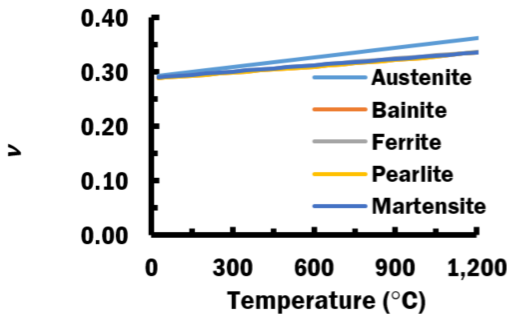
(c) Poisson's ratio
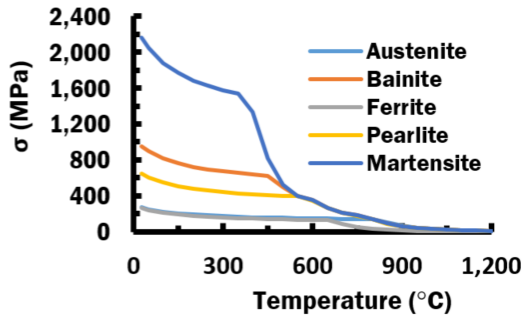
(d) Yield strength
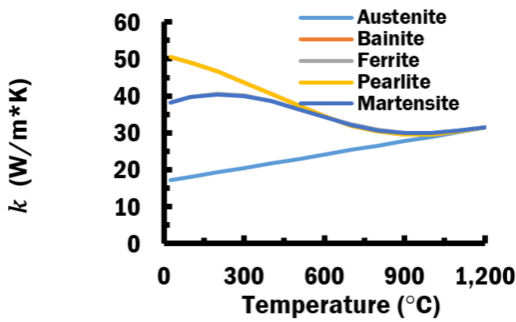
(e) Thermal conductivity
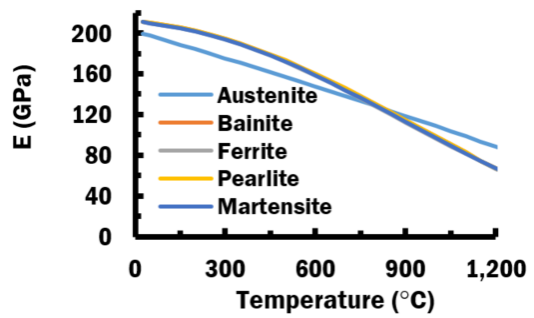
(f) Modulus of elasticity

Fig. 27 Temperature dependent properties of SCM 440[40, 41)]

(a) Section A-A'

(b) Section B-B'
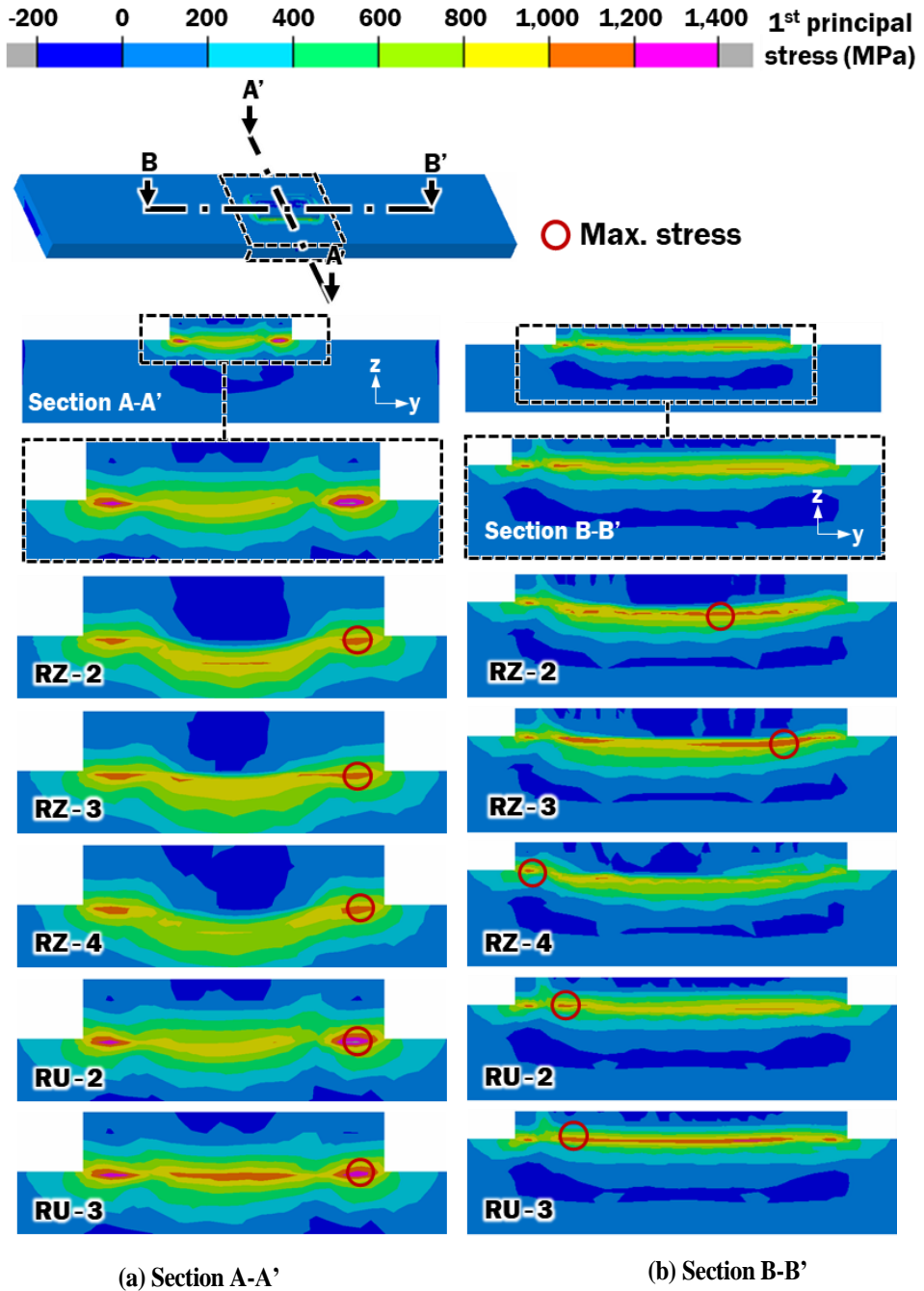
Fig. 28 Influence of deposition strategy on 1st principal stress distribution (Deposition material: G6, substrate: SCM 440)
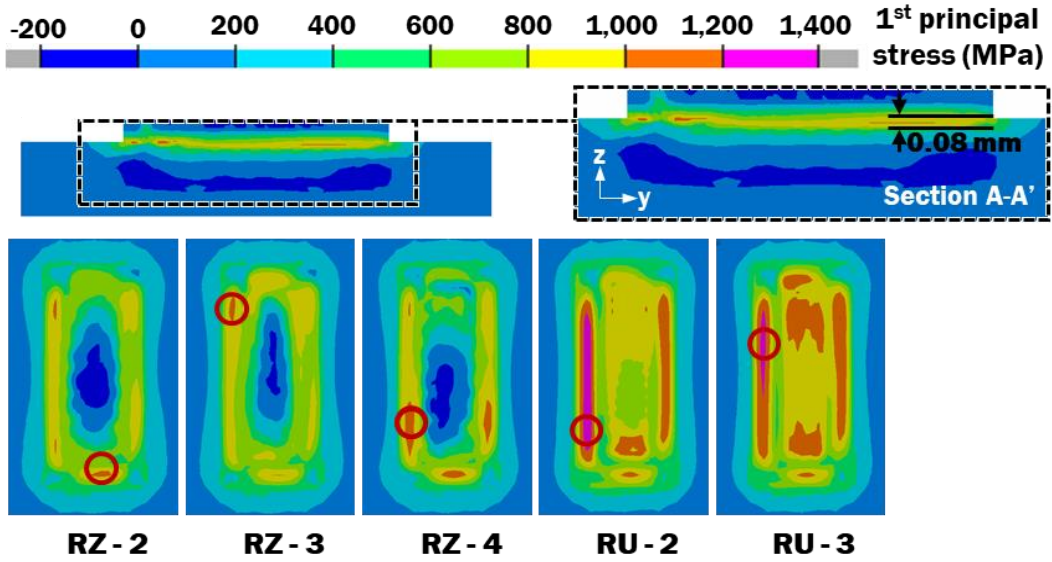
Fig. 29 Influence of deposition strategy on planar 1st principal stress distribution (Deposition material: G6, substrate: SCM 440)

(a) Section A-A'

(b) Section B-B'

(b) Planar stresses
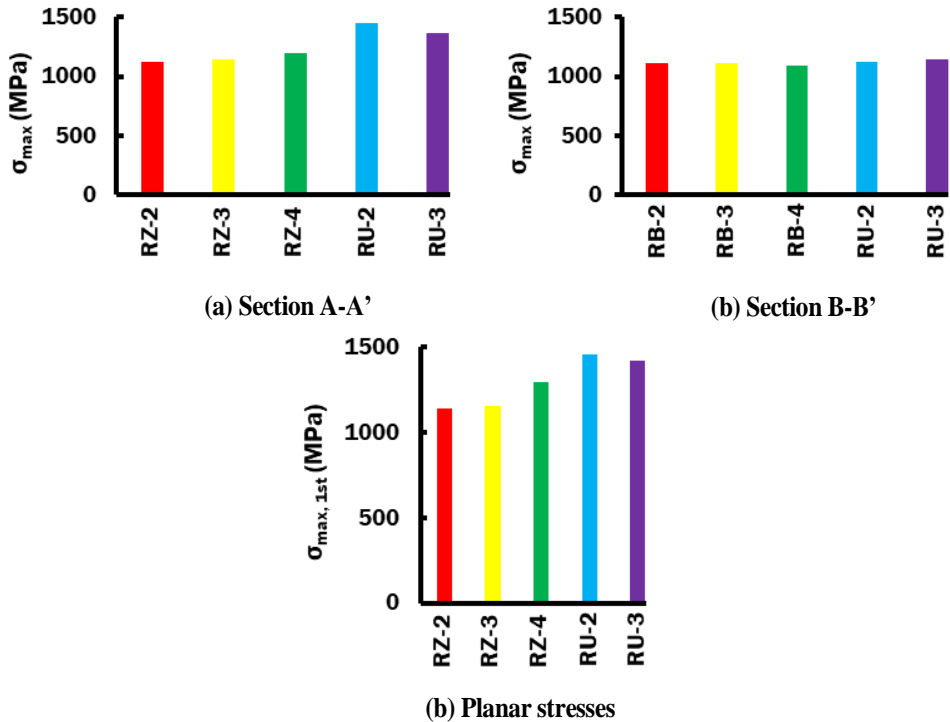
Fig. 30 Influence of deposition strategy on maximum 1st principal stress according to cross-section view (Deposition material: G6, substrate: SCM 440)
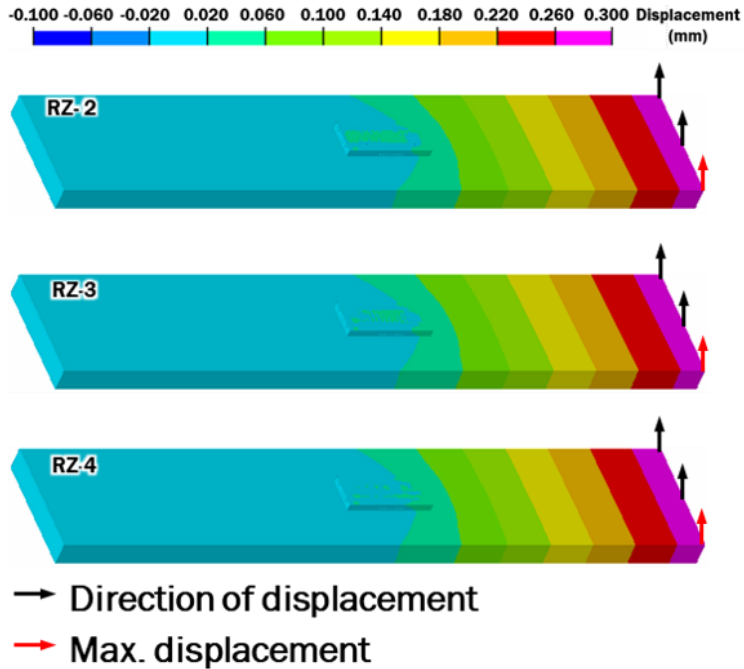
Fig. 31 Influence of selected deposition patterns on displacement distribution (Deposition material: G6, substrate: SCM 440)

closer to top surface of the substrate. The location of maximum stresses is similar for all cases and is located under the contour bead. Considerably higher maximum 1st principal stresses are in case of unidirectional deposition strategies in cross section A-A'. Stress distribution in cross-section B-B' is shown in Fig. 28 (b). When cross-section B-B' is compared to A-A' considerably lower stresses are observed for every case. The distribution of stress shows similar tendency where stress concentration depth is greater in case of zig-zag deposition strategies. This is due to inter-pass time required during unidirectional deposition which has effect on residual stress distribution. Although maximum stresses in cross-section B-B' are lower in case of unidirectional deposition strategies higher stresses are observed inside deposited bead. Fig. 30 shows maximum stresses. Section A-A' shows considerably higher maximum stresses. Unidirectional strategies show the higher maximum 1st principal stress.

Fig. 29 shows planar stress distribution. It was estimated that the maximum planar stresses

are at a depth of approximately at a depth of 80 µm. Zig-zag deposition strategies show somewhat symmetrical stress distribution while unidirectional deposition strategies show high stress concentration at one side of the substrate due to better symmetry and lower maximum stresses zig-zag strategies RZ-2, RZ-3 and RZ-4 are selected for farther displacement evaluation.
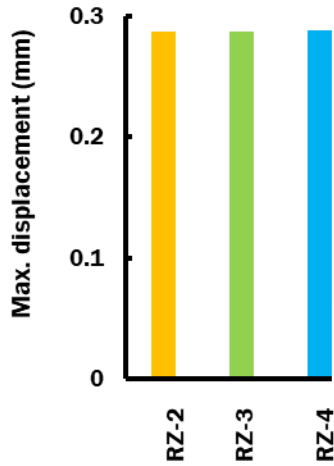
Fig. 32 Maximum displacement of selected deposition patterns (Deposition material: G6, substrate: SCM 440)
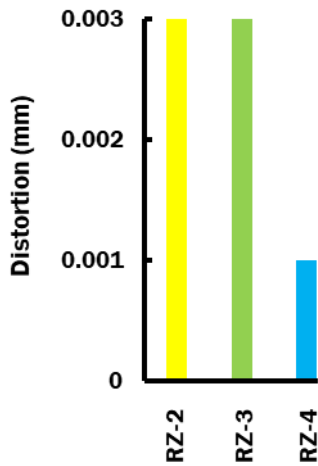
Fig. 33 Maximum distortion of selected deposition patterns (Deposition material: G6, substrate: SCM 440)

Upward displacement at the free end is observed in all models as shown in Fig 31. The maximum displacement is located at the edge of the FE models. When maximum displacement is compared the similar value was predicted for each case, as shown in Fig 32. When maximum distortion is compared e.g. difference of maximum displacement at opposite corners of the free end of the models. RZ-4 showed the lowest distortion which is 3 times less than RZ-2 and RZ-3 as can be seen on Fig. 33, hence RZ-4 strategy was selected as proper deposition pattern for G6 powder deposited over SCM 440.

III. THERMO-MECHANICAL CHARACTERISTICS ACCORDING TO SHAPE OF DEPOSITED MATERIAL

A. Description of the Analysis

More in-depth research and broad understanding of the DED process is necessary in order to drive technology forward and develop it to its full potential[36]. Finite element method is a great tool in order to understand the perplexing physical phenomenon that take place during deposition process in regards to different process parameters. Fundamentally, it can be divided into empirical and numerical analysis models. The empirical model is based on data obtained from experiment which systematized and summarized by various methods such as regression analysis or linear/non-linear analysis. After that the data is used as a base for the numerical modeling and analysis[37]. Analysis model is then developed for better understanding of the effects of process parameters but generally focuses only on one or two physical processes because analysis of all physical fields is highly challenging due to limitations of modern hardware. For example, melt pool models are analyzing the process of melting of powder until solidification to investigate cross section formation[38]. Thermo-mechanical analysis is focused on the properties of material after solidification, including distortion, stress and metal microstructure. These models are used to investigate various process parameters and deposition strategies such as deposition path, dwell time, preheating and etc[36]. The main goal of thermo-mechanical FEA is to estimate heat transfer and stress-strain characteristics of the part during deposition by DED.

When parts are manufactured by DED process usually substrate is required on top of which metal part is deposited. Depending on the part geometry and substrate material and dimensions the residual stress formation and distortion effects might vary significantly. For example, if the substrate is too thin it can deflect significantly which in turn will affect the part quality and

dimensional accuracy. In addition, increased width and length of deposition can also affect the part itself due to accumulation of distortions as a result of cyclic heat flux input. Author has no knowledge of existing studies of the aforementioned case. In this study, the residual stress formation and displacement are estimated and evaluated according to deposition shape and powder material. More specifically, thermo-mechanical characteristics of Inconel 718 deposited on AISI 1045 according to width (W) and length (L) and thermo-mechanical characteristics of Inconel 718 deposited on AISI 1045 substrate and G6 powder deposited on SCM 440 according to deposited height (H).

B. Effects of Deposition Width & Length

1. Finite Element Models

In this study, total of nine FEA models were created to investigate the effects of width and length of deposited bead on thermos-mechanical characteristics in the vicinity of deposited bead. In order to save computational time but maintain acceptable accuracy of the results of simulation fine mesh was created in the vicinity of deposited bead with the smallest element size of 0.01 mm. Fine mesh is required only in the surrounding area of deposited bead due to high temperature
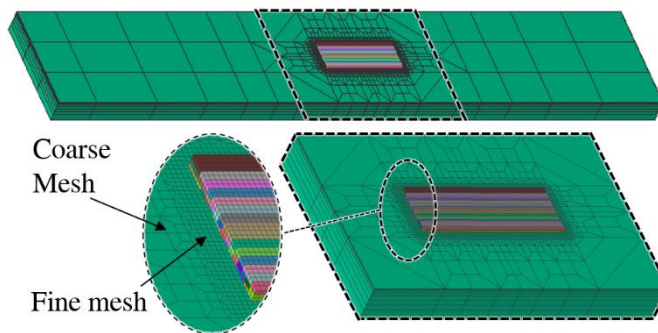
Fig. 34 Mesh structure of FE models for analysis of influence of deposited shape on post process thermo-mechanical characteristics (Deposition material: Inconel 718, substrate: AISI 1045)
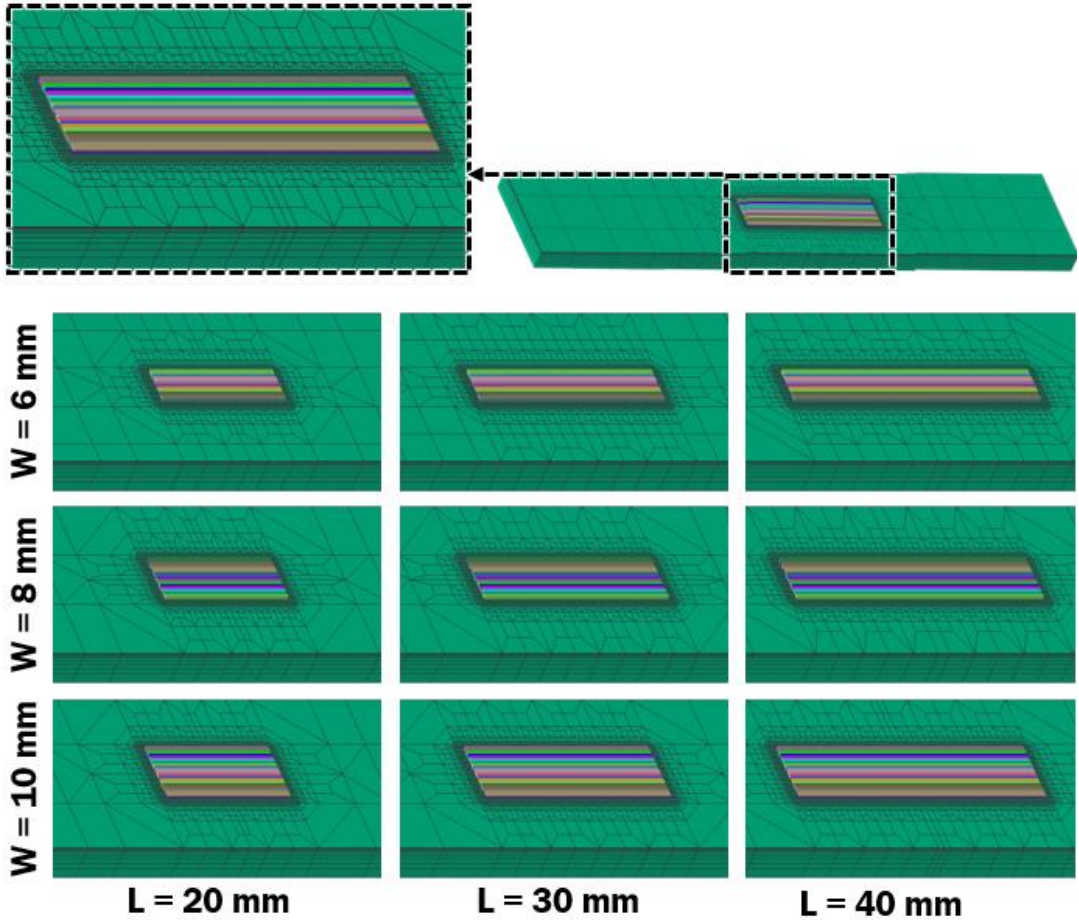
Fig. 35 Selected dimensions for width (W) and length (L) of deposition area

gradients and high heat flux in that region. In addition, the highest temperature change is also happening in that region. The thickness of each deposited layer is one element tall and each track four elements wide, making every element ¼ of the diameter of laser beam. Mesh structure of the models is shown on Fig. 34.

The deposition parameters are taken from the work of Ho et al. Table 7 shows the process parameters used for the analysis and Table 8 shows dimensional characteristics of deposited bead. The creation of model and analysis were performed in commercial software SysWeld[40]. When
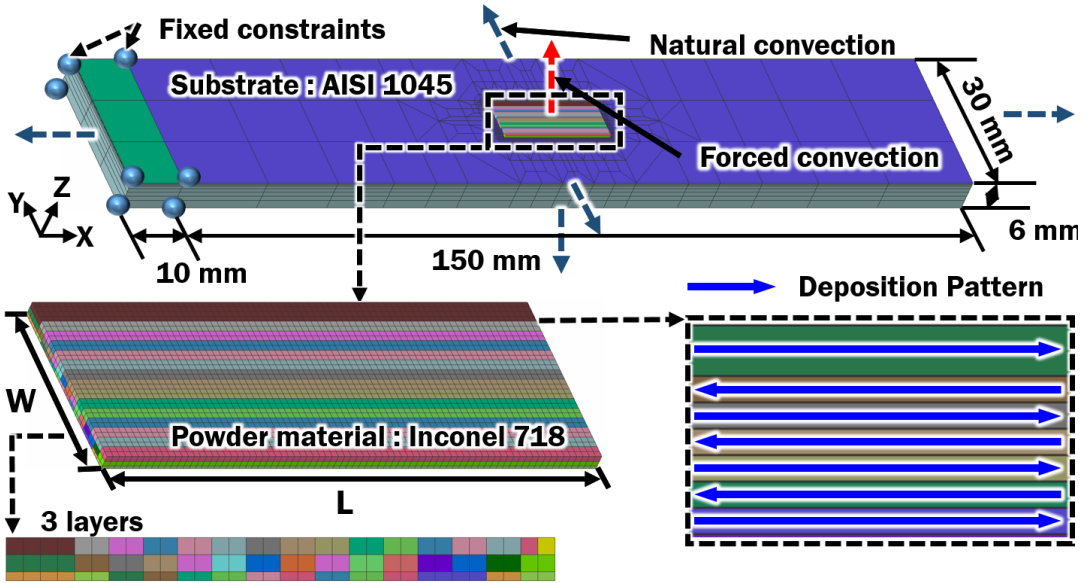
Fig. 36 Boundary conditions of FE models for analysis of effects of deposition shapes (Deposition material: Inconel 718, substrate: AISI 1045)

simulation of deposition process is compared to real DED process the analysis is performed in steps rather than continuously. The most sophisticated results are obtained by the activation technique. During that process some of the elements are activated at the location of heat source to simulate the material ejection process. After that the steady state heat transfer equations are solved at that location and heat source is moved to the next step. The final conditions of previous step are used as initial conditions of the next step. The distance traveled by heat source between steps depends on the step time. In addition, the accuracy also depends on step time. The smaller the step time is the closer the simulation to continuous deposition process. In this study the step time during analysis is 0.02 seconds which gives highly accurate results. Fig 35 shows selected dimensions of the width (W) and length (L). Since the goal of the study is to evaluate the effects of various W and L on the residual stress and displacement all the parameters of the analysis are the same for all models including power of laser, scan speed, gas flow rate, clamping conditions, ambient and initial temperatures. The number of nodes and number of elements for each case are

Table 7 Process parameters of the experiment (Deposition material: Inconel 718, substrate: AISI 1045)

1st bead width (mm)	Hatch distance (mm)	1st layer thickness (mm)	2nd-3rd layer thickness (mm)	Total height (mm)
1	0.5	0.135	0.25	0.635

Table 8 Dimensional characteristics of deposited bead (Deposition material: Inconel 718, substrate: AISI 1045)

P (W)	r (mm)	η	c	V (mm/min)	F (L/min)	S (f/min)
350	1	0.350	1/16	1000	7	10.3

shown in Table 9. The higher the number of nodes and elements the higher the time required for the analysis. The computational time ranging from around 12 hours for the smallest deposition area of 6 mm width and 20 mm length up to 120 hours for the largest area of deposition of 10 mm width and 40 mm length. Boundary conditions of the FE models are shown on Fig 36. Dimensions of the substrate are the same for all models, as shown in Fig 36.

The raster scanning pattern based on planar bead deposition only in one direction, which is very simple and robust to be used with any geometry of shape of the part. Although build accuracy can be negatively affected and more time is required to complete the deposition process by raster deposition strategy. Considering these models have a lot of beads zig-zag deposition strategy is selected to join all single beads into one continuous deposition process with reduced number of transmission motions and reduced deposition time.

Heat loss from each side of the substrate and the surface of deposition bead was considered in the analysis. Forced convection during deposition process was applied to the top surface which consist of radiative losses and energy losses due to blow of Ar gas. Total of 3 layers deposition was analyzed with the starting location of deposition from the fixed side to the free end of substrate. All beads are deposited in the direction parallel to the long side of the substrate. One sided clamp was used with clamp on the side with starting point of deposition. Dimensions of

the substrate are same for all models and were previously. Fixed clamping of 10 mm was applied at one end of the substrate as shown on Fig 36. The purpose of the study is to analyze the effects of deposited shape on residual stress and distortion. More specifically, to investigate the effects of change in width and length.

Table 9 Number of meshes and nodes according to deposition width (W) and length (L) (Deposition material: Inconel 718, substrate: AISI 1045)

W (mm)	6			8			10		
L (mm)	20	30	40	20	30	40	20	30	40
Nodes (EA)	32,772	39,159	46,094	46,102	55,434	65,376	59,285	71,559	84,515
3D Elements (EA)	29,868	35,904	42,404	42,200	51,020	60,368	54,388	65,992	78,188

2. Results & Discussions

According to predicted results after long cooling all the models are below 30°C which is close to the room temperature and sufficient to evaluate post-process thermo-mechanical characteristics of deposition process. Fig 37 shows ISO view of effective stress distribution for each study case. As can be seen from the Fig. 37 stresses on the surface of the models is comparatively low. Moreover, only the deposited area and small surrounding area exhibits residual stresses and the rest of the substrate is unaffected by effective stress.

Cross-sections through the starting side of deposition, through the center and ending side of the deposited bead of the models were selected to evaluate effective stress distribution as shown in the Fig 38, Fig 39 and Fig 40. In cross-section A-A' residual stress distribution can be observed as shown in Fig 38. For all cases the stress distributed similarly and the location of maximum stress is on the left side or under the first deposited bead. The maximum stress and stress concentration is under the deposited bead on the top surface of the substrate. In all cases width residual stress is lower with increasing the length of deposited bead.

Section B-B' in Fig 39 shows stress distribution through the mid-section of FE models. Similarly, the distribution of stress and the location of maximum stress is same for all cases except the 10 mm width and 30 mm length case which has maximum stress under the last deposited bead. In case of 6 mm width and 10 mm width the 20 mm length showed the lowest maximum stresses and 30 mm length case showed the lowest maximum residual stress, as shown in Fig 39. In case of 8 mm width case the maximum effective stresses are similar for each case. Overall, 10 mm width case shows the lowest stresses. The mid-section of the model has the highest importance as far as maximum stresses are concerned. This is due to steady state conditions inside the model. Most of the part is affected by the steady state conditions and show similar stresses across most of the inside of the part. This has high impact over mechanical properties of the deposited part.

Fig. 37 ISO view of effective stress distribution according to deposited width (W) and length (L) (Deposition material: Inconel 718, substrate: AISI 1045)

Cross-section C-C' goes through the end of the deposited bead on the free end of the substrate as shown in Fig 40. Maximum stress location is same for all cases. In each case 20 mm length models showed the highest maximum stress as shown on the graph in Fig. 41. In case of 6 mm and 10 mm the stress is lowest at 30 mm length with slight increase in value when deposited length is 40 mm.

Fig 42 shows ISO view of 1ˢᵗ principal stress distribution. Asymmetric stress distribuend is observed on the surface of the models. Similar pattern of stress distribution for all models is

Fig. 38 Effective stress distribution in A-A' section according to deposited width (W) and length (L) (Deposition material: Inconel 718, substrate: AISI 1045)

Fig. 39 Effective stress distribution in B-B' section according to deposited width (W) and length (L) (Deposition material: Inconel 718, substrate: AISI 1045)

Fig. 40 Effective stress distribution in C-C' section according to deposited width (W) and length (L) (Deposition material: Inconel 718, substrate: AISI 1045)

(a) Section A-A'

(b) Section B-B'

(c) Section C-C'

Fig. 41 Influence of deposited width (W) and length (L) on maximum effective stresses according to cross-section (Deposition material: Inconel 718, substrate: AISI 1045

observed. Which farther proves that stress distribution is primarily affected by the scanning pattern. Similarly, to effective stress evaluation three cross-sections were selected to analyze 1st principal stress distribution. Cross-sections A-A', B-B' and C-C' as shown in Fig.43-45.

Cross-section A-A' is located at the edge if the deposited bead on the closer to fixed side of substrate, as shown in Fig 43. The location of maximum stress for all models is located under the second bead. The excessive stress concentration region is under the deposited close to the top surface of the substrate. For all cases the maximum stress is lower with increasing length of deposited bead except 10 mm case which has same maximum stress for 30 mm and 40 mm length.

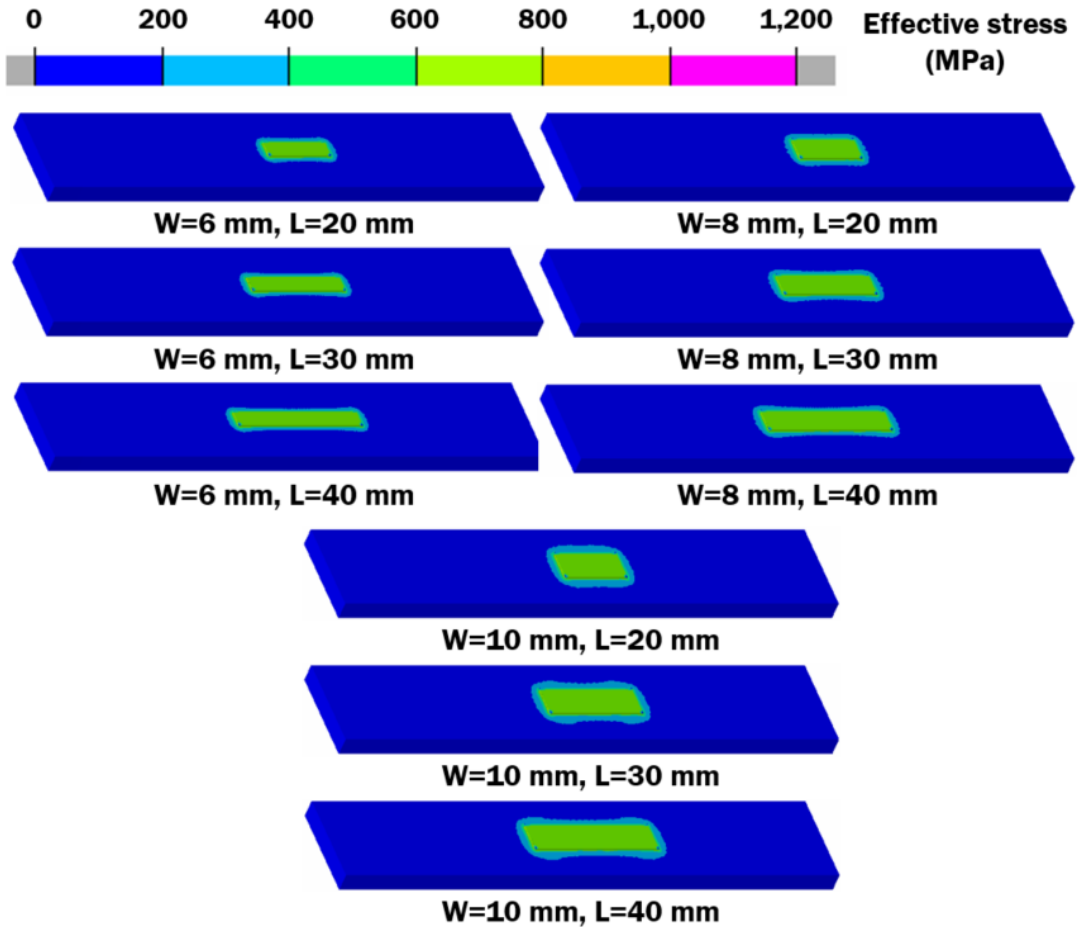Cross-section B-B' is the cut through the mid-section of the models as shown in Fig 44. The
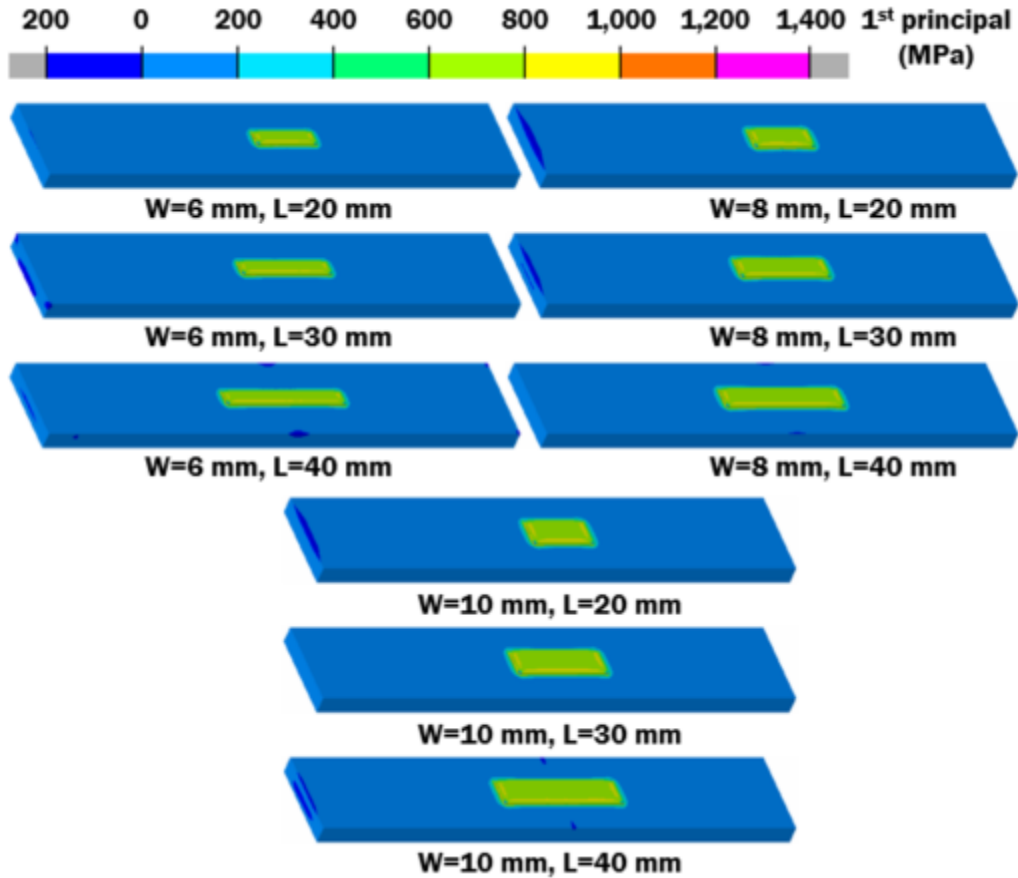
Fig. 42 ISO view of 1st principal stress distribution according to deposited width (W) and length (L) (Deposition material: Inconel 718, substrate: AISI 1045)

stress distribution pattern is same for all models through the mid-section. The stresses at the mid-section are considerably lower compared to the stresses at the edges of deposited bead. This is due to higher energy input at the start and at the end of deposited bead. The starting and ending section of deposited bead is called transition area and it is exposed to considerably higher energies which results in greater temperature gradients as well as greater residual stress. The maximum 1st principal stress location is exactly at the center of the models under the deposited bead on the top surface of the substrate. The magnitude of maximum stress is the highest in case of 20 mm length for each width case. In case of 30 mm and 40 mm length the difference in
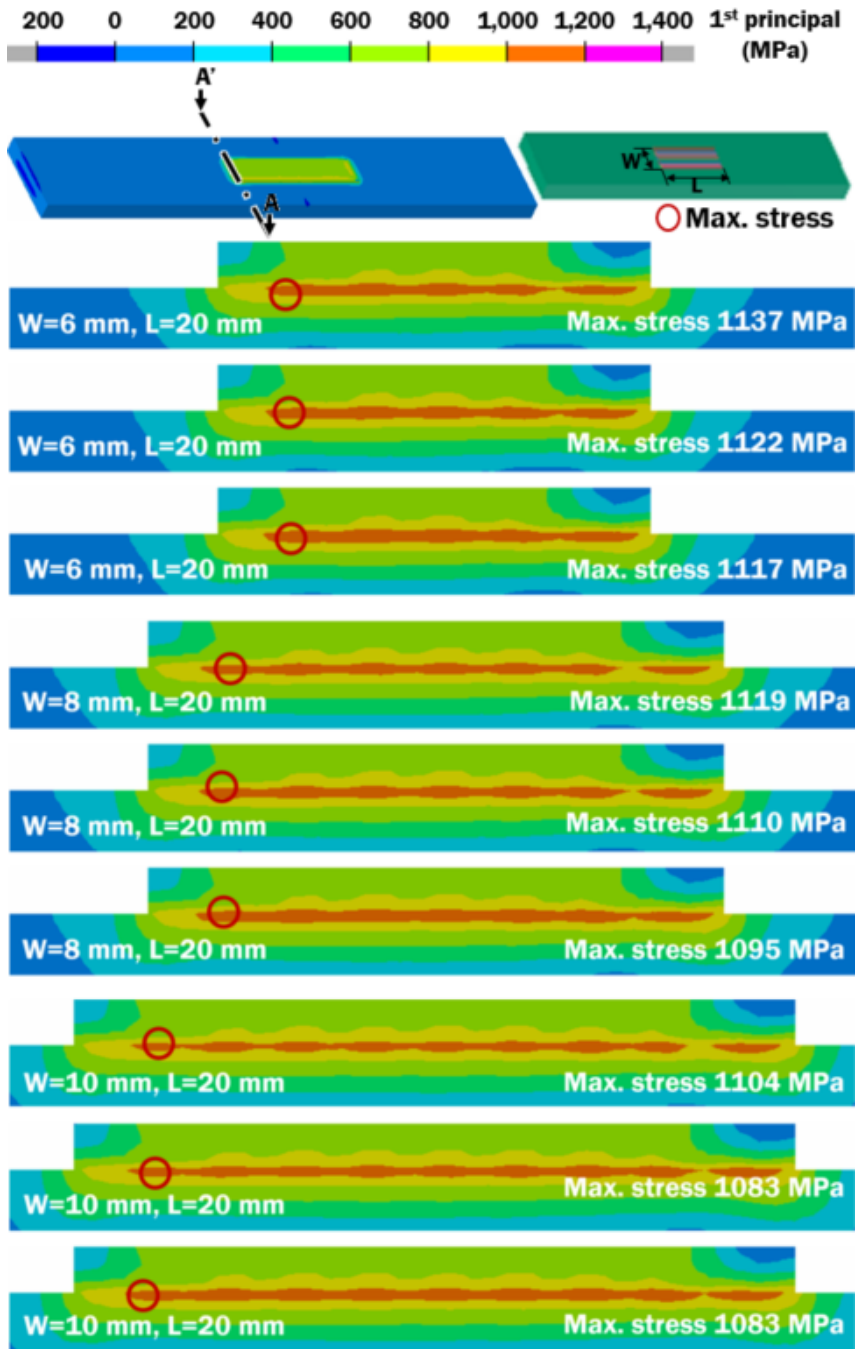
Fig. 43 1st principal stress in section A-A' according to deposited width (W) and length (L) (Deposition material: Inconel 718, substrate: AISI 1045)
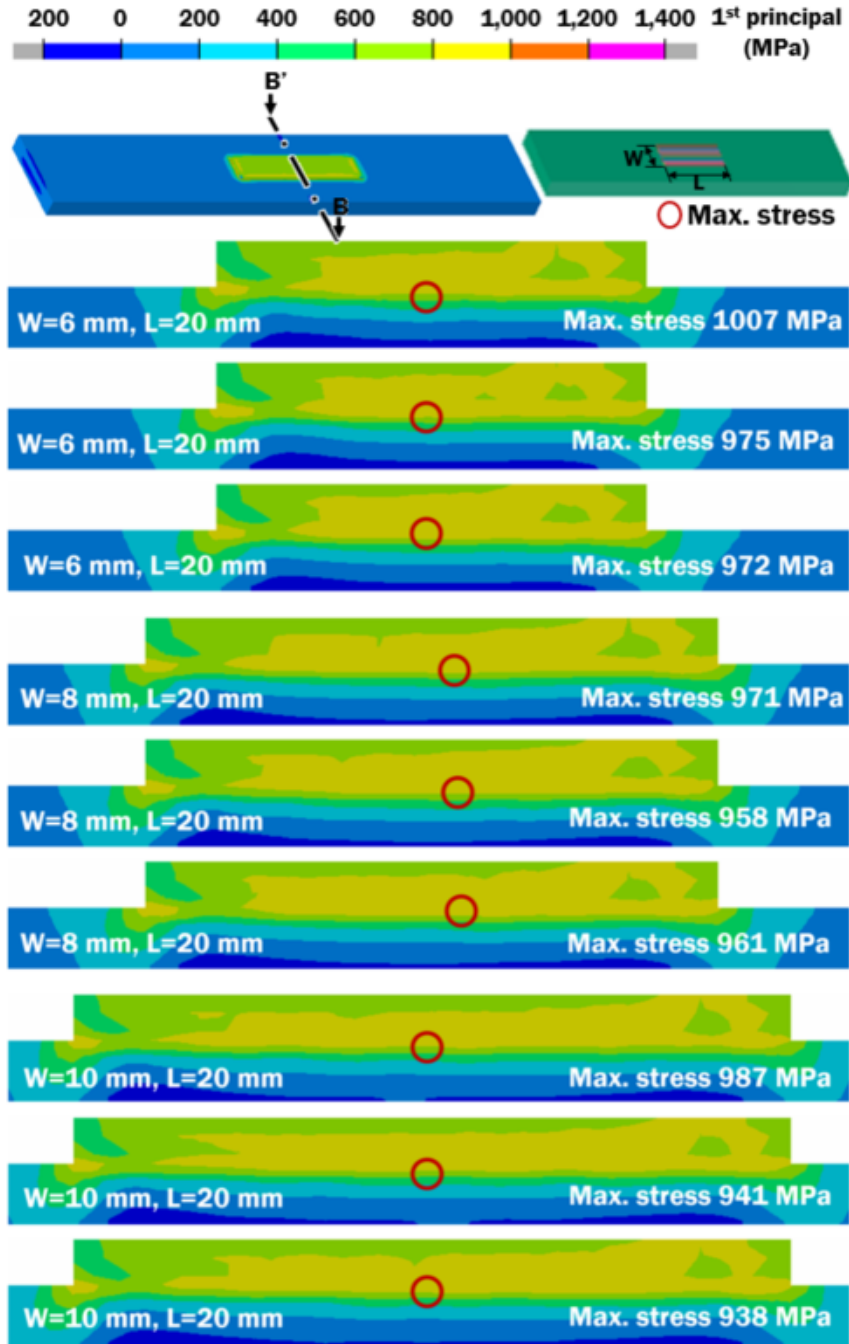
Fig. 44 1st principal stress distribution in section B-B' according to deposited width (W) and length (L) (Deposition material: Inconel 718, substrate: AISI 1045)
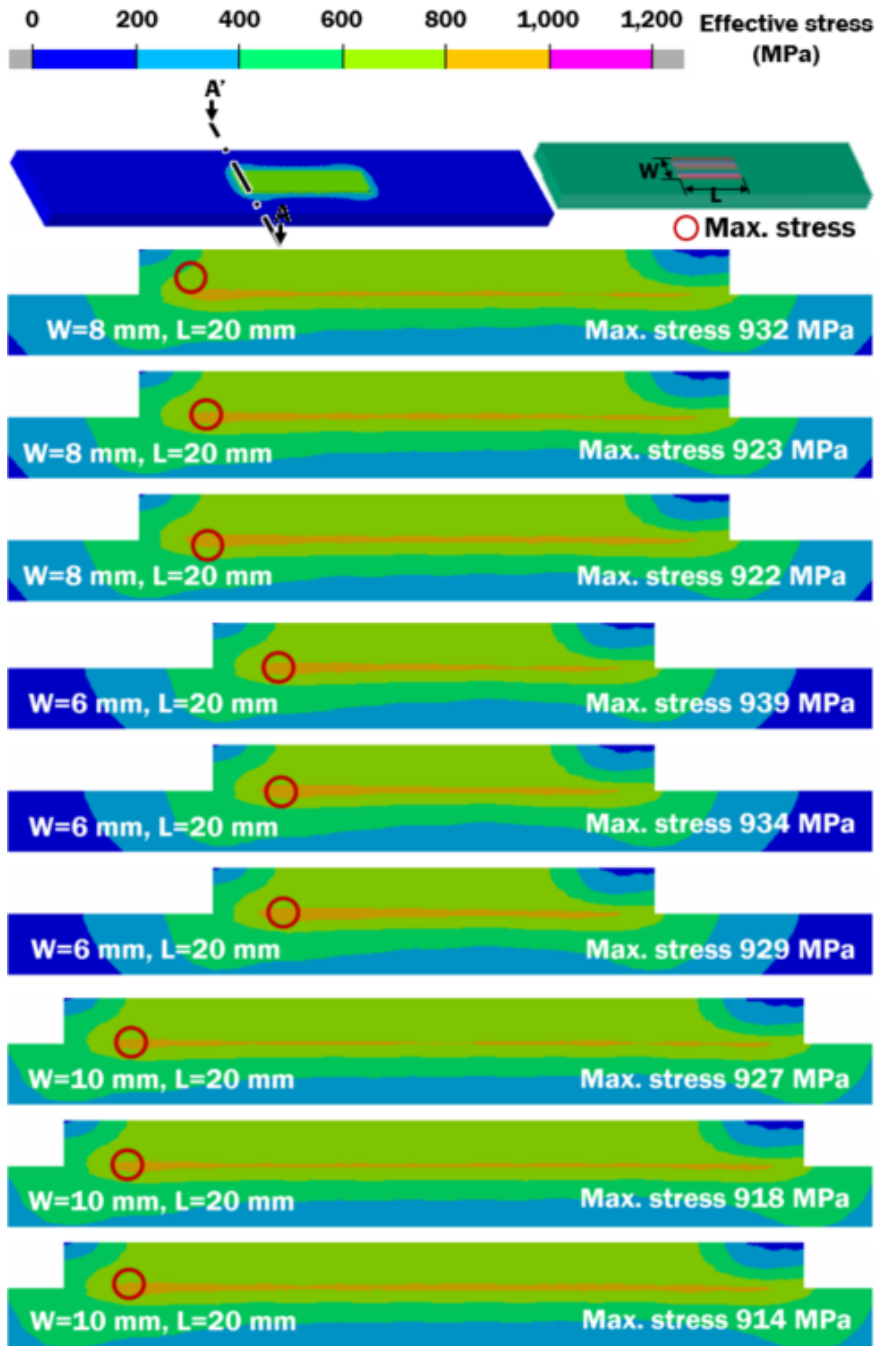
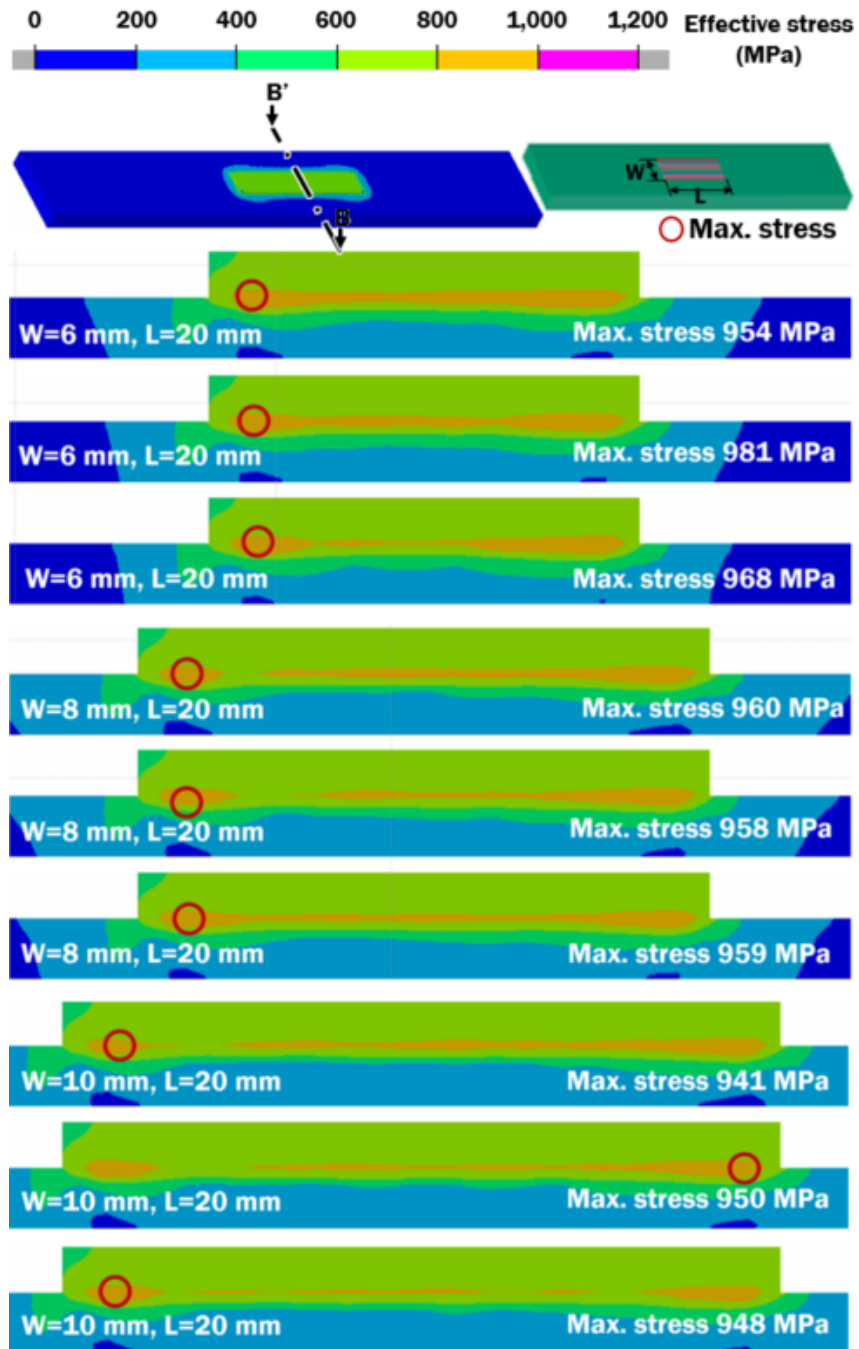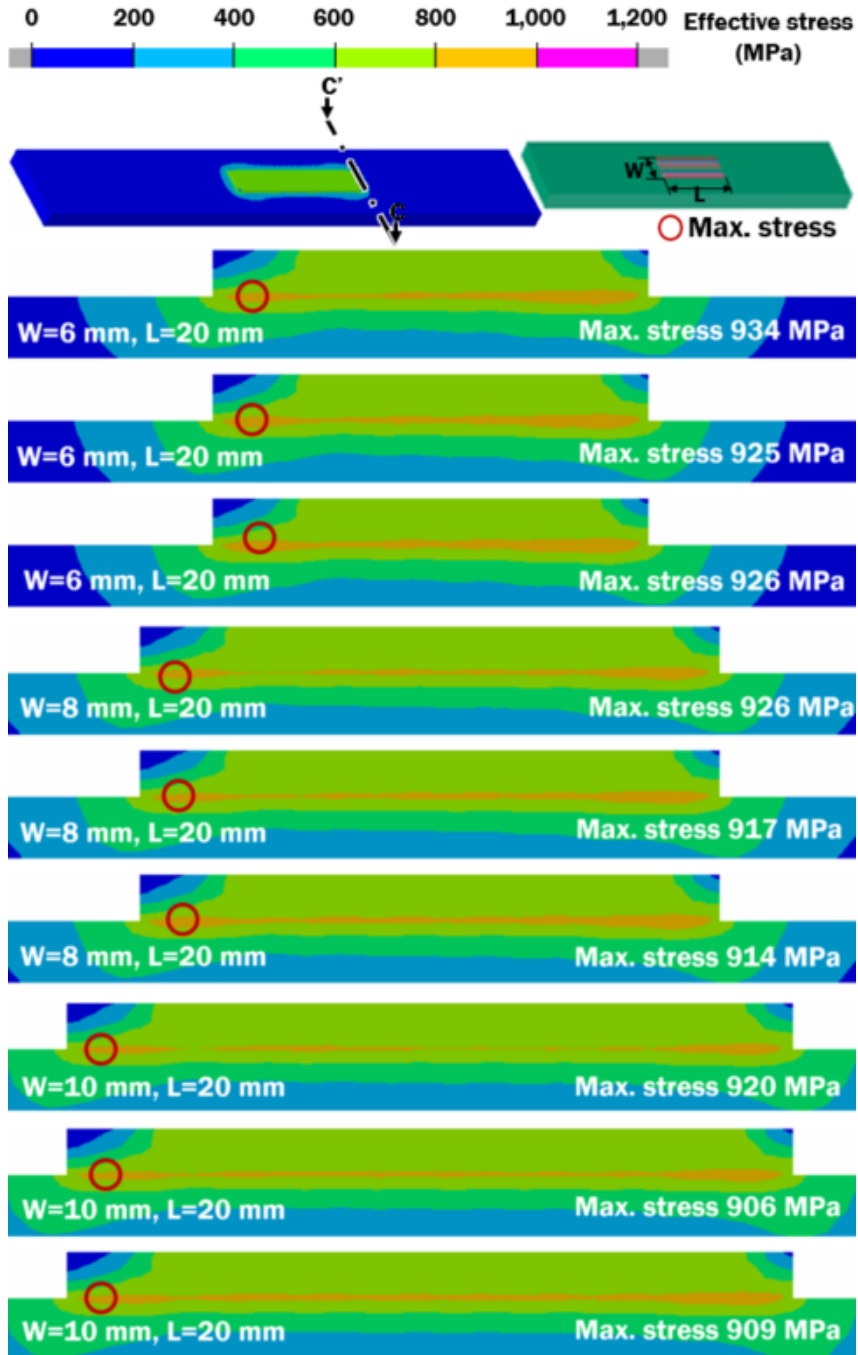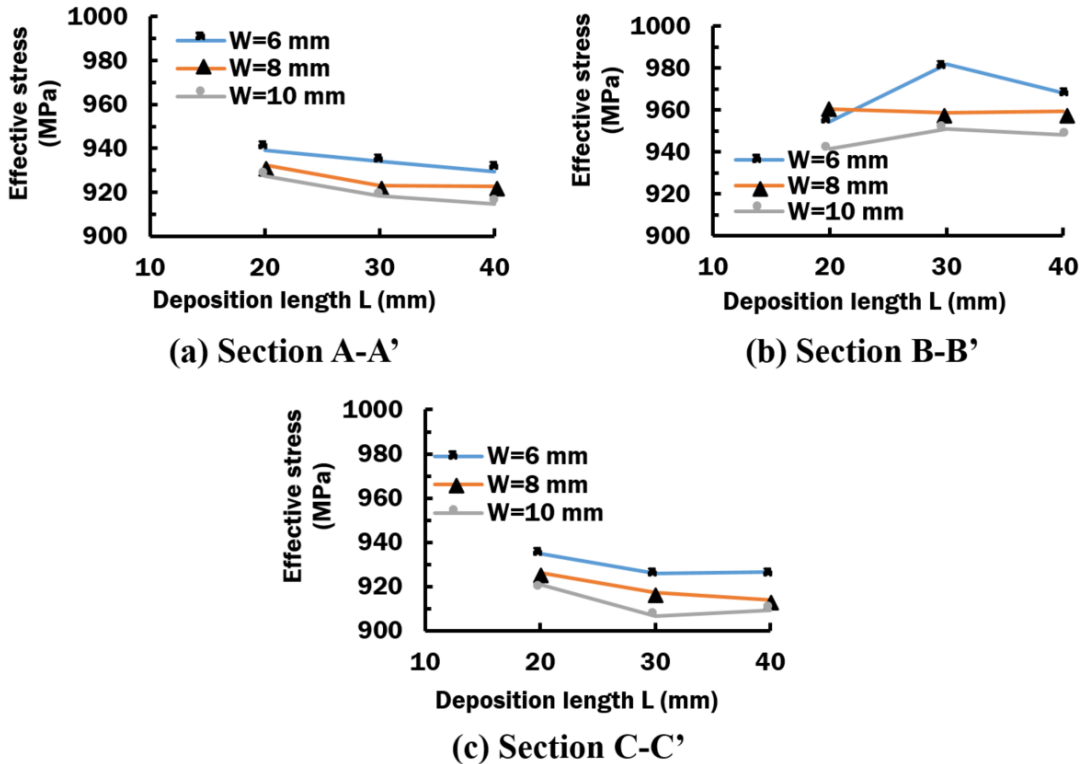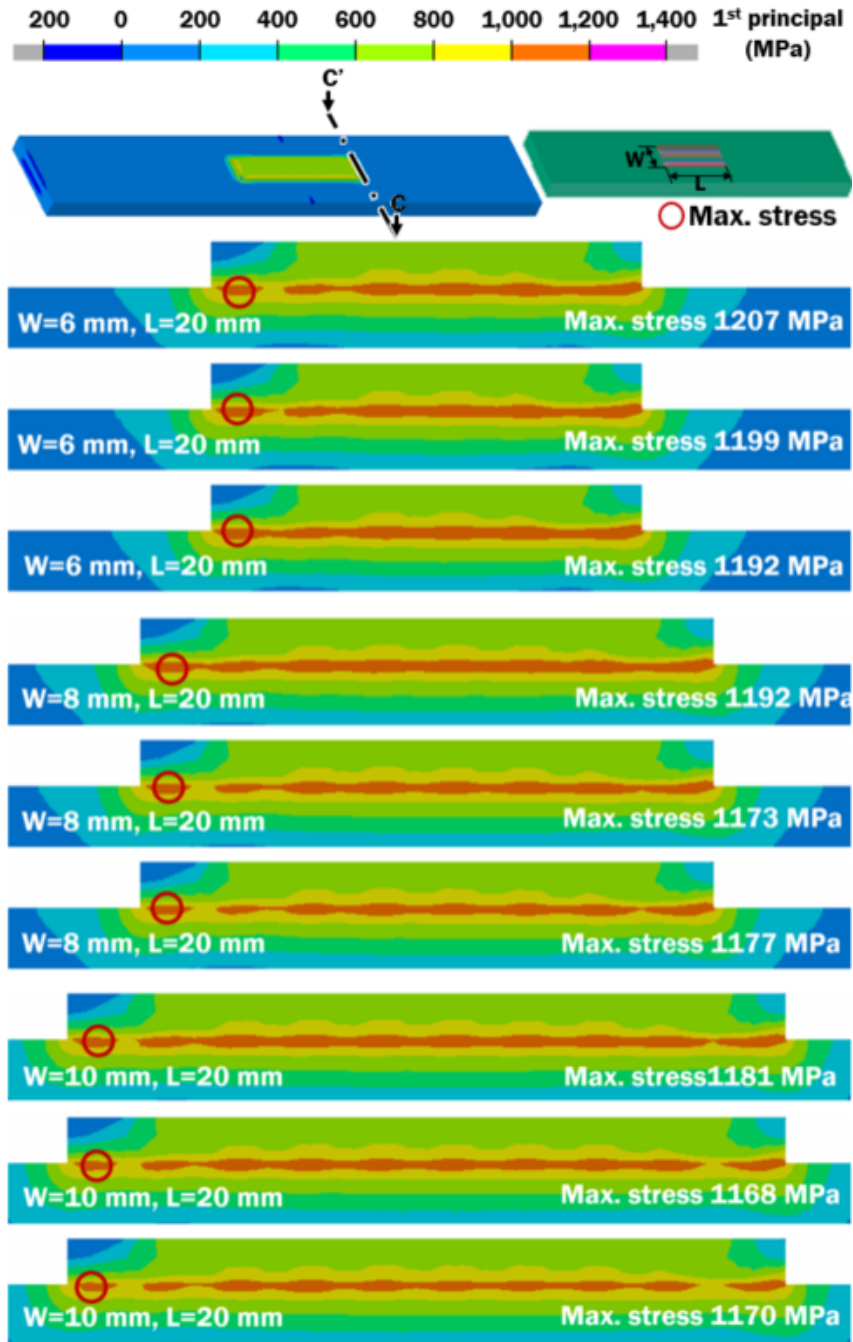**Fig. 45 1st principal stress distribution in section C-C' according to deposited width (W) and length (L) (Deposition material: Inconel 718, substrate: AISI 1045)**
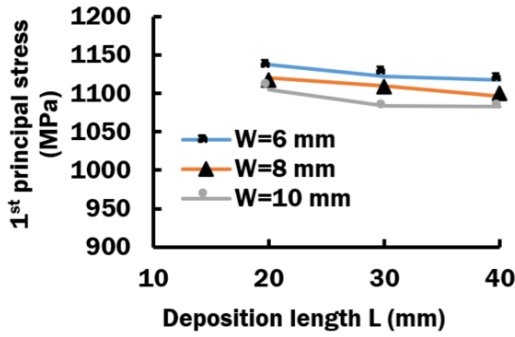
(a) Section A-A'
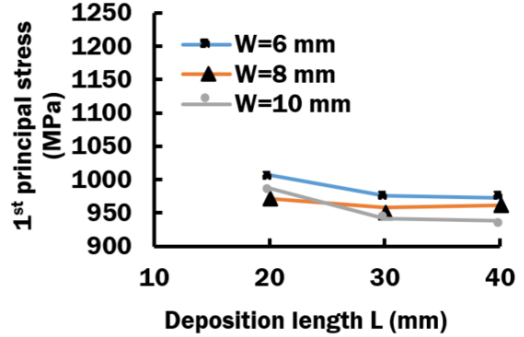
(b) Section B-B'
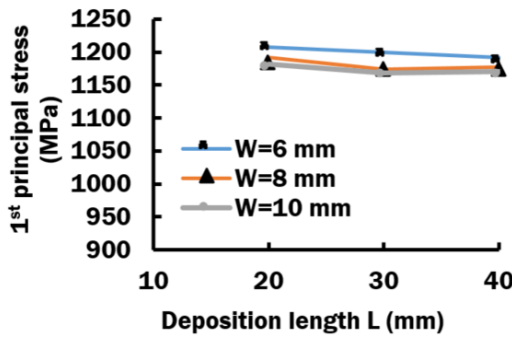
(c) Section C-C'

Fig. 46 Influence of deposited width (W) and length (L) on maximum 1st principal stresses according to cross-section (Deposition material: Inconel 718, substrate: AISI 1045)

maximum stress is low. The stress is lower with increased length in case of 6 mm and 10 mm width while opposite is true for the case of 8 mm width. The cross-section C-C' goes through the edge of the bead closer to the free end of the substrate as shown in Fig 45. Similarly, to other cross-section views the stress distribution pattern and location of maximum stress is similar for all models. Stress concentration region is under the deposited bead near the top surface of the substrate. The maximum stress location is under the 1st bead. In all cases the highest maximum stress is at 20 mm length. The stresses are lower with increased length in case of 6 mm width and 8 mm width. However, in case of 10 mm width the maximum stress is the lowest at the 30 mm length with slight increase at 40 mm length. The maximum stresses are summarized in Fig. 46. All cases showed similar pattern of displacement distribution as shown in Fig. 47. When
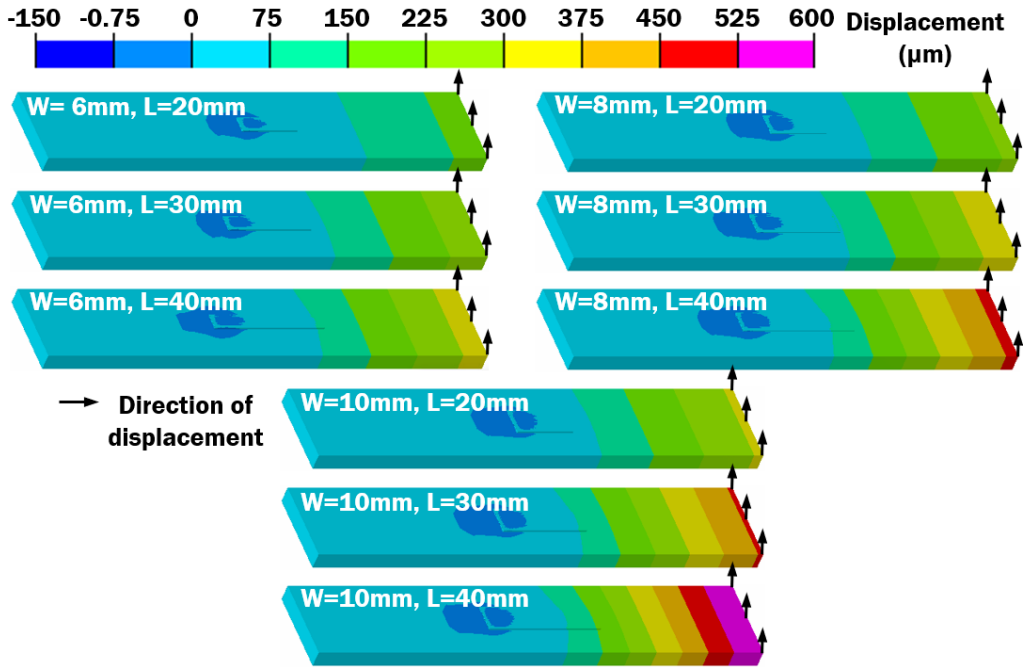
Fig. 47 Displacement distribution according to deposited width (W) and length (L) (Deposition material: Inconel 718, substrate: AISI 1045)
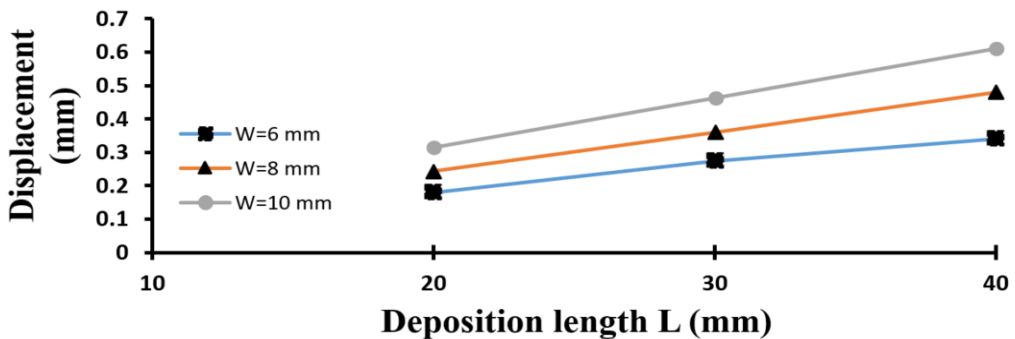
Fig. 48 Maximum displacement according to deposited width (W) and length (L) (Deposition material: Inconel 718, substrate: AISI 1045)

displacement is compared the higher dimensions contribute to higher maximum displacement as shown on Fig. 48. The increase in width as well as increase in length contribute to greater. This is due to increased force acting on substrate because larger force is acting on the part when bigger region is deposited. The increase in length contribute to higher distortion.

C. Thermo-Mechanical Characteristics of Inconel 718 Deposited on AISI 1045 Substrate According to Deposited Height

1. Finite Element Models

In order to analyze the effects of deposited total of three different height of deposition were selected. The selection was based on the number of layers. 6, 9 and 12 layers were selected for the analysis of thin wall deposition. The purpose of the analysis is to evaluate the changes in thermal stresses and displacement due to increased height of deposited bead. Table 10 shows number of nodes and meshes.

All the models have same boundary conditions as shown in Fig 49, except the height of deposited bead. Substrate dimensions and clamping conditions are same for all the models and heat loss due to convection was considered from all surfaces except clamped region. Simple zig-zag deposition strategy along the long side of the substrate was used for the analysis. The width of

Fig. 49 Boundary conditions of FE models for analysis of the influence of height of deposited wall (Deposition material: Inconel 718, substrate: AISI 1045)

Table 10 Number of layers, nodes and elements according to height (H) of the wall (Deposition material: Inconel 718, substrate: AISI 1045)

H (mm)	1.385	2.135	2.885
Number of layers	6	9	12
Nodes (EA)	24,630	28,273	31,918
3D Elements (EA)	22,410	25,770	29,130

the wall is 3.5 mm or six beads in each layer.

The initial and ambient temperature was set to 20℃ and total of 40 minutes cooling in ambient environment was used for the analysis.

2. Results & Discussion

Cut through the mid-section of the models was used in order to analyze the inside residual stress distribution as shown in Fig 50. The distribution pattern of effective stress is similar in all three models. Deposited material has higher stresses closer to the top surface and lower surfaces closer to substrate. However, the region very close to substrate has the highest stress concentration. Which can be observed by evaluating planar stress distribution. Excessive effective stress is under the edges of the deposited bead and maximum stress is at the corner of deposited bead on top surface of the substrate. From planar stress distribution maximum stresses can be found and evaluated. According to analysis results the maximum effective stress is lower when more layers are deposited. This is due to heat input from upper layers increases the temperature of the substrate causing stress relaxation. In addition, stress distribution results show that overall stresses in the vicinity of deposited bead is lower with increasing number of layers.

Predicted results for the displacement are show in Fig. 51. The results show that higher number of deposited layers contributes to greater displacement. This result is in line with the residual stress results. Higher displacement facilitates lower residual stresses.
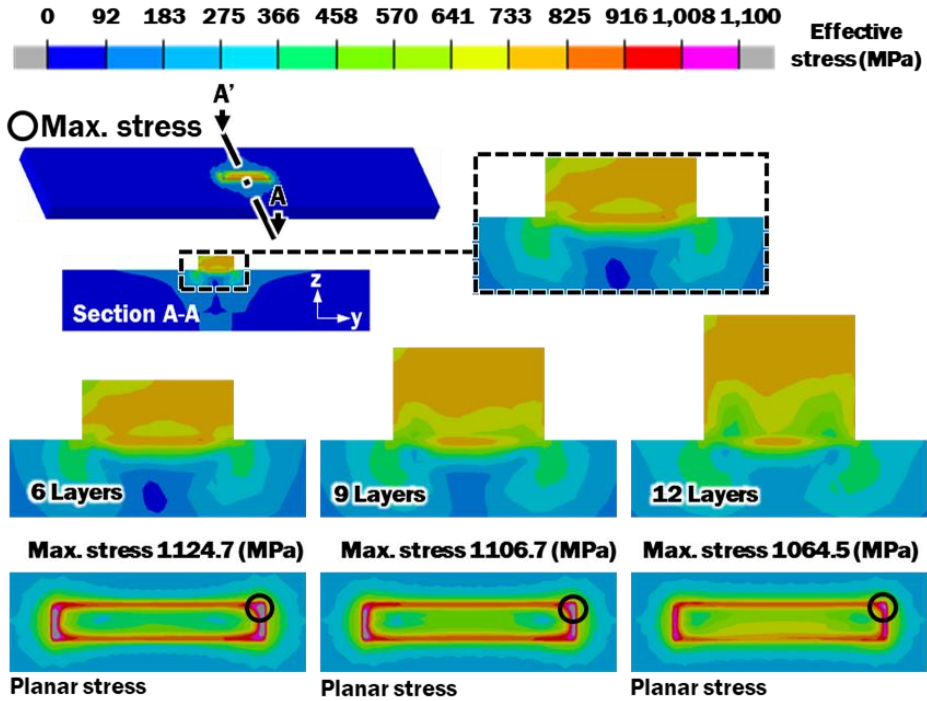
Fig. 50 Effective stress distribution according to deposited height (Deposition material: Inconel 718, substrate: AISI 1045)

**(a) Displacement distribution** **(b) Maximum Displacement**

Fig. 51 Influence of deposited height on displacement distribution and maximum displacement (Deposition material: Inconel 718, substrate: AISI 1045)

The difference in displacement between 6 and 9 layers is greater than the difference between 9 and 12 layers. This is due to decreasing effect of deposition on substrate with increasing of number of layers. With each additional layer heat is required to travel thicker material layer to reach the substrate hence decreasing the influence on the stress and displacement. However, long processing time can increase overall temperature of the substrate and give effect of stress and displacement relaxation.

D. Thermo-Mechanical Characteristics of G6 Deposited on SCM 440 Substrate According to Deposited Height

1. Finite Element Models

In this analysis G6 material was selected as a powder and SCM 440 as a substrate material. In order to investigate the effects of the height of deposited bead on the residual stress and displacement 3 cases were selected with 6, 9 and 12 layers of deposited clad. Each layer consists of 6 beads. Height of deposition clad and number of meshes and nodes is shown in Table 11.

Boundary conditions of FE models is shown in Fig 52. Fixed constraints are applied on one side and heat loss due to natural convection was applied to all surfaces. In addition, forced convection coefficient was applied on top surface during deposition process. The initial and ambient temperatures were set to 20°C and free air cooling was applied for 40 minutes.

Table 11 Number of layers, nodes and elements according to height (H) of the wall (Deposition material: G6, substrate: SCM 440)

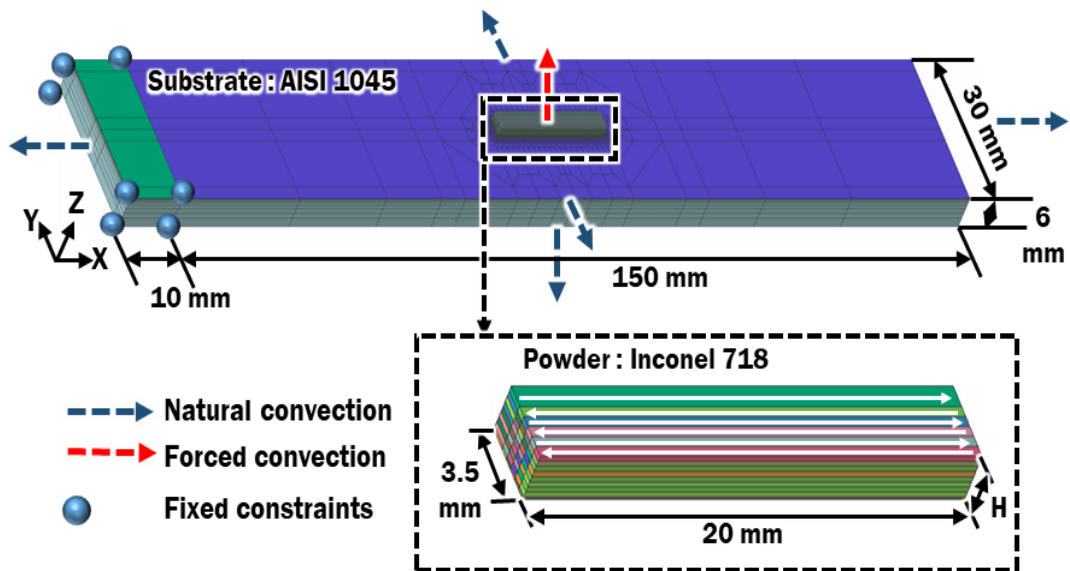| H (mm)	3.625	5.5	7.375
Number of layers	6	9	12
Nodes (EA)	22,812	26,025	29,238
3D Elements (EA)	20,740	23,740	26,740
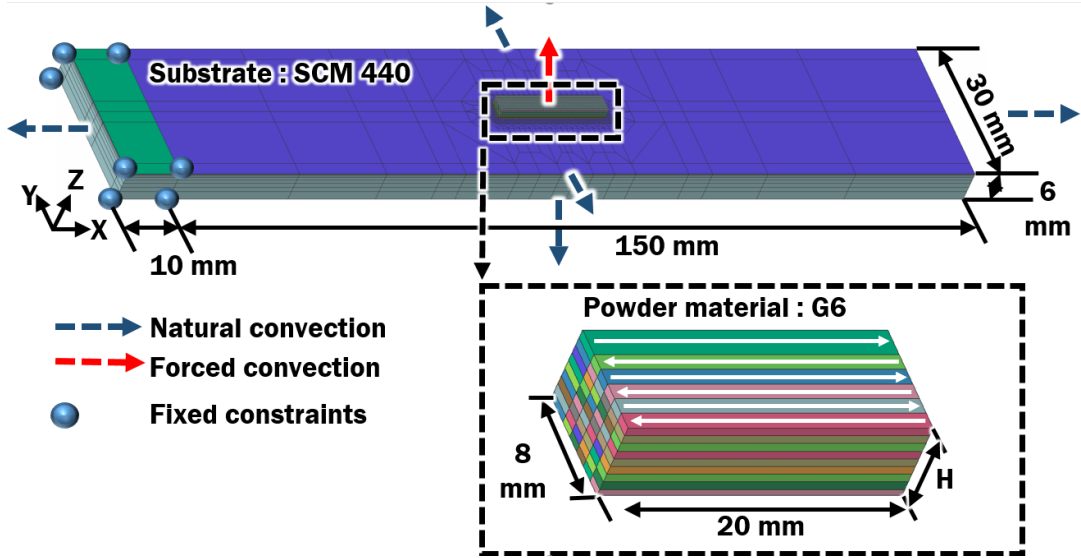
Fig. 52 Boundary conditions of FE models for analysis of the influence of height of deposited wall (Deposition material: Inconel G6, substrate: SCM 440)

2. Results & Discussion

In order to analyze internal thermal residual stress distribution section, cut through the center was selected as shown in Fig. 53. The mid-section stresses can show how stresses are distributed throughout the majority of the deposited part and substrate. Excessive stress concentration region is located under deposited bead close to top surface of the substrate. High stresses are primarily distributed inside substrate. Location of excessive stresses is slightly deeper with each additional bead. The depth of maximum stresses is approximately 80 µm from the top surface of the substrate. Stress distribution is similar in all three cases. The distribution of stresses is asymmetrical. The location of the maximum stress is same for all three cases. According to predicted results the overall stresses as well as maximum effective stress is decreased with increase of deposited layers. Stresses are significantly decreased between each case which can be attributed to high energy input because heat from the deposition nozzle increases overall
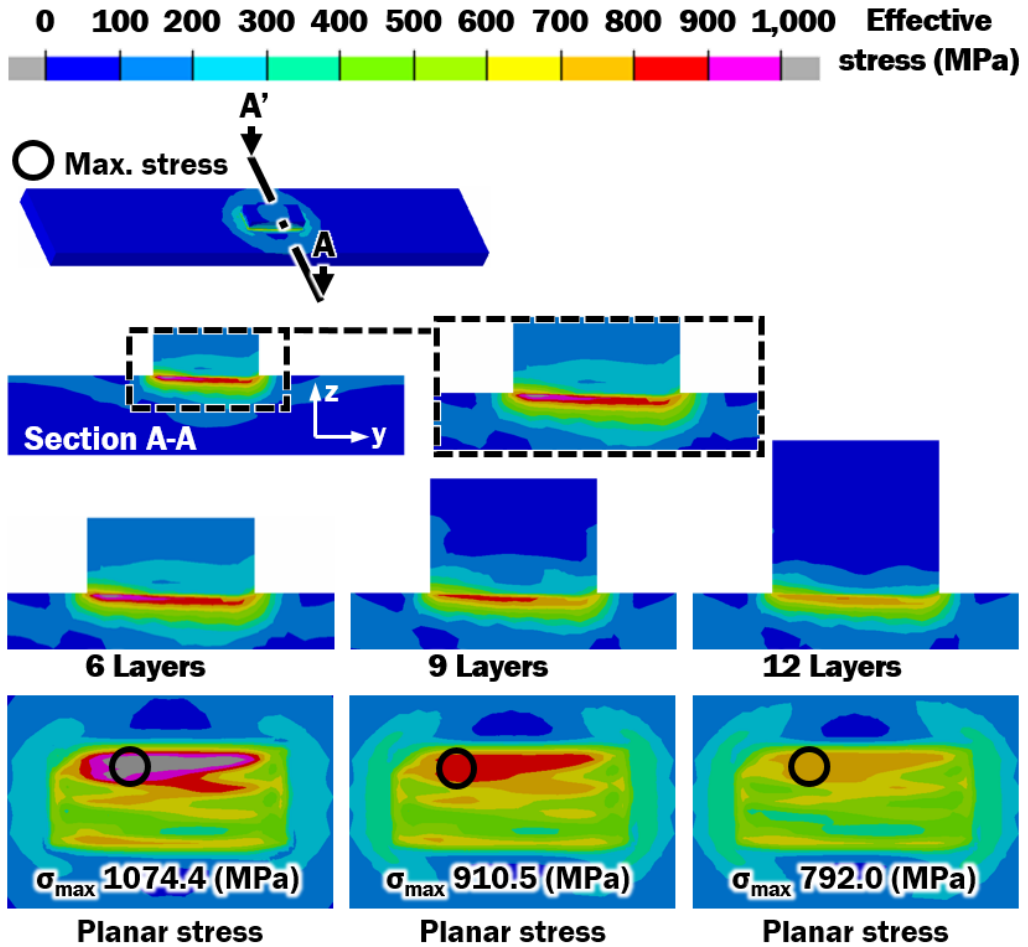
Fig. 53 Influence of deposition height on effective stress distribution (Deposition material: Inconel G6, substrate: SCM 440)

temperature of the substrate and results in stress relaxation.

The displacement results are shown in Fig. 54. According to obtained results the displacement is increasing with increasing the number of deposited layers. The rate of displacement increase is lower with increasing of the height of deposition. The difference in maximum displacement between 6 layers and 9 layers is 0.110 mm but only 0.024 mm between 9 layers and 12 layers wall. This result show that increasing height of deposited clad the effect of energy and high
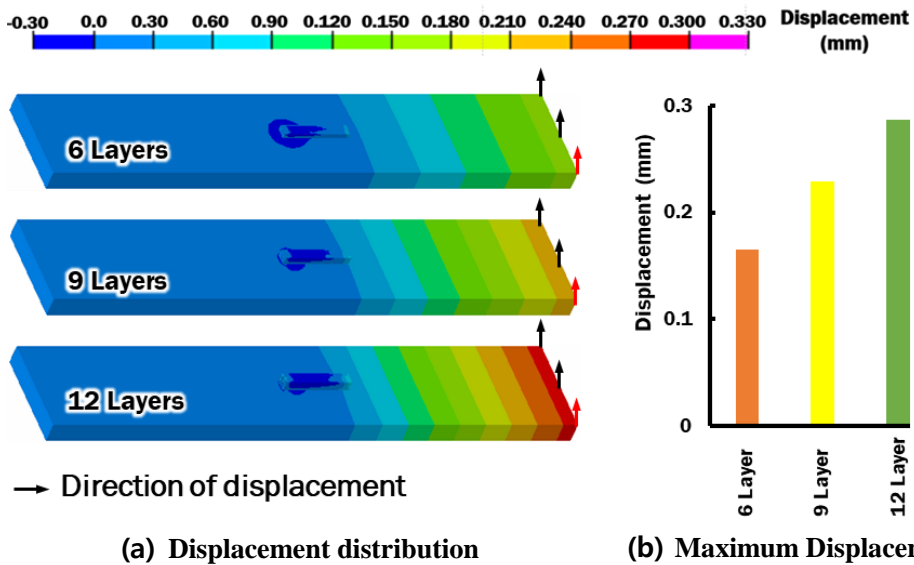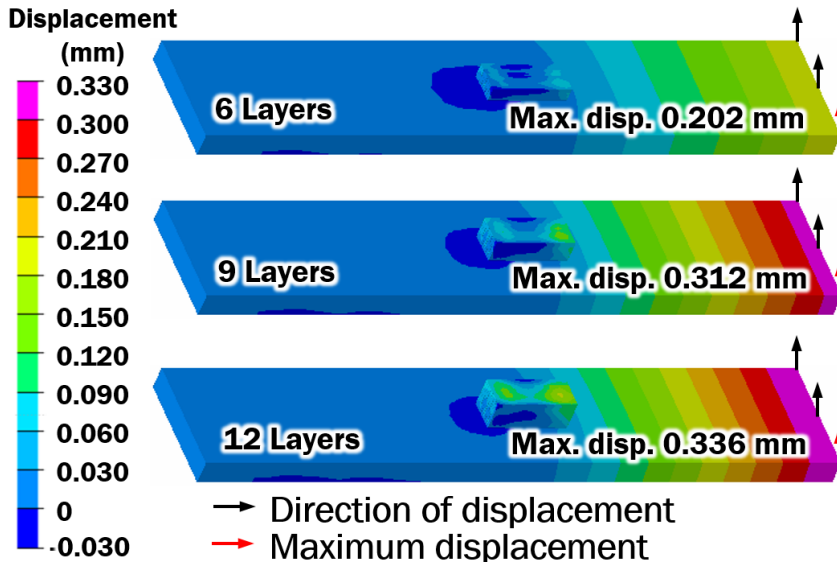
Fig. 54 Influence of deposition height on displacement distribution and maximum displacement (Deposition material: Inconel G6, substrate: SCM 440)

temperature input on substrate reduces. In addition, this result show that the lower stresses in case of taller deposited clad resulted in increased displacement.

E. Thermo-Mechanical Characteristics of Inconel 718 Wall Deposited on AISI 1045 Substrate by Proper Deposition Pattern

1. Finite Element Models

In this analysis selected proper deposition pattern for Inconel 718 powder was used to deposit thin wall. Boundary conditions of the analysis models are shown in Fig. 55. 9 layers deposition analysis was selected for the analysis. The results are compared to 9 layers deposited by simple zig-zag_X scanning pattern and this wall will be denoted farther in the text as zig-zag_X wall. Similarly, to previous analysis, heat losses due to convection and radiation were estimated using temperature dependent properties of materials and gases. Proper deposition pattern is based on

Fig. 55 Boundary conditions of FE models for the evaluation of effects of proper deposition strategy (Deposition material: Inconel Inconel 718, substrate: AISI 1045)

RZ-7 deposition pattern which has all odd number layers starting from the first deposited along the short side of substrate and even layers are deposited along the long side of substrate. Wall deposited by selected deposition pattern will be denoted farther as RZ-7 wall. For both cases the deposited clad has exact same dimensions. The comparison is based on the residual stresses and displacement results.

2. Results & Discussion

The predicted results of effective stress show change in stress distribution inside the deposited wall as can be seen in Fig. 56. RZ-7 wall shows lower stresses closer to the surfaces of the build material while zig-zag_X wall shows stresses distributed throughout the wall including the outside surfaces. In order to evaluate maximum stresses planar stress distribution was investigated. Excessive stress concentration shows in case of zig-zag_X wall shows stresses at the edges between deposited wall and substrate. However, in case of RZ-7 wall excessive stresses are more scattered and located under the layers deposited after contour bead. Surface stresses are
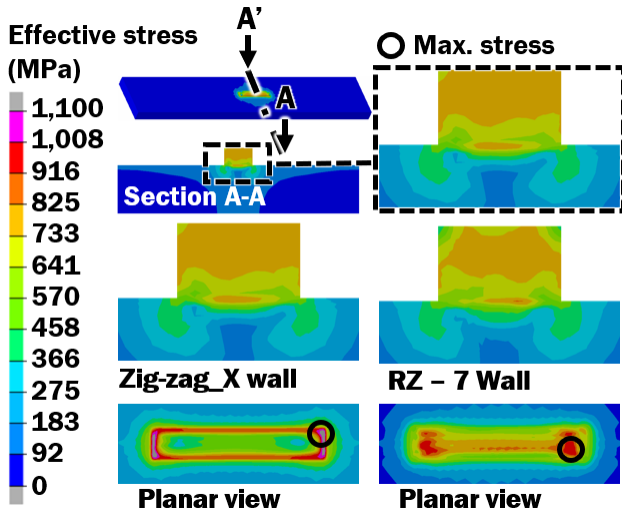
(a) Effective stress distribution
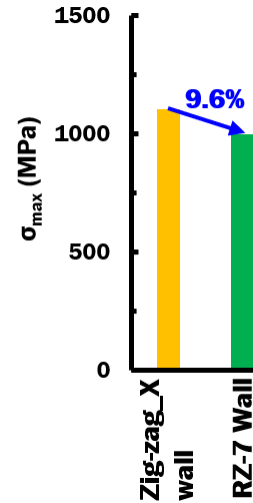
(b) Max. effective stress

Fig. 56 Comparison of effective stress results between RZ-7 and zig-zag_X walls (Deposition material: Inconel Inconel 718, substrate: AISI 1045)

(a) 1st principal stress distribution

(b) Max. 1st principal stress

Fig. 57 Comparison of 1st principal stress results between RZ-7 and zig-zag_X walls (Deposition material: Inconel 718, substrate: AISI 1045)

more dangerous because they can become the cause of crack propagation. The maximum effective stress magnitude was reduced by 9.6 % when proper deposition path is applied as shown

(a) Displacement distribution **(b) Max. displacement**
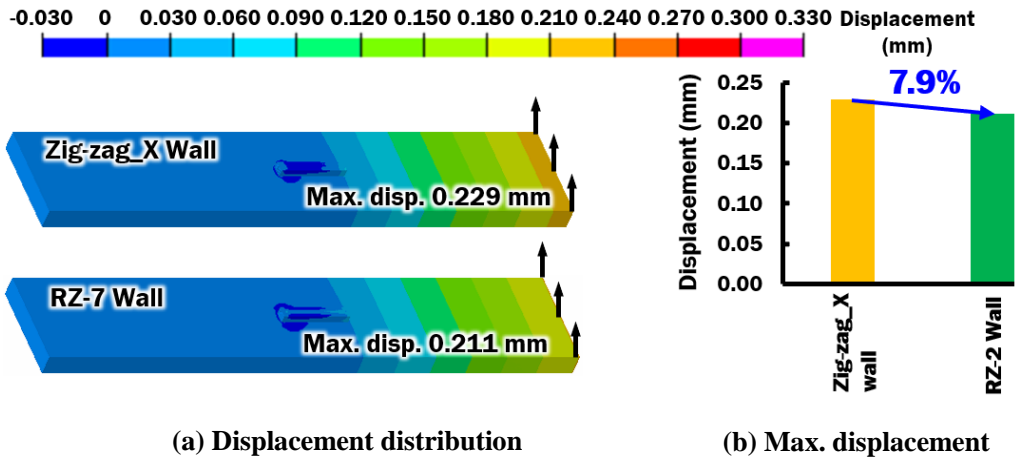
Fig. 58 Comparison of displacement results between RZ-7 and zig-zag_X walls (Deposition material: Inconel 718, substrate: AISI 1045)

in Fig. 56 (b). From this result it can be noted that proper deposition pattern can improve stress distribution and reduce maximum stresses in the vicinity of deposited region.

The results for 1st principal stress is illustrated in Fig. 57. Stress distribution in mid-section shows that stress concentration region is at the corners between wall and substrate. zig-zag_X wall shows higher stresses along the surface inside the wall and RZ-7 shows higher stresses along the top surface. Planar stress distribution was investigating to evaluate maximum stresses. Excessive 1st principal stress concentration region is similar for both cases however proper deposition pattern shows lower planar stresses and maximum first principal stress is reduced by 4.1% as illustrated on Fig. 57 (b).

The displacement results can be found on Fig. 58. The analysis results show upward displacement at the unclamped side of the substrate for both cases. The selected strategy RZ-7 showed 7.9 % decrease in the maximum displacement compared to zig-zag_X wall by zig-zag strategy, as can be seen on Fig. 58 (b). From this result it can be noted that the proper deposition strategy can lower residual stress in the vicinity of deposited region as well as displacement in the substrate.

F. Thermo-Mechanical Characteristics of G6 Wall Deposited on SCM 440 Substrate by Proper Deposition Pattern

1. Finite Element Models

Analysis of G6 powder deposition on SCM 440 resulted in minimum distortion when RZ-4 strategy is applied, hence this strategy was selected for farther analysis of wall deposition. Total
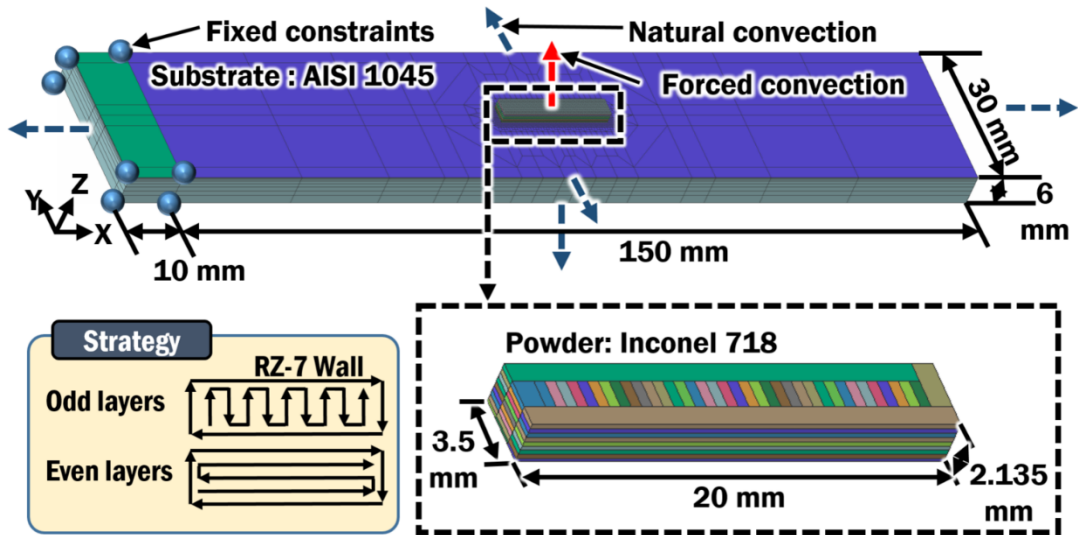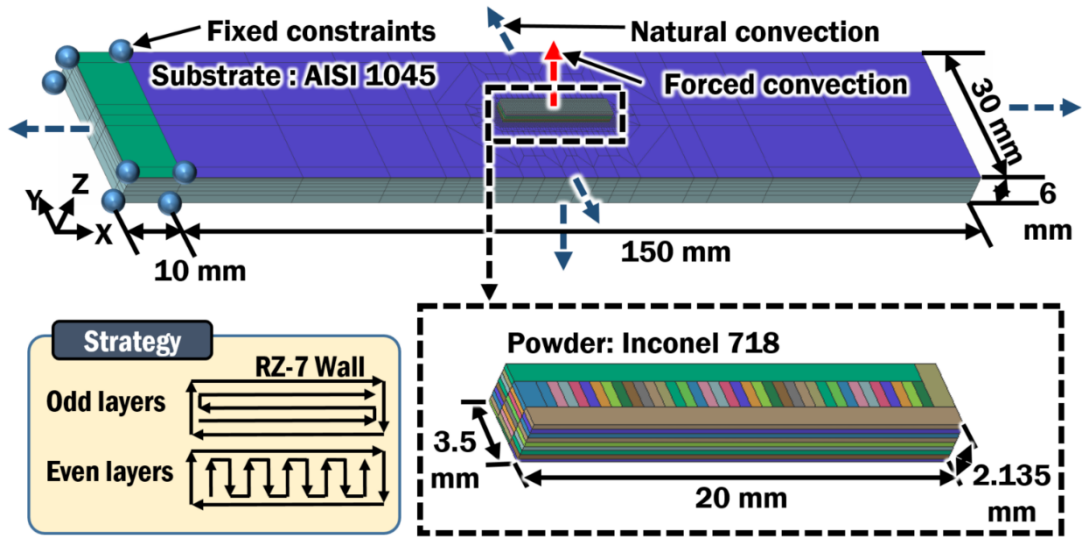

Fig. 59 Boundary conditions of FE models for the evaluation of effects of proper deposition strategy (Deposition material: G6, substrate: SCM 440)

of 9 layers were deposited with the height of 5.5 mm as shown in Fig. 59. Boundary conditions and deposition strategy are shown in Fig. 59. RZ-4 deposition pattern consists of odd layers deposited along the length and even layers along the width of the substrate. Post process thermo-mechanical characteristics by RZ-4 strategy is compared to simple zig-zag in x direction pattern for deposition of multi-bead 9 layer wall. Wall deposited by zig-zag strategy will be denoted farther as zig-zag_X wall and wall by selected strategy is denoted as RZ-4 wall. Same boundary conditions such as clamping, dimensions of substrate and bead are used. Heat losses were
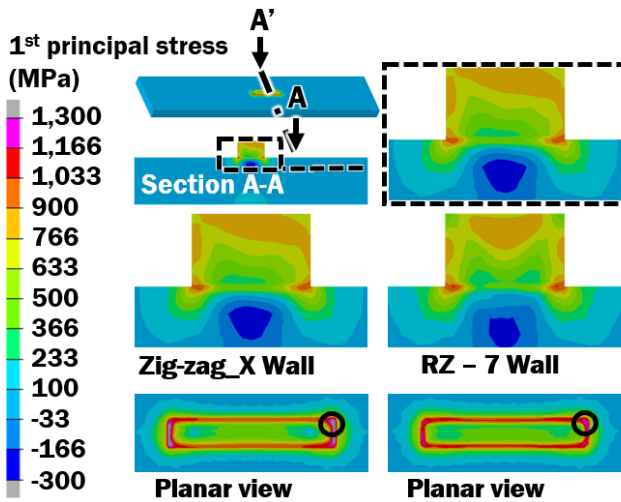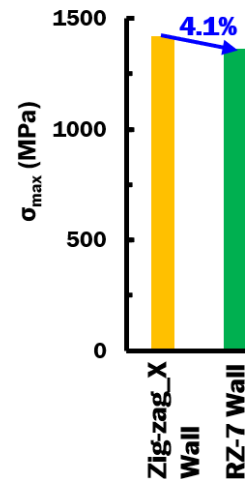
(a) Effective stress distribution **(b) Max. effective stress**
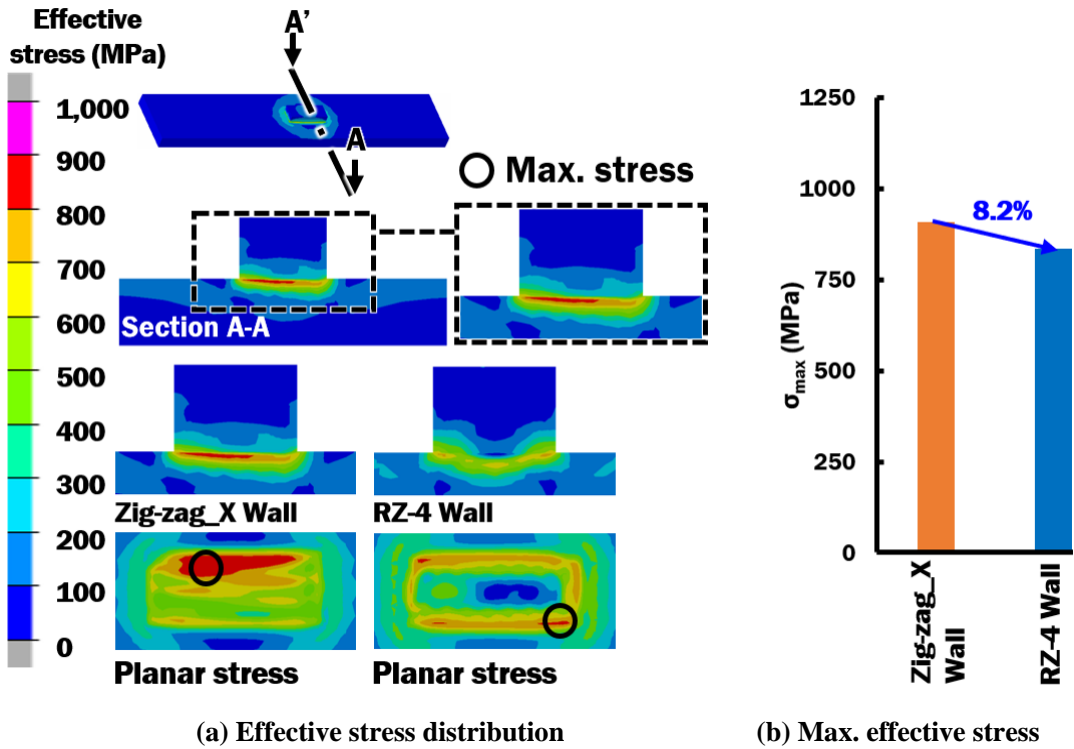
Fig. 60 Comparison of the effective stress results between RZ-4 wall and zig-zag_X walls (Deposition material: G6, substrate: SCM 440)

estimated using temperature dependent properties of Ar and Air. Results are compared in terms of residual stress and displacement.

2. Results & Discussion

Fig 60 shows analysis results for effective stress distribution for two walls. According to predicted results deposition of zig-zag_X wall showed asymmetrical stress distribution. Stress magnitude is varying greatly throughout the model. RZ-4 wall on the other hand showed symmetrical and uniformly distributed stress in cross-section through the mid-section. In order to evaluate maximum stresses due to deposition process planar effective stress distribution is

(a) 1st principal stress distribution   **(b) Max. 1st principal stress**
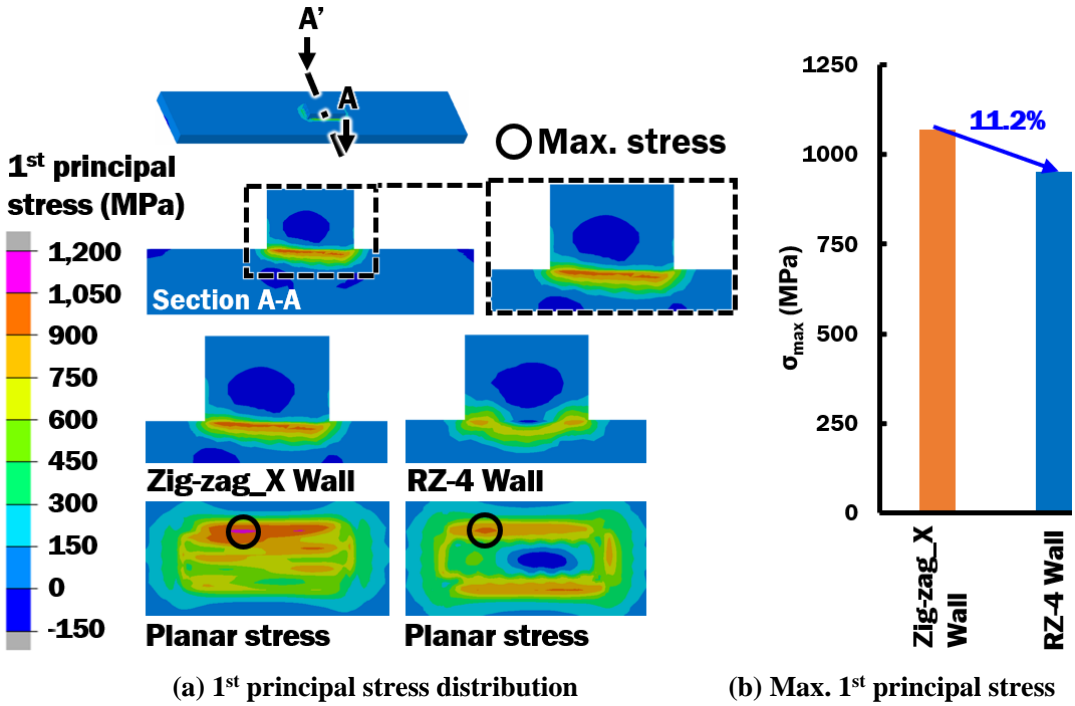
Fig. 61 Comparison of 1st principal stress results between RZ-4 wall and zig-zag_X wall (Deposition material: G6, substrate: SCM 440)

evaluated as shown in Fig 60 (a). The depth of excessive residual stresses is approximately 80 µm. RZ-4 wall showed uniform effective stress distribution with two axis symmetry. zig-zag_X wall, however, showed asymmetric stress distribution with highly concentrated stress on one side of the substrate. Reduction of maximum residual stress by 8.2 % was obtained due to RZ-4 deposition strategy as shown in Fig. 60 (b).

Results of the analysis for 1st principal stress are shown in Fig. 61 Similarly to effective stress, 1st principal stress distribution in cross section cut through the center shows asymmetrical distribution for zig-zag_X wall and symmetrical distribution in case of RZ-4 wall as can be observed form Fig 61 (a). Evaluation of maximum stresses and excessively concentrated stress region is accomplished through investigation of planar stress distribution which is approximately 80 µm deep. RZ-4 wall showed more symmetrical stress distribution compared to zig-zag_X

(a) 1st principal stress distribution   (b) Max. 1st principal stress
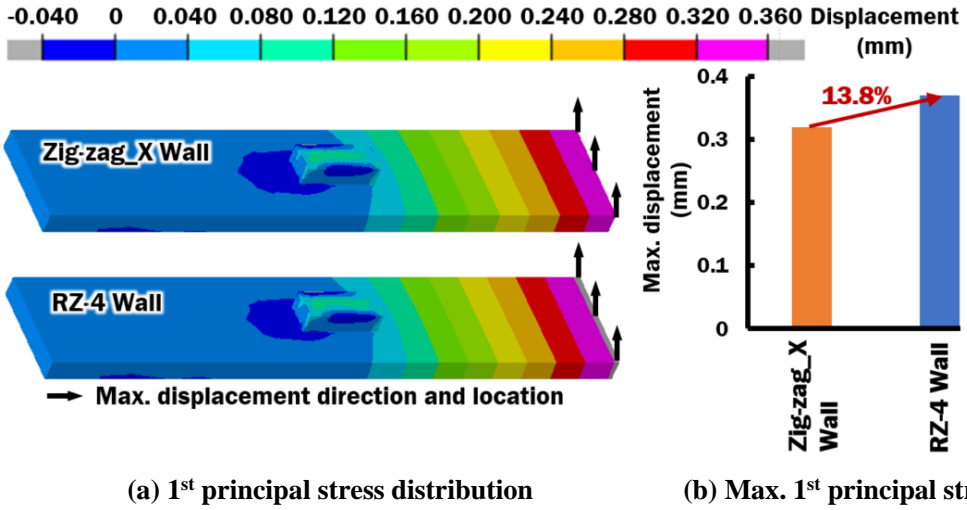
Fig. 62 Comparison of displacement results between RZ-4 wall and 9 layers wall (Deposition material: G6, substrate: SCM 440)

wall. Maximum 1st principal stress was reduced by 11.2 % when proper deposition strategy is applied, as can be seen on Fig. 61 (b).

Displacement distribution and maximum displacement are shown in Fig. 62. Upward displacement in both cases can be observed. Maximum displacement is at the free end of the substrate. When maximum displacement is compared selected deposition pattern showed 13.8% increase in maximum displacement as shown in Fig 62 (b).

From the results of above post process thermos-mechanical characteristics evaluation it can be noted that selected deposition path can reduce effective and 1st principal stress but failed to control the displacement. Thus deposition of G6 powder on SCM 440 substrate requires farther evaluation.

IV. CONCLUSION & FUTURE WORKS

Effects of deposition strategies on thermo-mechanical characteristics of Inconel 718 deposited on AISI 1045 and G6 deposited on SCM 440 substrate were investigated. It was revealed in this work that deposition path has significant influence on residual stress distribution as well as effects on displacement and distortion. According to the results of the analysis excessive stress concentration region is under deposited area near the top surface of substrate in case of Inconel 718 and AISI 1045 and at a depth of around 80 µm in case of G6 and SCM440. Zig-zag deposition strategies showed better uniformity and symmetry of stress compared to raster deposition strategies. Contour bead significantly reduced maximum stresses in all cases of deposition and RZ-3 in case of Inconel 718 deposition and RZ-4 in case of G6 deposition showed low maximum 1st principal stress, low distortion and uniform stress distribution hence they are selected as proper deposition patterns.

Thermo-mechanical analysis according to the shape of deposited bead were investigated. Three different width and three different length for each width were selected for analysis of 3 layers deposition. According to predicted results, the effect of increased width and length of deposition does not have significant effect on residual stress distribution and maximum stresses however the major trend is showing slight decrease in stresses with larger area of deposition. According to deposition area displacement is increased with increasing area of deposition bead and increasing height of deposition bead results in lower residual stress but higher displacement. Residual stresses are not affected by the shape of deposited clad. Deposition of Inconel 718 by the RZ-7 strategy resulted in reduced effective and 1st principal stresses as well as displacement. Deposition of wall by G6 powder using the RZ-4 strategy resulted in reduced effective and 1st principal stress, however, significantly increased displacement. Possible reasons for different behavior of G6 deposited on SCM 440 can be difference in thermos-physical material properties. Another factor is the difference in characteristic dimensions of deposited bead and different

parameters of deposition nozzle such as laser power, scanning speed and shield gas flow rate.

For the future works additional scanning pattern are to be investigated. In this study the starting point for each layer in each case study was the same but starting each layer with different starting point can have significant effect on post process thermo-mechanical characteristics of deposited material and substrate. In addition, effects of material properties should be investigated. As the next step, other process parameters combined with deposition strategies can be investigated including scan speed, laser power, powder flow rate and etc.

REFERENCES

1. ASTM International. Standard Terminology for Additive Manufacturing Technologies; ASTM International F2792-12a; ASTM International: West Conshohocken, PA, USA, 2012.

2. Pham, D.T., Gault, R.S., "A comparison of rapid prototyping technologies, Int. J. Mach. Tools Manuf,, Vol. 38, pp. 1257-1287, 1998.

3. Scott, J.A., Weber, C.L., Newsome, S., Wohlers, T.T., "Additive Manufacturing: Status and Opportunities," 2012.

4. Ahn, D. G., "Directed Energy Deposition (DED) Process: State of the Art," International Journal of Precision Engineering and Manufacturing-Green Technology, Vol. 8, No. 2, pp. 703–742, 2021.

5. Mudge, R. P., Wald. N. R., "Laser Engineered Net Shaping Advances Additive Manufacturing and Repair," Welding, pp 44-48, 2007.

6. Hedges, Martin, and Neil Calder. "Near Net Shape Rapid Manufacture & Repair by LENS," edited by Neotech Services, 2006.

7. Alfaify, A., Saleh, M., Abdullah, F. M., Al-Ahmari, A. M., "Design for Additive Manufacturing: A Systematic Review," Sustainability, Vol. 12, No. 19, pp. 7936. 2020.

8. Vayre, B., Vignat, F., Villeneuve, F., "Designing for additive manufacturing," Procedia CIRP, Vol. 3, pp. 632–637, 2012.

9. Laverne, F., Segonds, F., Anwer, N., Le Coq, M., "DFAM in the design process: A proposal of classification to foster early design stages," In Proceedings of the Confere 2014 Croatie, Sibenik, Croatia, Vol. 3–4, 2014.

10. Edgar, J., Tint, S., "Additive manufacturing technologies: 3D printing, rapid prototyping, and direct digital manufacturing," Johns. Matthey Technol. Rev., Vol. 59, pp. 193–198, 2015.

11. Ameen, W., Al-Ahmari, A., Abdulhameed, O., "Design for metal additive manufacturing: An investigation of key design application on electron beam melting," Int. J. Mech. Aerosp. Ind. Mechatron. Manuf. Eng., Vol. 13, pp. 264–269, 2019.

12. Thompson, M.K., Moroni, G., Vaneker, T., Fadel, G., Campbell, R.I., Gibson, I., Bernard, A., Schulz, J., Graf, P., Ahuja, B., "Design for Additive Manufacturing: Trends, opportunities, considerations, and constraints," CIRP Ann., Vol. 65, pp. 737–760, 2016.

13. Setaki, F., Tenpierik, M., Turrin, M., van Timmeren, A., "Acoustic absorbers by additive manufacturing," Build. Environ., Vol. 72, pp. 188–200, 2014.

14. Dietrich, D.M., Cudney, E., "Impact of integrative design on additive manufacturing quality," Int. J. Rapid Manuf., Vol. 2, pp. 121–131, 2011.

15. Jiang, J., Ma, Y., "Path Planning Strategies to Optimize Accuracy, Quality, Build Time and Material Use in Additive Manufacturing: A Review," Micromachines, Vol. 11, No. 7, pp. 633, 2020.

16. Ahn, D. G., "Direct metal additive manufacturing processes and their sustainable applications for green technology: A review" International Journal of Precision Engineering and Manufacturing-Green Technology, Vol. 3, No. 4, pp 381–395, 2016.

17. Ahn, D. G., "Applications of laser assisted metal rapid tooling process to manufacture of molding & forming tools— State of the art," International Journal of Precision Engineering and Manufacturing, Vol. 12, No. 5, pp. 925–938, 2011.

18. Negi, S., Nambolan, A. A., Kapil, S., Joshi, P. S., Karunakaran, K. P., Bhargava, P., "Review on electron beam based additive manufacturing," Rapid Prototyping Journal, Vol. 26, No.3, pp. 485–498, 2020.

19. U.S. Department of Energy, "Quadrennial Technology Review 2015," Quadrennial Technology Review 2015, Available at: https://www.energy.gov/sites/prod/files/2015/11/f27/QTR20156AAdditive%20Manufacturing.pdf

20. Chua, B. L., Lee, H. J., Ahn, D.-G., and Kim, J. G., "Influence of Process Parameters on Temperature and Residual Stress Distributions of the Deposited Part by a Ti-6Al-4V Wire Feeding Type Direct Energy Deposition Process," Journal of Mechanical Science and Technology, Vol. 32, No. 11, pp. 5363–5372, 2018.

21. Yang, Q., Zhang, P., Cheng, L., Min, Z., Chyu, M., and To, A. C., "Finite Element Modeling and Validation of Thermomechanical Behavior of Ti-6Al-4V in Directed Energy Deposition Additive Manufacturing," Additive Manufacturing, Vol. 12, pp. 169–177, 2016.

22. Wang, L., Felicelli, S., Gooroochurn, Y., Wang, P. T., and Horstemeyer, M. F., "Optimization of the LENS® Process for Steady Molten Pool Size," Materials Science and Engineering: A, Vol. 474, No. 1–2, pp. 148–156, 2008.

23. Lindgren, L.-E., Lundbäck, A., Fisk, M., Pederson, R., and Andersson, J., "Simulation of Additive Manufacturing Using Coupled Constitutive and Microstructure Models," Additive Manufacturing, Vol. 12, pp. 144–158, 2016.

24. Chua, B. L., "Investigation of Development of Thermo-Mechanical Analysis Method for a Wire Feeding Type Directed Energy Deposition Process," (Unpublished doctoral dissertation or master's thesis), Chosun University, South Korea, 2019.

25. Nickel, A. H., Barnett, D. M., and Prinz, F. B., "Thermal Stresses and Deposition Patterns in Layered Manufacturing," Materials Science and Engineering: A, Vol. 317, No. 1–2, pp. 59–64, 2001.

26. Mughal, M. P., Mufti, R. A., and Fawad, H., "The Mechanical Effects of Deposition Patterns in Welding-Based Layered Manufacturing," Proceedings of the Institution of Mechanical Engineers, Part B: Journal of Engineering Manufacture, Vol. 221, No. 10, pp. 1499–1509, 2007.

27. Deus, A. M. and Mazumder, J., "Three-Dimensional Finite Element Models for the Calculation of Temperature and Residual Stress Fields in Laser Cladding," Proc. of the 25th International Congress on Applications of Laser and Electro-Optics, 2006.

28. Chiumenti, M., Cervera, M., Salmi, A., Agelet de Saracibar, C., Dialami, N., and Matsui, K., "Finite Element Modeling of Multi-Pass Welding and Shaped Metal Deposition Processes," Computer Methods in Applied Mechanics and Engineering, Vol. 199, No. 37–40, pp. 2343– 2359, 2010.

29. Ding, J., Colegrove, P., Mehnen, J., Ganguly, S., Sequeira Almeida, P. M., Wang, F., and Williams, S., "Thermo-Mechanical Analysis of Wire and Arc Additive Layer Manufacturing Process on Large Multi-Layer Parts," Computational Materials Science, Vol. 50, pp. 3315– 3322, 2011.

30. Zhang, C., Li, L., and Deceuster, A., "Thermomechanical Analysis of Multi-Bead Pulsed Laser Powder Deposition of a Nickel-Based Superalloy," Journal of Materials Processing Technology, Vol. 211, No. 9, pp. 1478–1487, 2011.

31. Farahmand, P. and Kovacevic, R., "An Experimental–Numerical Investigation of Heat Distribution and Stress Field in Single- and Multi-Track Laser Cladding by a High-Power Direct Diode Laser," Optics & Laser Technology, Vol. 63, pp. 154–168, 2014.

32. Crespo, A. and Vilar, R., "Finite Element Analysis of the Rapid Manufacturing of Ti–6Al–4V Parts by Laser Powder Deposition," Scripta Materialia, Vol. 63, No. 1, pp. 140–143, 2010.

33. Denlinger, E. R. and Michaleris, P., "Effect of Stress Relaxation on Distortion in Additive Manufacturing Process Modeling," Additive Manufacturing, Vol. 12, pp. 51–59, 2016.

34. Lee, Y. S., Bandari, Y., Simunovic, S., Richardson, B., and Kirka, M. M., "Correlations of Interlayer Time with Distortion of Large Ti-6Al-4V Components in Laser Metal Deposition with Wire," Proc. of the 29th Annual International Solid Freeform Fabrication Symposium, pp. 606–622, 2018.

35. Ambielli, J. F., "Industrial Process Design for Manufacturing Inconel 718 Extremely Large Forged Rings," Theses and Dissertations, pp. 1222, 2011.

36. Ren, K., Chew, Y., Fuh, J., Zhang, Y., Bi, G., "Thermo-mechanical analyses for optimized

path planning in laser aided additive manufacturing processes," Materials & Design, Vol.162, pp. 80–93, 2019.

37. El Cheikh, H., Courant, B., Branchu, S., Hascoët, J. Y., Guillén R., "Analysis and prediction of single laser tracks geometrical characteristics in coaxial laser cladding process," Opt. Lasers Eng., Vol. 50, No. 3, pp. 413–422, 2012.

38. Morville, S., Carin, M., Peyre, P., Gharbi, M., Carron, D., Le Masson, P., Fabbro, R., "2D longitudinal modeling of heat transfer and fluid flow during multilayered direct laser metal deposition process," J. Laser Appl., Vol. 24, No. 3, pp. 032008. 2012.

39. Agarwal, G., Gao, H., Amirthalingam, M., Hermans, M., "Study of solidification cracking susceptibility during laser welding in an advanced high strength automotive steel," Metals, Vol 8, p 673, 2018.

40. Sysweld, Visual-Environment Version 15.5, ESI Group Inc. 2021.

41. JmatPro, JmatPro version 12.0, Sente Software Ltd. 2021.

42. Alfaify, A., Saleh, M., Abdullah, F. M., Al-Ahmari, A. M., "Design for Additive Manufacturing: A Systematic Review," Sustainability, Vol. 12, No 19, pp. 7936, 2020.

43. Dilberoglu, U. M., Gharehpapagh, B., Yaman, U., Dolen, M., "The Role of Additive Manufacturing in the Era of Industry 4.0," Procedia Manufacturing, Vol. 11, pp. 545–554, 2017.

44. Shamsaei, N., Yadollahi, A., Bian, L., Thompson, S. M., "An overview of Direct Laser Deposition for additive manufacturing; Part II: Mechanical behavior, process parameter optimization and control," Additive Manufacturing, Vol. 8, pp 12–35, 2015.

45. Dai, K., Shaw, L., "Distortion minimization of laser-processed components through control of laser scanning patterns," Rapid Prototyping Journal, Vol. 8, No.5, 270–276, 2002.

46. Farahmand, P., Kovacevic, R., "An experimental–numerical investigation of heat distribution and stress field in single- and multi-track laser cladding by a high-power direct diode laser," Optics & Laser Technology, Vol. 63, pp. 154–168, 2014.

47. Yan, L., Zhang, Y., Liou, F., "A conceptual design of residual stress reduction with multiple shape laser beams in direct laser deposition," Finite Elements in Analysis and Design, Vol. 144, pp. 30–37, 2018.

48. Kim, H., Lee, K. K., Ahn, D. G., Lee, H., "Effects of Deposition Strategy and Preheating Temperature on Thermo-Mechanical Characteristics of Inconel 718 Super-Alloy Deposited on AISI 1045 Substrate Using a DED Process," Materials, Vol. 14, No. 7, pp. 1794, 2021.

ACKNOWLEDGMENTS

Undertaking this master's degree journey has been truly life-changing for me. Despite the challenges I encountered at the beginning and throughout my stay in Korea, I believe that coming here was one of the best decisions I have made so far. While finishing my master's degree requirements and writing this thesis, I have only felt humbled, grateful, and appreciative of all the help and support I have received along the way. I came across a number of people and institutions whose contributions helped my studies and research in various ways, and they deserve special recognition. It gives me great pleasure to express my appreciation to them.

I am extremely grateful for the opportunity to conduct this master's degree research study in the field of novel additive manufacturing technology. First and foremost, I would like to acknowledge and express my heartfelt gratitude to Professor Ahn Dong-Gyu, my research adviser, for his unwavering guidance, enthusiasm, and invaluable support over the years. I consider myself very fortunate to work with such a considerate and encouraging professor as him. Without his mentoring, meticulous supervision at every phase of my academic work, and persistent assistance with this thesis, finishing my degree would not have been possible.

Second, I would like to thank my committee members, Professor Kim Chang-Lae, and Professor Lee Jeong-Won, for their insights and advice in developing my research.

I am also very grateful to all the former and current members of CAD/CAM/CAE laboratory, Kwang-Kyu Lee, Ho Kim, Sun-Ho Baek, Kim Dan-A, Ji-Wan Yang, Im Seong-Hoon, Dong-Il Jeong, who provided me with their invaluable academic support and assistance, as well as their enjoyable camaraderie. They made me feel like I was not alone in my graduate school journey, especially during my thesis research.

I want to express my gratitude to the organizations and institutions that made studies and research possible in South Korea and Chosun University. I am immensely thankful to the South Korean government and the National Institute for International Education (NIIED) for selecting

me as the Global Korea Scholarship recipient (GKS). Its generosity has enabled me to embark on this journey.

Last but not least, my heartfelt appreciation goes to my family, my parents, brothers, and my wife, who have always supported, encouraged, prayed for, and believed in me in all of my endeavors and life decisions. I do not think I could have overcome the difficulties of studying away from home without their love and support. And, of course, I am eternally grateful to Allah, the Almighty, for blessing me with His graces, strength, and sustenance.

CURRICULUM VITAE

Gwangju, 61448 Republic of Korea • aliyev.alisultan@gmail.com • Mobile (+82) 1025601571
• Gender: M • DOB: 12 September 1994• Citizenship: Kazakhstani • Married

EDUCATION

Master of Science, Mechanical Engineering   Sept 2020 - Aug 2022
Chosun University, South Korea   GPA: 4.42/4.5
Global Korea Scholarship Recipient / Full Scholarship

Korean Language Program, TOPIK Level IV Passed   Sept 2019 - Aug 2020
Keimyung University, South Korea

Bachelor of Science, Mechanical Engineering   Sept 2013 - Aug 2017
Eastern Mediterranean University, North Cyprus   GPA: 3.42/ 4.0
University Scholarship Recipient –High Academic Excellence/ Full Scholarship

English Language Program, IELTS 7.5 Band   Aug 2012 - Jun 2013
EMU Foreign Language and Preparatory School, North Cyprus

SKILLS

Computer: AUTOCAD, SolidWorks, Catia, NX Graphics, Abaqus, SysWeld
Language: Professional Fluency in English and Russian, Conversational Turkish and Korean

ACADEMIC/WORK EXPERIENCE

Junior Research Assistant, Chosun University, Gwangju, South Korea
Sept 2020 – Present

- Research Lab: CAD/CAM/CAE/CAT/ Additive Manufacturing
- Research: Developing 3D Printing Application Technology

Mechanical Engineer, TOO Mechanic Steel KZ, Almaty Kazakhstan
Jan 2019 – Apr 2019

- Product development for customers. Calculated cost and estimate the final price of the products. Oversaw the design and development of the manufacturing of parts. Finalized designs and estimated required operations.
- Created drawing using CAD applications (AutoCad, SolidWorks)
- Conducted feasibility study (possibility of designing of a product using available machines, which include: Lathe, Gear Shaper, Drill press, Grinding, Welding, WireCut, WaterJet, PlasmaCut, Guillotine, Rolling, Shear(sheet metal))

Transport Lead, GATE (GAMMA & TEKFEN) Construction, Tengiz Oilfield, Kazakhstan
Aug 2018- Jan 2019

- Supervised, and coordinated of all transportation matters within the organization
- Organized schedules & routes
- Ensured that vehicles are safe and meet legal requirements

Team Leader, Technical Office Dept. Renaissance Construction, Russian Federation
Aug 2017 – Jun 2018

- Managed rental equipment invoices for the chief executive manager's approval. Worked with partner organizations in solving invoices issues. Prepared weekly reports for the top manager.
- Coordinated with other technical office departments located in the other sites.
- Estimated the required type and amount of equipment for specific work. Analyzed prices for the specific types of equipment in various regions.
- Distributed work among the team members and control staff.
- Created an inspiring team environment with an open communication culture. Developed training needs and provide coaching. Resolved issues or conflicts among the team members. Assisted with the orientation and adaptation to the new members.

Mechanical Engineer Trainee, A&T ENERGO Company, Tasotkel Hydro Power plant, Kazakhstan, Jul 2016 – Aug 2016

- Maintenance of the turbine schedule. Assisted in operating the turbines when necessary
- Evaluated and monitored the turbine performance

RESEARCH AND PUBLICATIONS

- Investigation of the Influence of Radius and Corner Position on the Residual Stress Distribution in the Vicinity of the Repaired Region via Directed Energy Deposition by using Finite Element Analysis

- A. Aliyev, K. K. Lee, D.G. Ahn, *Investigation of the influence of radius and corner position on the residual stress distribution in the vicinity of the repaired region via directed energy deposition by using finite element analysis*, The Korean Society of Manufacturing Process Engineers, Vol. *20, No.* 7, 33–40, 2021

CONFERENCES, WORKSHOPS, & PRESENTATIONS

- A. Aliyev, K. K. Lee, D.G. Ahn, *A Study on Residual Stress Characteristics According to Deposition Path to Deposit Inconel 718 on AISI 1045 Substrate with Thin Beam Structure*, The Korean Society of Mechanical Engineers Spring Conference, Yeosu, April 27-30 2022, (Oral)
- A. Aliyev, K. K. Lee, D.G. Ahn, *Investigation of the Effects of Deposition Strategies on Thermo-mechanical Characteristics of G6 steel Deposited on SCM440 Substrate by DED using FEA,* The Korean Society for Technology of Plastic International Symposium on Technology of Plasticity (IS-KSTP30),Busan South Korea, November 24-26 2021 (Oral)
- A. Aliyev, K. K. Lee, D.G. Ahn, *A Study on Thermo-mechanical Characteristics in the Vicinity of Inconel 718 Deposited Region on AISI1045 substrate by a DED process According to Deposition Strategies,* The Korean Society of Manufacturing Engineers Autumn Conference, Jeju South Korea, December 01-03 2021, (Oral)
- Korea Workshop Lecture Series on Advanced Technology, Korea's National Security, and Culture. Organized by the Korea Foundation and the Keimyung Institute for International Studies, Participant, Seoul South Korea, 17 September to 1 October 2021
- A. Aliyev, K. K. Lee, D.G. Ahn, *A Study on the Effect of Inner Radius of a Part on Residual Stress Characteristics in the Deposited Region for the Case of Repair of Arc Shaped Part Using a DED Process,* The Korean Society of Mechanical Engineers online conference, 17 July 2021 (Poster)